Chem Soc Rev

REVIEW ARTICLE

View Article Online
View Journal | View Issue

Cite this: *Chem. Soc. Rev.*, 2017, **46**, 7787

Enantiomer surface chemistry: conglomerate *versus* racemate formation on surfaces

Soham Dutta[a] and Andrew J. Gellman *[ab]

Research on surface chirality is motivated by the need to develop functional chiral surfaces for enantiospecific applications. While molecular chirality in 3D has been the subject of study for almost two centuries, many aspects of 2D chiral surface chemistry have yet to be addressed. In 3D, racemic mixtures of chiral molecules tend to aggregate into racemate (molecularly heterochiral) crystals much more frequently than conglomerate (molecularly homochiral) crystals. Whether chiral adsorbates on surfaces preferentially aggregate into heterochiral rather than homochiral domains (2D crystals or clusters) is not known. In this review, we have made the first attempt to answer the following question based on available data: in 2D racemic mixtures adsorbed on surfaces, is there a clear preference for homochiral or heterochiral aggregation? The current hypothesis is that homochiral packing is preferred on surfaces; in contrast to 3D where heterochiral packing is more common. In this review, we present a simple hierarchical scheme to categorize the chirality of adsorbate–surface systems. We then review the body of work using scanning tunneling microscopy predominantly to study aggregation of racemic adsorbates. Our analysis of the existing literature suggests that there is no clear evidence of any preference for either homochiral or heterochiral aggregation at the molecular level by chiral and prochiral adsorbates on surfaces.

Received 28th July 2017

DOI: 10.1039/c7cs00555e

rsc.li/chem-soc-rev

1. Introduction to chirality

The term chirality refers to the existence of a sense of handedness to the structure of an object, *i.e.* it is non-superimposable onto its mirror image. The word chiral was coined in 1894 by Lord Kelvin and is derived from the Greek word kheir meaning hand.[1]

[a] *Department of Chemical Engineering, Carnegie Mellon University, Pittsburgh, PA 15213, USA. E-mail: gellman@cmu.edu; Tel: +1-412-268-3848*
[b] *W. E. Scott Institute for Energy Innovation, Carnegie Mellon University, Pittsburgh, PA 15213, USA*

Soham Dutta

Soham Dutta is a PhD student in the Department of Chemical Engineering at Carnegie Mellon University in Pittsburgh, Pennsylvania, USA. He received his Bachelor of Engg. at Siddaganga Institute of Technology, Tumkur, India and his Master of Science at Carnegie Mellon University. He is currently a member of the Catalysis and Surface Science laboratory and is studying decomposition and aggregation of chiral molecules on single crystal metal surfaces. Fundamental understanding of such phenomena has applications in enantiomer separation, enantioselective catalysis and supramolecular chirality.

Andrew J. Gellman

Andrew Gellman is the Thomas Lord Professor of Chemical Engineering at Carnegie Mellon University. He received a BS in Chemistry from the California Institute of Technology and a PhD in Chemistry from the University of California at Berkeley. His research expertise is in the field of surface science and surface chemistry with emphasis on catalysis, corrosion, chirality and enantioselectivity. In addition, his group has developed of tools and methods for high throughput study of alloy surfaces spanning alloy composition space and for studies of structure sensitive properties of crystalline surfaces spanning surface orientation space.

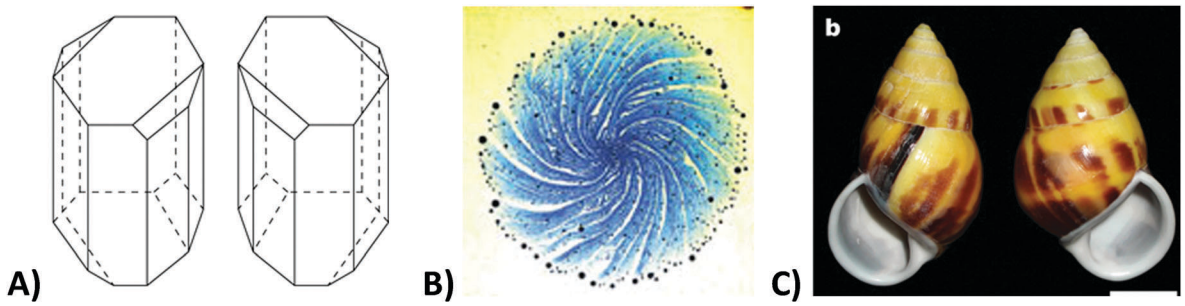

Fig. 1 Chirality manifests itself throughout nature in various forms. This figure compiles a few such examples. (A) The hemihedral crystal shapes of (2*R*,3*R*)-(+)- and (2*S*,3*S*)-(−)-sodium ammonium tartrate tetrahydrate observed by Pasteur. Pasteur visually identified and separated these crystals based on their shape. After separating the crystals into two enantiomorphous groups and dissolving them, he found that the two solutions rotated light in opposite directions. Reprinted from ref. 5 Copyright 2001 with permission from Elsevier. (B) Bacterial colonies (like this one for *Paenibacillus vortex*) can exhibit chirality. The branches are all oriented with the same spiral sense of direction due to the orientation of the bacterial flagella, thus imparting chirality to the structure. Reprinted by permission from Macmillan Publishers Ltd: Nature ref. 6 Copyright 2001. (C) Left- and right-handed shells of the species *Amphidromus perversus* exhibiting chiral dimorphism. Adapted by permission from Macmillan Publishers Ltd: Nature ref. 7 Copyright 2009.

Chirality is ubiquitous in nature at all length scales, ranging from the celestial where circularly polarized light emanates from large regions of space[2] to macroscopic objects (living and non-living) to molecules and down to the interactions between fundamental particles.[3] The pervasiveness of chirality is demonstrated by biotic and abiotic examples as shown in Fig. 1.[4–7]

In the context of a geometrically rigid body such as a crystal, a structure is said to be chiral, if it lacks mirror plane symmetry and thus, it is not superimposable onto its mirror image. This definition, when applied to chiral molecules, implies the existence of both left- and right-handed forms (the molecule and its non-superimposable mirror image) called enantiomers. A molecule with a central atom bonded to various substituents is chiral (example shown in Fig. 2A[8]), if there are no combinations of mirror, rotation and inversion symmetry operations that transform the molecular structure into itself.[9] In the early 1800's, molecular chirality was observed, but not understood, by detecting the optical activity of enantiomers, *i.e.* their ability to rotate linearly polarized light by equal magnitudes but in opposite directions. While scientists such as Mitscherlich, Biot and others had demonstrated optical activity by chemical compounds in the early 19th century,[10] the origin of optical activity in molecular chirality was discovered by Louis Pasteur in 1848.[11,12] Pasteur found that crystals of sodium ammonium tartrate tetrahydrate ($Na^+NH_4^+C_4H_4O_6^{2-}\cdot 4H_2O$) had chiral shapes as shown in Fig. 1A, and that dissolution of enantiomorphous crystals yielded solutions that rotated light in equal but opposite directions. Solutions containing equimolar amounts of the enantiomorphous crystals did not rotate light. Pasteur's experiment was the first to establish a link between enantiomorphism at the macroscopic level (crystal shape) and at the molecular level and to establish the link to optical activity.[13] His work laid the foundation of the field of stereochemistry.

The notations used to designate the handedness of molecular enantiomers have evolved over the years; hence, we will briefly review them before proceeding further. Notations including D/L, *d*/*l*, +/−, *P*/*M* and *R*/*S* are used to designate the handedness of enantiomers.[14] When chirality is determined

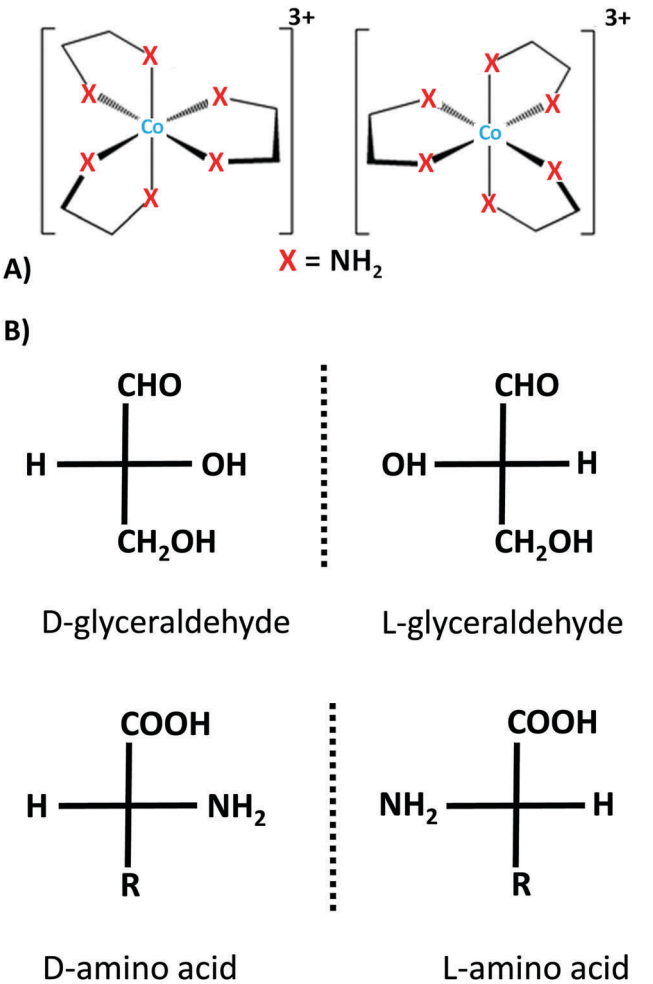

Fig. 2 (A) Enantiomers of the coordination compound [Co(ethylenediamine)$_3$]$^{3+}$ seen across a mirror plane. The ligands are tilted to accommodate the *cis* arrangement of the N atoms, leading to a break in mirror and inversion symmetry. Adapted from ref. 8 with permission from the Royal Society of Chemistry. (B) Fischer projections of D- and L-glyceraldehyde and the amino acid molecular structures.

exclusively from optical activity measurements, the terms levorotatory (*l*) or (−) and dextrorotatory (*d*) or (+) are used, depending on whether linearly polarized light is rotated to the left or the right, respectively, when observed looking towards the polarized light source along the direction of propagation. While Fischer introduced the *d*/*l* nomenclature for chiral compounds in 1890, it was not until the early 20th century that Rosanoff (1906) and Wohl & Freudenberg (1923) established glyceraldehyde ($CH_2OH(CHOH)CHO$) as the reference for assignment of many other chiral molecules.[15–17] The assignment of chirality based on glyceraldehyde has come to be known as the Fischer convention.[18,19] To establish the convention, glyceraldehyde was denoted as either (D-) or (L-) depending upon whether the –OH group lay on the right or the left side of its Fischer projection (Fig. 2B). To denote the chirality of related molecules, their molecular structures were compared to that of D- and L-glyceraldehyde. It is relevant to point out that the direct correlation between the Fischer convention *d*/*l* nomenclature and optical activity was not established until 1951 when Bijvoet and co-workers used anomalous X-ray scattering to determine the absolute chirality of (+)-sodium rubidium tartrate crystals.[20] As the library of chiral chemical compounds expanded in the 20th century, the Cahn Ingold Prelog (CIP) convention was introduced. This convention designated the absolute chirality about a tetrahedral carbon atom as either rectus (*R*) or sinister (*S*) depending on the stereographic arrangement of its four different substituents.[18,19] In addition to chiral carbon centers which are conventionally associated with chiral molecules, chirality can also originate from molecular structures that lacks a mirror plane perpendicular to a molecular axis: *e.g.* biaryl molecules, ferrocene ($Fe(C_5H_5)_2$), and helical structures such as helicenes.[21] To differentiate helically chiral molecules from chiral molecules with a chiral center, helical molecules are categorized using the convention *M* (minus) and *P* (plus) to denote left-handed and right-handed helices, respectively.[22,23] In this review, wherever there is a need to distinguish between two enantiomers of a chiral compound, we have decided to use the convention adopted by the authors of the original work being discussed.

From a societal perspective, the most important manifestation of molecular chirality is found in the biomolecules essential for life on Earth. Most such molecules (amino acids, sugars, DNA, *etc.*) have structures that are chiral and, therefore, exist in two enantiomeric forms. However, in life on Earth these molecules are homochiral, *i.e.* chiral biomolecules are found only in one enantiomeric form.[24,25] For example, only the L-enantiomers of amino acids are present in naturally occurring proteins. The molecular backbones of DNA and RNA contain only D-sugars. Replacing some of the amino acids in proteins or replacing the sugar subunits in DNA with their mirror images would drastically change the *in vivo* properties of these biomolecules, rendering them incompatible with life.[26,27] The origin of homochirality in life on Earth has been the subject of much research over the past century as it may provide clues to the processes that led to the origin of life itself.[25,28–30] The reasons for biomolecular homochirality are not known although a number of contributing factors have been proposed. These include, but are not limited to, minute energy differences between enantiomers induced by parity violation in the weak force,[31] stochastic fluctuations in enantiomeric excess (ee)[32] and chiral amplification of enantiomeric excess on inorganic surfaces.[33]

The most important social consequence of the biomolecular homochirality of life is that chirality influences the physiological response of living organisms to ingested chiral compounds such as pharmaceuticals.[34] The tragic birth defects resulting from ingestion of a racemic (enantiomerically equimolar) mixture of D- and L-Thalidomide™ by pregnant women in the late 1950's ultimately led to our appreciation of the need for stereochemical control of chiral pharmaceuticals.[35,36] Rising awareness of the differences in physiological impact of enantiomers and issuance of regulations for chiral drug development have led to a steady growth in the production of single enantiomer drugs.[37–40] This has led to a market with >200 billion USD annual sales of enantiopure drugs in 2005 and its growth at a rate of 15% since 2010.[41,42] It is estimated that ~95% of all drugs marketed by 2020 will be chiral.[43,44]

In the 20th century, chirality research was focused on asymmetric synthesis of single enantiomer compounds and decades of significant work was recognized by the 2001 Nobel prize in chemistry.[45–47] However, in the 21st century, research on chirality has expanded to include fields such as chiral nanostructures,[8,48] chiral surfaces,[49–51] molecular motors,[52–54] and spintronics.[55] One of the most active fields has been supramolecular chirality,[56,57] *i.e.* the growth of extended, periodic chiral structures in two- (2D) and three-dimensions (3D). Self-assembly principles are used to prepare functional surfaces and solids with enantiospecific properties. Fundamental to understanding supramolecular chirality are the interactions between the chiral components (molecules or clusters) of the structure. Generally speaking, racemic mixtures of chiral adsorbates can aggregate in either of two ways: homochirally or heterochirally. Homochiral aggregation refers to the clustering of like enantiomers of the chiral moiety whereas; heterochiral aggregation refers to racemic clustering of opposite enantiomers. The primary focus of this review is to determine the differences in the aggregation tendencies of chiral molecules adsorbed on surfaces *versus* in 3D. Common wisdom holds that, in 3D enantiomers prefer to crystalize heterochirally (racemate) rather than homochirally (conglomerate).[58] It has been suggested that the opposite is true for enantiomer aggregation on surfaces.[59] This review addresses this hypothesis directly.

Key to designing 2D supramolecular chiral structures on surfaces is an understanding of how chiral adsorbates interact with surfaces and with each other. Which forces govern the organization of racemic/non-racemic mixtures of chiral adsorbates into chiral supramolecular structures? What kind of enantiomer aggregation behavior (homochiral or heterochiral) is favored on surfaces? This review documents a comprehensive survey of experimental studies of chiral and prochiral molecules adsorbed on surfaces in order to extract the current state of understanding and attempt to answer the questions above. To understand these systems fully, we have included in this

review adsorbates that are achiral and non-prochiral but, nonetheless, form chiral structures on surfaces. The review includes observations at both liquid–solid (L–S) and gas–solid (G–S) interfaces. Unfortunately, the majority of studies of chiral adsorbates on surfaces have been limited to enantiopure molecules rather than mixtures of enantiomers.[49,60–62] There are a number of reviews of enantiopure chiral adsorbates on surfaces,[56,63,64] however, such studies cannot comment on inter-enantiomer interactions that ultimately lead to stable homochiral or heterochiral assemblies on the surface. Hence, this review excludes studies of enantiopure adsorbates on surfaces.

The outline of this review is as follows: we begin by comparing chiral aggregation in 2D *versus* 3D. Then, we introduce a classification which categorizes chirality at multiple levels for adsorbate–surface systems. Next, we divide adsorbate–surface systems into four groups depending on the chirality of the adsorbate (chiral, prochiral, conformationally chiral and achiral) and discuss each group separately. Our survey of these adsorbate–systems reveals that both homochiral and heterochiral aggregation have been observed at the molecular and at the cluster level when chiral, prochiral and conformationally chiral molecules adsorb onto surfaces. We did not find a clear preference for homochiral over heterochiral aggregation on surfaces;[59,65] however, homochiral aggregation is certainly more common on surfaces than it is in 3D.[58]

2. Chirality in two dimensions

2.1 Two-dimensional chirality

Chirality in two-dimensions is an increasingly important area of research, driven by applications to various surface chemical processes (catalysis, separations, sensing, *etc.*). If the surface in use is chiral, these processes can be enantioselective. Intrinsic surface chirality can be expressed either by surfaces of bulk materials such quartz[66] and calcite[67] or by single crystal surfaces of achiral bulk materials such as metals cut along low-symmetry directions (naturally chiral surfaces).[68,69] Alternatively, an achiral surface can be modified to become chiral either by chiral templating or by chiral imprinting. Chiral templating refers to the process of rendering a surface chiral by adsorption of chiral molecules, for example, adsorption of *R*- or *S*-tartaric acid (TA, HOOCCH(OH)CH(OH)COOH) on Cu(110).[60,70] Chiral imprinting refers to the reconstruction of an achiral surface by a chiral adsorbate such that the surface exposes intrinsically chiral structures or facets.[71–73]

The most common industrial application of chiral surfaces is in the field of chromatographic separations in which chiral stationary phases are used to separate enantiomer mixtures into enantiopure compounds.[74–78] Remarkably, enantiomer separation has also been observed during chromatography of non-racemic mixtures over achiral stationary phases that, in principle, do not prefer either enantiomer.[79–81] This phenomenon is attributed to enantiomer aggregation, exactly the subject of this review. In the field of enantioselective catalysis, heterogeneous catalysts are of great interest as alternatives to conventional asymmetric homogeneous catalysts used for synthesis of enantiopure compounds.[49,82–85] Homogeneous catalytic processes, although well developed and highly enantioselective, suffer from the need for product separation from the homogeneous catalyst.[86–88] In contrast, heterogeneous enantioselective processes have inherent advantages such as reduced waste generation and significantly fewer downstream separation issues. The highly enantiospecific hydrogenation of α-ketoesters by heterogeneous cinchonidine-modified Pt catalysts has motivated much research on the mechanistic origin of enantioselectivity on surfaces.[89–92] In addition to chromatography and catalysis, advanced materials development utilizes principles of chiral recognition and organization in 2D for preparation of self-assembled systems,[93,94] liquid crystals,[95] molecular electronics[96–98] and sensors.[99,100] Lastly, study of chirality on surfaces may yield clues to the origin of homochirality in life on Earth. It has been suggested that nonlinear chiral amplification mechanisms on inorganic mineral surfaces may have led to enantiomeric excess in the primordial soup and consequently, to biomolecular homochirality.[66,101] Understanding the fundamental forces that guide chiral molecular aggregation on surfaces is crucial to enabling the design of functional enantiospecific surfaces and thereby maximizing their potential.[102–105]

2.2 Chiral molecular packing in 3D and 2D

In 3D, racemic mixtures of enantiomers crystallize in one of three ways: as a racemate, a conglomerate or a random solid solution (RSS) (Fig. 3).[58] Racemate crystals have unit cells containing equal numbers of both enantiomers as shown in the case of DL-alanine (Fig. 3B[106]) whereas; conglomerates are

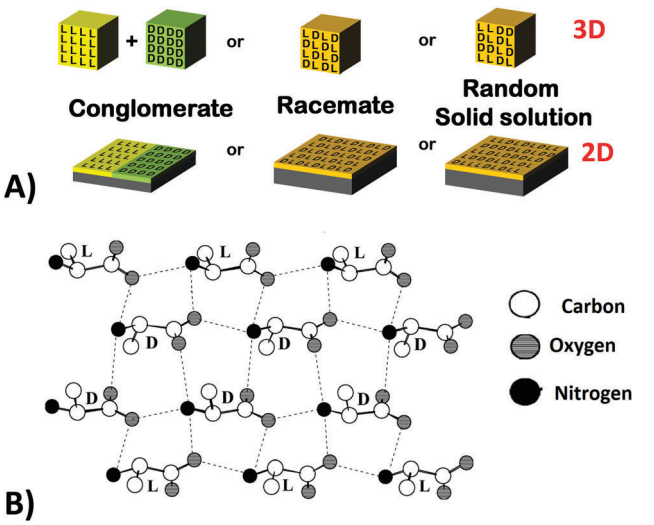

Fig. 3 (A) Three types of packing arrangements adopted by chiral molecules crystallized in 2D and 3D. 3D crystallization of a racemic mixture can result in a mixture of enantiomerically pure 3D crystals (conglomerate), racemate crystals, or a RSS. Adsorption can result in a 2D conglomerate, a 2D racemate, or a 2D random solution on the surface. (B) 3D crystal structure of DL-alanine ($CH_3NH_2CHCOOH$) racemate with both L- and D-enantiomers in the unit cell. Adapted with permission from ref. 106 Copyright 2010 American Chemical Society.

physical mixtures of enantiopure crystals. A RSS is one in which both enantiomers are randomly distributed on the crystal lattice and there is no long range periodicity; a rare occurrence. In addition, there are more complex crystal structures such as kryptoracemates (false conglomerates whose crystals on dissolution lead to optically inactive solutions) and crystallographically independent molecules (molecules that crystallize in large-unit cell structures of ~50 or more molecules causing molecules in the same unit cell to be exposed to different local environments).[107]

Based on a survey of ~1300 chiral molecules, Collet *et al.* reported that ~90% of racemic mixtures crystallize from solution into racemate crystals.[58] Estimates are that 5–10% of neutral, chiral organic molecules crystallize as conglomerates, while ionic and zwitterionic organic molecules are 2–3 times more likely to form conglomerates.[58,107] RSS are very rare and may result from kinetic trapping in metastable structures.[58,108,109] In 1895, it was suggested by Wallach that the prevalence of racemates over conglomerates could be attributed to a higher packing density of racemate crystals over conglomerate crystals; however, this correlation was based on a limited set of nine compounds.[110–112]

In 1991, Dunitz *et al.* tried to validate Wallach's rule by analyzing the structures of racemate and conglomerate crystals reported in the Cambridge Structural Database.[113] Dunitz concluded that, although there was a small difference in the densities of racemate and conglomerate structures (racemates being higher in density), the difference was due to sampling bias in the available data. There is no evidence to suggest that the density difference leads to racemate *vs.* conglomerate packing, thus questioning Wallach's rule.[113] Comparisons of the densities of racemic *vs.* enantiopure compounds have revealed many instances in which Wallach's rule does not apply, so stable modes of packing cannot be explained merely on the basis of density.[113–119] In fact, the generality of the estimated 5–10% conglomerate formation reported by Collet *et al.*[58] has been questioned due to the limitation of the original survey to crystallization processes performed at ambient temperature conditions.[117] Several other investigations have revealed that, under some conditions, conglomerate formation is preferred over racemate formation.[117,120,121] For example, conglomerates are twice as likely to form in organic salts than in inorganic salts[117] and conglomerates are also more likely to form at low crystallization temperatures than at high temperatures.[120,121] To date, a fundamental understanding of what governs crystallization of chiral compounds into stable conglomerates or racemates has been elusive.

The first experiments to study chiral molecules on surfaces were performed using chiral amphiphiles at air–water interfaces.[122,123] Based on observations from those experiments, it was hypothesized that the likelihood of racemate formation on surfaces is greatly reduced with respect to its likelihood in 3D.[59] The postulated rationale is that symmetry elements such as inversion, glide planes parallel to surface and twofold screw axes cannot exist at asymmetric interfaces, thus reducing the number of chiral symmetry groups available to molecules when they are constrained to 2D surfaces. For the case of mixed crystals (consisting of a guest molecule included in the bulk of another crystal), it has been demonstrated that the overall symmetry of the mixed crystal must be the same as the host crystal symmetry for occlusion of the guest crystal and hence, the mixed crystal could be referred to as homochiral.[124] In a general sense, if this hypothesis is true and is applied to racemic mixtures deposited on surfaces, it suggests that on surfaces conglomerates may be more prevalent than racemates. One of the most comprehensive attempts undertaken to date to understand chiral organization in 2D has been made by Matzger and co-workers.[125] They surveyed the two-dimensional structural database (2DSD) to determine the unit cell structures of long alkyl chain amphiphiles adsorbed at solution-HOPG (highly oriented pyrolytic graphite) interfaces. They qualified their findings by noting that the dataset was limited to HOPG surfaces, *i.e.* physisorbed systems, thus excluding chemisorption and that the dataset was also limited to adsorbates with long alkyl chains. Nonetheless, they concluded that within these constraints, 70–80% of the ordered surface structures formed have chiral unit cells and exist in enantiomorphous domains.[125] This finding by Matzger *et al.*, that chiral lattices are more common than achiral lattices (for long alkyl chain amphiphiles on HOPG), must not be incorrectly interpreted to suggest that chiral adsorbates preferentially form conglomerate domains (homochiral at the molecular level) in 2D. The Matzger study exclusively surveyed adsorbates that are either conformationally chiral or achiral in 3D. Therefore, conclusions regarding the frequency of conglomerate *vs.* racemate packing in 2D cannot be drawn. Nonetheless, the Matzger study is the first review of a significant sample of adsorbate–surface systems (359 unique monolayers) and demonstrated that when achiral and conformationally chiral adsorbates self-assemble in 2D, there is a preference for lattice level chirality.

2.3 Early studies of enantiomers on air–water interfaces

Before the advent of scanning tunneling microscopy (STM) in the late 20th century, chirality in 2D was studied using Langmuir–Blodgett films (L–B) of chiral amphiphiles at the air–water interface. Amphiphiles (lipids) are well-suited for such experiments because the combination of a hydrophilic polar head group with a hydrophobic aliphatic tail confines these molecules to the water surface; thus easily forming 2D monolayers. Techniques such as area–pressure isotherms, optical measurements (Brewster angle and fluorescence microscopy) and grazing incidence X-ray diffraction (GIXD) were used to probe these L–B films.[126] Stewart *et al.* reviewed the use of area-pressure isotherms to compare monolayer packing of racemic and enantiopure mixtures of surfactants.[123] Use of differential scanning calorimetry and X-ray diffraction enabled detection of phase transitions in saturated monolayers.[123] Using racemic α-amino acid amphiphiles (*R*-CH(NH_2)COOH) such as aminostearic acid, aminolauric acid, aminomyristic acid and lysine derivatives, Weissbuch *et al.* found that an odd number of carbon atoms in the alkyl chain led to resolution into conglomerate domains while amphiphiles with an even number of carbon atoms formed racemic domains.[65]

Nandi *et al.* have reviewed the available literature on L–B experiments and found that to rigorously differentiate between conglomerate or racemate formation by chiral amphiphiles in 2D, area-pressure isotherms need to be supplemented with optical measurements. Chiral resolution into racemate or conglomerate domains is not always clearly indicated by the area-pressure isotherms alone.[126]

With the advent of high resolution STM, it is now possible to discriminate between enantiomers at both L–S and G–S interfaces.[64,127–129] The vast majority of systems reviewed herein have been studied using STM. In addition to STM, other surface science techniques such as X-ray photoelectron spectroscopy (XPS) and reflection absorption infrared spectroscopy (RAIRS) can be used to determine the chemical state and orientation of adsorbates on surfaces.[130,131]

3. Current review

3.1 Scope and purpose of review

Several authors have reviewed the organization of chiral and prochiral molecules adsorbed on surfaces in enantiopure form and as racemic mixtures.[72,132–136] Most of these reviews have focused on specific types of adsorbates or surfaces and, in most cases, only on enantiopure adsorbates. Hence, there is a need for a comprehensive review that focuses on the behavior of enantiomer mixtures and prochiral adsorbates which necessarily adsorb as racemic mixtures on achiral surfaces. In particular, there is no existing review focusing on the tendency of adsorbed racemic mixtures to aggregate into homochiral (conglomerate) or heterochiral (racemate) structures. This review includes studies of chiral adsorbates (molecules that are enantiomorphous in 3D), prochiral adsorbates (achiral molecules that become enantiomorphous once adsorbed in 2D), conformationally chiral adsorbates (molecules that are energetically stable in achiral forms but with energetically accessible chiral conformations) and achiral adsorbates (neither chiral nor prochiral). Focusing on studies of enantiomer mixtures sheds light on homochiral and heterochiral enantiomer interactions that lead to the formation of conglomerate or racemate domains (or clusters) on surfaces.

This review has multiple objectives. It will assess the current state of knowledge on the packing of the aforementioned types of adsorbates in 2D. It will assess whether there is a tendency for preferential aggregation into homochiral or heterochiral structures. It will also serve as a database for benchmarking of efforts to model and predict chiral aggregation on surfaces. To limit the scope of this review, specific classes of adsorbate systems have not been included because they have been reviewed by others or fall outside our scope of interest. Such systems include: enantiopure adsorbates, studies performed at air–water interfaces, studies that induce chirality *via* seed molecules or external fields,[61] chirality of liquid-crystals in 3D and 2D,[137] studies of chirality in 3D or in 1D,[138] and studies based purely on simulation or modeling. Also, in the sections that include surveys of conformationally chiral and achiral adsorbates (Sections 7 and 8), the only studies included are those in which the authors have explicitly focused on the chirality of the overlayer formed by these adsorbates.

Our survey of the literature on mixtures of chiral adsorbates includes 154 unique adsorbate–surface systems in which chiral aggregation has been studied experimentally. In the next section, we discuss the categorization of adsorbate–surface systems based on the origin of their chirality. It must be noted that for molecules on surfaces, chirality can be expressed at multiple levels from molecular to cluster to lattice level chirality. We have attempted to develop a generic approach to classifying the origins of chirality in order to encompass all possible examples of chiral aggregation observed in these systems.

Before discussing classification, it is important to clarify the terminology that we use to describe chirality. Traditionally, the terms conglomerate and racemate have been used to describe crystals that result from crystallization of racemic mixtures in 3D. Conglomerates are physical mixtures of crystals that are themselves enantiomerically pure. Racemates are crystals in which each unit cell contains both enantiomers in equal numbers. Many researchers discussing surface chirality have used the terms racemate and heterochiral interchangeably and the terms conglomerate and homochiral interchangeably. To avoid confusion especially when discussing chirality at multiple levels in this review, we will use the terms homochiral and heterochiral with a prefix indicating the level of chirality: molecular-, cluster- or lattice-level.

3.2 Classification of adsorbate chirality on surfaces

A number of authors have attempted to classify chiral organization of adsorbates on surfaces.[56,62–64,125] Some have divided surface chirality into point-, organizational-, conformational- and prochirality.[62–64] Point chirality refers to chirality arising due to asymmetric registration of the adsorbate with the substrate lattice. Organizational chirality arises from the structures of clusters formed by aggregation of adsorbed molecules. Prochirality is an intrinsic property of achiral molecules that assume non-superimposable mirror-image adsorbate configurations that we refer to as surface enantiomers.

Another classification scheme relies on the use of plane symmetry groups. In 3D, there are 32 point groups and 230 space groups.[64] However, due to a reduction in the number of available symmetry elements on going from 3D to 2D, only 17 plane groups are available in 2D. Of these, only 5 are chiral and exist in two enantiomorphous forms. The survey by Matzger *et al.* focused on molecules with long-alkyl chains adsorbed on HOPG and categorized each of those adsorbate–surface systems into one of the 17 2D plane groups. Matzger *et al.* found that approximately 70–80% of those systems belong to the 5 chiral plane groups.[125]

It is important to note that considering chirality of monolayers adsorbed on surfaces is not exactly the same as 2D chirality. The surface adds a third dimension and breaks the mirror symmetry parallel to the 2D plane.

3.2.1 Classifying adsorbates. In this work, we have divided all the adsorbate–surface systems reviewed into four sections depending on the type of adsorbate studied: chiral (Ch),

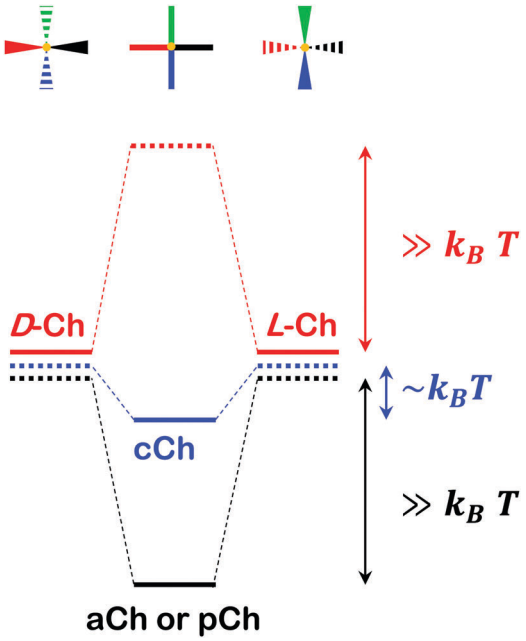

Fig. 4 The energetic relationships between stereoisomeric molecular conformations. The diagrams at the top show a tetrahedral chiral enantiomer, an achiral configuration of the same bonds and the opposite enantiomer of the original chiral configuration. Achiral (aCh) and prochiral (pCh) molecules are energetically stable with respect to chiral conformations of the same bonds. Chiral (D-Ch and L-Ch) molecules are energetically stable with respect to achiral conformations of the same bonds. The chiral and achiral conformations of conformationally chiral (cCh) molecules have energies differing by a few k_BT and interconvert rapidly, if the barriers between conformations are low.

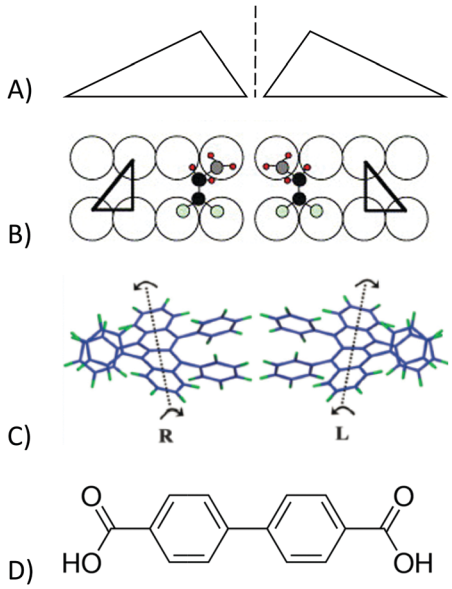

Fig. 5 (A) A scalene triangle in 3D can be superimposed on its mirror image by a half-rotation out of its plane. This rotation operation does not exist when constrained to 2D. (B) The two enantiomorphous configurations adopted by prochiral Gly (NH_2CH_2COOH) adsorbed on the Cu(110) surface. The orientation of the $-NH_2$ group with respect to the C–C bond renders the mirror images non-superimposable. Reprinted from ref. 131 Copyright 2005, with permission from Elsevier. (C) Conformationally chiral rubrene which can adopt chiral configurations in 3D, shown as *R* and L but has a low racemization barrier which prevents isolation of the enantiopure pure enantiomers. Reproduced from ref. 332 with permission from the PCCP Owner Societies. (D) Biphenyl-4,4′-dicarboxylic acid, example of an achiral molecule in 3D which is not chiral even after it adsorbs in 2D because it adsorbs with a mirror plane perpendicular to the surface.

prochiral (pCh), conformationally chiral (cCh) or achiral (aCh). The differences between these types of molecules are illustrated using the energy level diagram shown in Fig. 4.

(a) Chiral adsorbates (Ch) – molecules whose stable structures in 3D are intrinsically chiral; *i.e.* they lack mirror and inversion symmetry and rotation of the mirror image cannot superimpose it on the original molecule. Also, as shown in Fig. 4, chiral molecules typically have very high barriers to racemization ($\gg k_BT$).[139,140] For our purposes, any molecule that can be isolated in enantiopure form at ambient temperature and does not racemize on experimental timescales has been categorized as chiral. This is an important distinction because, as we will later see, molecules such as rubrene can be chiral in 3D but not easily resolvable into their enantiopure forms at ambient conditions. This review only includes studies in which mixtures of such enantiomers have been adsorbed on surfaces. Those studies in which only one enantiomer has been deposited on a surface are not relevant to the purposes of this review.

(b) Prochiral adsorbates (pCh) – this group encompasses molecules that are achiral in 3D but prochiral in the sense that adsorption renders them chiral. Such molecules have mirror images which can be superimposed on an R^{n+1} Euclidean plane through a half-turn about the mirror plane but are not be allowed the same operation on an R^n Euclidean plane.[141] For example, as shown in Fig. 5A, a scalene triangle (example adapted from Mislow *et al.*) can be superimposed on its mirror image by a half-turn in 3D (R^3) but when confined to 2D (R^2), the mirror images are non-superimposable. Thus, prochiral adsorbates include molecules that have only one mirror plane in 3D. They adopt chiral configurations simply by being constrained to 2D by adsorption onto a featureless surface such that the molecular mirror plane is not oriented perpendicular to the surface. Although prochiral molecules with non-superimposable adsorbate configurations are not molecular enantiomers, we refer to them as surface enantiomers. For example, the amino acid glycine (Gly) is prochiral and adopts two enantiomorphous conformations once adsorbed in 2D (shown in Fig. 5B). It adsorbs such that its mirror plane (in the gas phase) is tilted away from the surface normal and thus, is not a symmetry element of the adsorbate–surface system.

(c) Conformationally chiral (cCh) adsorbates – cCh adsorbates have chiral and achiral conformations in close energetic proximity to one another. In 3D, conformationally chiral molecules racemize rapidly. However, when adsorbed in 2D, they can adopt stable chiral conformations that can be visually observed using STM, as has been reported by various authors.[139,140] The adsorbates categorized in this section typically cannot be isolated in enantiopure form at ambient temperature. Examples of cCh molecules include rubrene[142,143] and dendrimer molecules.[144]

(d) Achiral adsorbates (aCh) – this group includes adsorbates that are achiral in 3D but not prochiral in the sense that simply constraining them to a featureless 2D plane does not render them chiral. These are atoms or linear molecules that have an infinite number of mirror planes and cannot avoid adsorption such that a mirror plane is perpendicular to the surface. While these adsorbates do not form surface enantiomers, their interactions with one another in clusters or their interaction in isolation with the structure of the surface can break mirror symmetry and result in the formation of chiral assemblies. An example is shown in Fig. 5D of the molecule biphenyl-4,4′-dicarboxylic acid which is an achiral molecule in 3D and assumes a flat non-chiral conformation when adsorbed on Au(111) in 2D due to interaction of the π electrons with the surface.[145] Other examples of achiral molecules include atoms/molecules which can adsorb onto an achiral surface in low symmetry sites that break the mirror symmetry of the surface.

In this review, studies involving the four types of adsorbates on both L–S and G–S interfaces have been included. Our search found only one example of an adsorbate–surface system that has been probed at both L–S and G–S interfaces; prochiral methylacetoacetate/Ni(111).[146–148] This system exhibits differences in surface chemistry at L–S *versus* G–S interfaces. However, the lack of any other such studies makes it impossible to conclude generally that the chirality of a given adsorbate–surface system is influenced by the ambient phase.

3.2.2 Classifying the chirality of adsorbate overlayers. The adsorbate–surface systems formed by chiral, prochiral, conformationally chiral and achiral adsorbates have been categorized in the following sections based on the type of chirality expressed. The formation of chiral structures by adsorption of atoms or molecules onto surfaces is quite common. Obviously, when a rigid chiral molecule is adsorbed on a surface, the resulting adsorbate–surface complex is chiral. The lack of mirror symmetry in the rigid adsorbate, breaks any pre-existing mirror symmetry of the substrate. Note that, in principle, the interaction with the surface could distort a flexible chiral molecule into a conformation that is achiral or distort an achiral molecule into an adsorbate that is chiral. What is not so obvious is that even the adsorption of isolated atoms onto surfaces can result in the formation of chiral complexes that break the symmetry of the surface. Herein, we will summarize some of the sources of chirality generated during adsorption of isolated atoms, molecules (chiral, prochiral, conformationally chiral and achiral), clusters and periodic 2D overlayers onto surfaces with various types of symmetry. This discussion serves as the basis for classifying the chirality observed in each system at three different levels: molecular-chirality, cluster-chirality and lattice-chirality. This expands on previous discussions by Bombis *et al.* and by Raval *et al.* and provides a framework for considering the formation of homochiral and heterochiral clusters and overlayers as discussed throughout the rest of this review.[62–64]

Initially, we discuss the origins of chirality in isolated species adsorbed on surfaces. The first group of adsorbates includes molecules that are chiral, prochiral or conformationally chiral in the gas phase. Note that conformationally chiral molecules can adopt conformations that are chiral or prochiral, in spite of the fact that their stable conformations are achiral. Chiral adsorbates arise from molecular structures that are chiral in the gas phases or from prochiral structures adsorbing such that no mirror planes are oriented normal to the surface. These species are denoted σ_v^0 (zero vertical mirror planes) and exist as two enantiomers (red L and blue ⅃ in Fig. 6A) on the surface. The dashed line between the two indicates their enantiomorphous relationship. The second group includes those molecules whose adsorbed structures have a finite number of mirror symmetry planes vertical to the surface when projected onto a structureless surface; imagine H_2 oriented parallel to the surface. These species are denoted σ_v^n, indicating the existence of *n* vertical mirror planes and they are achiral adsorbates (green | in Fig. 6A). The third group of adsorbates includes those species whose projected structures on the structureless surface have an infinite number of mirror planes

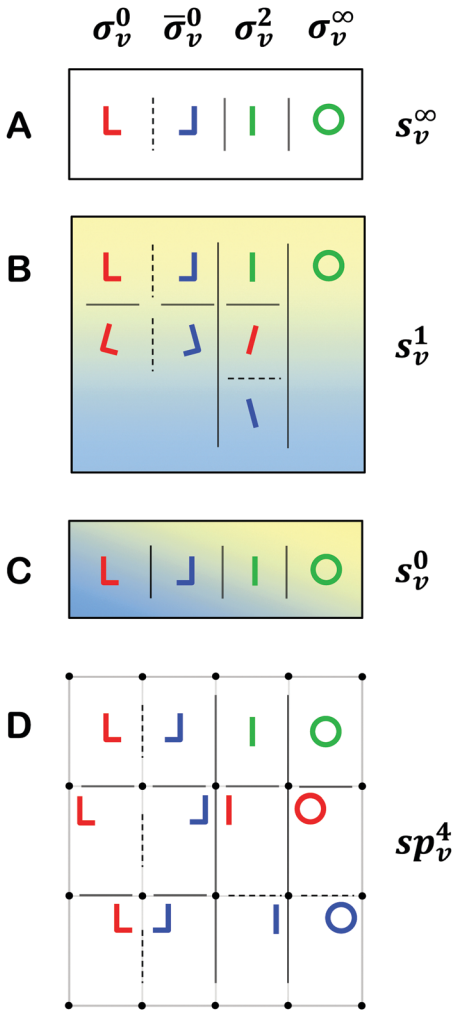

Fig. 6 Schematic representation of the adsorption of species with varying degrees of mirror symmetry (σ_v^0, σ_v^n, σ_v^∞) on surfaces with various combinations of symmetry: (A) s_v^∞, (B) s_v^1, (C) s_v^0, and (D) sp_v^4 as defined in the text. Species separate by solid lines are inequivalent. Those separated by dashed lines are enantiomers. Blue and red symbols represent the two enantiomers of chiral adsorbed species while green symbols represent achiral species.

normal to the surface; imagine an atom or H_2 oriented vertically. These are denoted σ_v^∞ (green ○ in Fig. 6A) and they are achiral on a structureless surface.

Four types of surfaces will be considered in this discussion (Fig. 6A–D). The first is a structureless plane (Fig. 6A) with an infinite number of vertical mirror planes, and denoted s_v^∞. This might be an accurate model for a liquid surface. The second has one or more, n, vertical mirror symmetry planes, s_v^n, but no other features (Fig. 6B). The third is structureless and has no mirror symmetry, s_v^0, (Fig. 6C). Finally, we consider a surface which has structure in the form of periodicity, combined with symmetry elements in the form of mirror planes, sp_v^n, (Fig. 6D). This would be representative of an achiral single crystal surface. Note that one could also consider periodic surfaces without mirror symmetry, sp_v^0; these are naturally chiral.[68] We do not include them here because they are not found among the surfaces considered in this review.

3.2.2.1 Chirality at the molecular level. On a featureless plane, s_v^∞, chirality can only arise from the adsorption of molecules that are chiral in the gas phase or those that are prochiral in the sense that adsorption breaks the mirror symmetry of the gas phase species. Prochiral molecules experience adsorption-induced chirality. Similarly, conformationally chiral molecules can adopt chiral conformations in the adsorbed state. Fig. 6A illustrates these possibilities using a structure with an L-shape that is planar and achiral in the gas phase, but whose adsorption results in two enantiomers, σ_v^0 and $\bar{\sigma}_v^0$, that cannot be superimposed by any proper 2D symmetry operations that restrict the molecule to the 2D plane; *i.e.* no flipping it over. The only real difference between enantiomers formed by adsorption of chiral and prochiral molecules is that prochiral molecules can invert their chirality by flipping. This is consequential, because the only means of forming molecularly homochiral domains of chiral adsorbates is by homochiral aggregation through diffusion across the surface. In contrast, prochiral adsorbates can form molecularly homochiral domains by chirality inversion through flipping over on the surface; without the need for lateral diffusion. For the adsorption of chiral or prochiral species, σ_v^0, on an s_v^∞ surface, rotation of either enantiomer through any angle about the surface normal yields equivalent species having the chirality of the original species. The species σ_v^n and σ_v^∞ are achiral on s_v^∞ surfaces because they have mirror symmetry planes normal to the surface.

The presence of mirror planes in the surface structure creates a directionality that will impart chirality to adsorbed species whose mirror symmetry planes are not aligned with those of the surface. A single vertical mirror plane is indicated in Fig. 6B by the vertical color gradient of the surface. The two enantiomers of the chiral σ_v^0 species are still related by mirror symmetry through the vertical mirror plane of the surface. Note, however, that rotation of either species renders it inequivalent to its original configuration (Fig. 6B). In Fig. 6, enantiomorphs are separated by dashed black lines while inequivalent species are separate by solid black lines. Species with a finite number of mirror planes, σ_v^n, remain achiral, if one of those mirror planes is coplanar with the surface mirror plane (Fig. 6B, first row). However, rotation such that the adsorbate and surface mirror planes are no longer aligned results in orientational chirality (Fig. 6B, rows 2 and 3). Rotation of σ_v^n species by equal angles in opposite directions results in the formation of enantiomorphs. Not surprisingly, the molecule with σ_v^∞ experiences no symmetry breaking as a result of rotation about the surface normal.

If a surface lacks mirror symmetry (Fig. 6C), then it is intrinsically chiral; *i.e.* it is not superimposable on its mirror image and can adopt two enantiomorphous forms, s_v^0 and $\bar{s}_v^0$.[68,69] We attempt to illustrate this with the tilted color gradient in Fig. 6C. The consequence for chiral enantiomorphs σ_v^0 and $\bar{\sigma}_v^0$ adsorbed on one of the two surface enantiomers is that they are no longer equivalent, $\sigma_v^0/s_v^0 \neq \bar{\sigma}_v^0/s_v^0$, as indicated by the solid black line. The adsorbate/surface complexes exhibit diastereomerism, $\sigma_v^0/s_v^0 \equiv \bar{\sigma}_v^0/\bar{s}_v^0 \neq \sigma_v^0/\bar{s}_v^0 \equiv \bar{\sigma}_v^0/s_v^0$, because there are two sources of chirality, the adsorbate and the surface. This is analogous to the case of an organic compound such as TA that has two chiral centers; *R*,*R*-TA ≡ *S*,*S*-TA ≠ *R*,*S*-TA. The inequivalence of diastereomers resulting from the adsorption of chiral species onto an intrinsically chiral surface results in the enantiodifferentiation of the properties (adsorption energetics, reaction kinetics, *etc.*) of the two molecular enantiomers.[149–151] This is the root origin of enantiospecific surface chemistry and enantioselective processes such as adsorption-based separations and asymmetric catalysis. On the other hand, the adsorption of achiral adsorbates σ_v^n and σ_v^∞ onto intrinsically chiral surfaces leaves the adsorbates achiral. Although the adsorbate–surface systems are chiral, the chirality originates with the surface. Physical properties such as the adsorption energetics of achiral adsorbates are identical on both surface enantiomers.

Finally, we consider the impact of surface periodicity on adsorbate chirality. Fig. 6D illustrates the adsorbates on a surface that is periodic, *e.g.* the single crystal surfaces typically used in the work that is reviewed herein. The surface lattice points are depicted by the black dots that are positioned at the intersections of mirror symmetry planes and could represent surface atoms. The adsorption of chiral species, σ_v^0 and $\bar{\sigma}_v^0$, imparts chirality to the surface. The different registries of the adsorbates in the unit cells renders the structures in rows 1–3 of Fig. 6D inequivalent. If the mirror planes of σ_v^n and σ_v^∞ species are aligned with mirror planes of the surface, as shown in Fig. 6D row 1, then the structures are achiral (green in our color scheme). Note that, if the σ_v^n species is rotated or oriented such that its mirror symmetry planes are not aligned any of those of the surface, it will display orientational chirality (as in Fig. 6B). The σ_v^n and σ_v^∞ species can also exhibit chirality on the periodic surface, if they are displaced laterally such that their mirror symmetry planes are no longer coincident with those of the surface (Fig. 6D, rows 2 and 3). We refer to this as registrational chirality. This is one route by which adsorption of atoms onto achiral surfaces can yield chiral surfaces. Of course, the energetics of both enantiomers of the surface structure are identical and so a chiral surface generated by adsorption of achiral species will have an equal number of both surface enantiomers.

The work reviewed herein uses adsorbates that are chiral, prochiral, conformationally chiral or achiral. In the following, a system will be categorized as being molecular-level homochiral, if the overlayer consists of domains (aggregates of adsorbates with long range order) that contain only one adsorbed enantiomorph. The system will be molecular-level heterochiral, if both enantiomers are present in each domain and in equimolar quantities.

3.2.2.2 Chirality at the cluster level. The primary objective of this review is to determine whether racemic mixtures of chiral adsorbates on surfaces tend to form overlayer structures or domains that are homochiral or heterochiral at the molecular or cluster levels. By clusters we refer to aggregates consisting of some uniform number of adsorbate species and we differentiate clusters from domains of adsorbates that have long range periodicity. Adsorption of a prochiral molecule on an achiral surface yields a racemic mixture of surface enantiomers. In contrast, chiral molecules can be adsorbed in enantiomerically pure form (most commonly studied), as racemic mixtures (less common) or as mixtures with control over their enantiomeric excess (uncommon). Probing of heterochiral adsorbate–adsorbate interactions requires the use of enantiomer mixtures. In 3D, racemic mixtures of chiral compounds crystallize into either racemates (equal numbers of both enantiomers in each unit cell) or into conglomerates (physical mixtures of enantiomerically pure crystals). Very rarely do they form RSS of enantiomers.[108,109] Because this review focusses on the enantiospecific clustering of chiral adsorbates in 2D, we have restricted ourselves to studies using racemic mixtures in which there is competition between homochiral and heterochiral interactions.

Following from the previous section we begin by considering the types of cluster structures that can be formed on structureless s_v^∞ surfaces. We try to elucidate all possible cluster types based on combinations of adsorbed monomers as identified in Fig. 7. In the figure we have limited ourselves to tetramers, but the discussion is otherwise generally true for clusters of arbitrary size.

There are seven types of chiral and achiral clusters that can be formed from racemic mixtures of chiral (including prochiral and conformationally chiral) and achiral adsorbates, three from the chiral σ_v^0 and $\bar{\sigma}_v^0$ species and four from the achiral σ_v^n and σ_v^∞ species. Fig. 7A depicts the two enantiomers of chiral clusters that are homochiral at the molecular level. It is not possible to create a molecular level homochiral cluster that is achiral. Rows B and C, depict clusters that are both heterochiral at the molecular level but chiral and achiral, respectively, at the cluster level. Rows D through G depict clusters that are achiral at the molecular level but can be either chiral or achiral at the cluster level.

The inclusion of mirror symmetry into the surface, s_v^n, can impart orientational chirality to molecules with a finite number of mirror planes, σ_v^n. As a consequence, they can exist as enantiomers on the surface and can form chiral and achiral clusters on the s_v^1 surface analogous to those formed by the

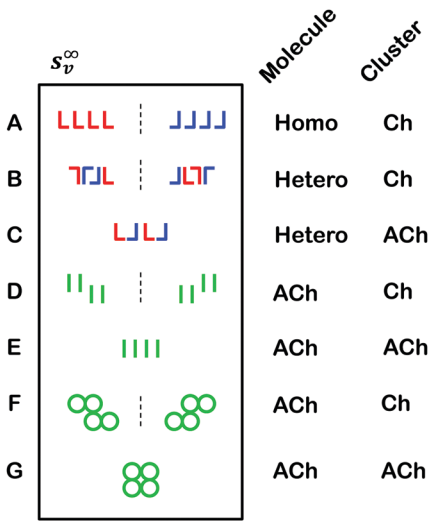

Fig. 7 The evolution of chirality from molecules into clusters on an isotropic surface. The columns to the right indicate whether the clusters are chiral and whether they are molecularly homochiral, heterochiral or achiral.

chiral σ_v^0 and $\bar{\sigma}_v^0$ species on the featureless s_v^∞ surfaces. These are illustrated in Fig. 8 rows A–C. The σ_v^∞ species remain achiral on the s_v^n surface because they are rotationally invariant. However, the presence of the surface mirror planes creates the possibility of clusters of σ_v^∞ species that are orientationally chiral as illustrated in Fig. 8 row D. The addition of periodicity to the surface as illustrated in Fig. 6D has much the same impact on cluster chirality as on molecular chirality. Clusters that are achiral can be rendered chiral by adsorption in such a way that their mirror planes are no longer coincident with those of the surface lattice. This would be registration chirality.

A system will be categorized as cluster-level homochiral, if the overlayer forms domains of single enantiomer chiral clusters such as those shown in Fig. 7 rows D and F and in Fig. 8 rows A, B and D. However, if both enantiomers of these chiral clusters are present in the same domain and with equal probability, such a system will be categorized as cluster-level heterochiral.

3.2.2.3 Chirality at the lattice level. Rather than forming isolated clusters as is typical at low coverages, many adsorbates at high coverages form adsorbate structures that are periodic,

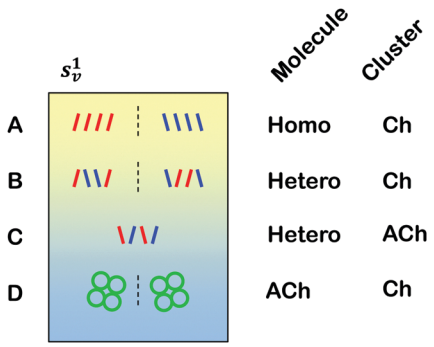

Fig. 8 Evolution of chirality from molecules to clusters on a featureless surface with one mirror vertical mirror plane.

often in registry with the surface lattice, and having structures that ideally extend across the entire surface with uniform local coverage. These are referred to as domains and the symmetry of the surface often dictates that there are several symmetry equivalent structures existing with equal probability. The periodic lattice is an array of identical unit cells with the same structure and orientation repeated with translational periodicity across the surface. The contents of the unit cell can be single atoms, single molecules, or many of each. For the purpose of this discussion, the contents of the unit cells can be considered analogous to the clusters just described in Section 3.2.2.2. These clusters can be chiral or achiral and they can be formed of homochiral, heterochiral or achiral molecular species. The key point is that the lattice can be chiral independent of contents.

Adsorbate overlayer lattices themselves can be chiral with respect to the surface lattice, independent of the chirality of their contents or basis. Fig. 9 depicts two types of lattices on a fourfold symmetric surface (lattice points indicated by black dots). Row A is a (2×2) lattice and rows B, C and D are denoted $(\sqrt{5}\times\sqrt{5})R26^\circ$ in Wood's notation.[152] We have represented the unit cell contents using the symbols ⌊, ⌋, ‖, and ◎ to imply that the contents of each unit cell can be a cluster of atoms or molecules with various symmetry properties. The unit cell contents be chiral or prochiral in the absence of the surface (⌊, ⌋). The contents can have a finite number of vertical mirror symmetry planes (‖). Lastly, the cell contents can have an infinite number of vertical mirror planes (◎). The (2×2) lattice is symmetric and its mirror planes are coincident with those of the surface. In Fig. 9A the surface is rendered chiral by the fact that the contents (basis) of each unit cell exhibits chirality and, therefore, the adsorbate layer exists in two enantiomorphous domains. Fig. 9B–D exhibit lattice chirality independent of the contents of the unit cell. Even if each unit cell contains just one atom positioned at the fourfold symmetry point of the surface lattice (Fig. 9D), the structure is chiral and exists in two enantiomorphous domains on the surface.

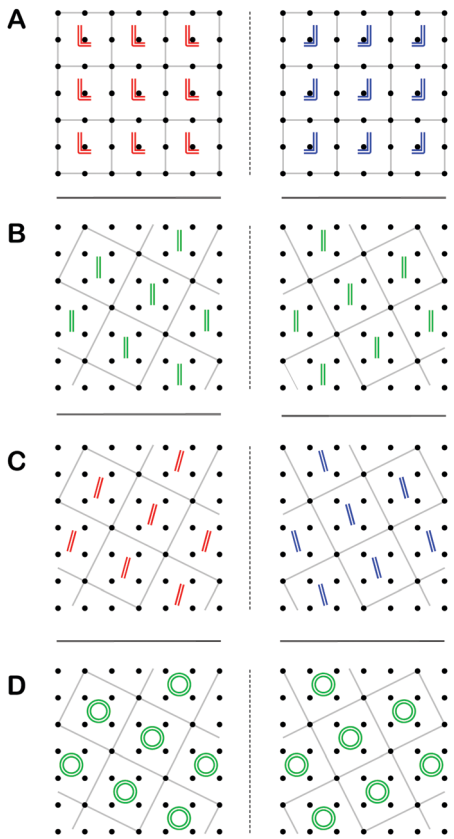

Fig. 9 Illustration of (A) $a(2 \times 2)$ and (B–D), $a(\sqrt{5} \times \sqrt{5})R26^\circ$ lattice on a fourfold symmetric substrate. The contents of the lattices are clusters of atoms or molecules that may be chiral (red and blue) or not (green) with respect to the substrate. The $(\sqrt{5} \times \sqrt{5})R26^\circ$ lattice is intrinsically chiral and creates enantiomorphous domains.

Wherever possible in this review, we indicate whether lattices with long range order are chiral or achiral. The more important issue is whether the contents of each unit cell is molecularly homochiral or heterochiral or formed of clusters that are homochiral or heterochiral.

3.2.2.4 Assigning chirality to each system. As discussed above, chirality can be expressed at multiple levels (molecular, cluster and lattice), simultaneously. Under each of the four groups of adsorbates (chiral, prochiral, conformationally chiral and achiral), we have assessed suitable published studies of adsorbed mixtures and categorized each adsorbate–surface system as homochiral or heterochiral at the molecular- and cluster-level while also indicating observations of lattice chirality. Hence, there are five possible categories and a given adsorbate–surface system can be assigned to multiple categories. Each of the four adsorbate groups (chiral, prochiral, conformationally chiral and achiral) will be discussed in a separate section below and the systems within that group have been summarized in tables at the end of each section. A few considerations associated with the categorization of adsorbate–surface systems are listed below.

– When tabulating the adsorbate–substrate systems, L–S interfaces and G–S interfaces have been tabulated separately. The numbers of observations of homochiral and heterochiral systems for studies at L–S and G–S interfaces are totaled separately. This was done to ascertain whether the ambient environment influences the tendency to form homochiral or heterochiral structures on surfaces.

– Each adsorbate–surface system has been categorized in the summary tables at the end of each section. Since one adsorbate–surface system can exhibit chirality at multiple levels, as depicted in Fig. 6–9, assignments of homochirality or heterochirality are reported only at the molecular and cluster levels.

– adsorbate–surface systems that show a transition from one type of chiral aggregation to the other (*e.g.* the coverage dependent transition of the 7[H]/Ag(100) system from homochiral to heterochiral packing at the molecular level[153]) or a coexistence of homochiral and heterochiral packing have been assigned to both categories.

– In addition to the five categories, some systems shave been categorized as 'random solid solutions' (RSS) or exhibiting a 'no organization' state of organization. The former refers to

the formation of random solid solutions of molecular or cluster enantiomers. The latter refers to no observation of any level of adsorbate organization on the surface. There are relatively fewer systems listed in these categories compared to the five categories of chiral aggregation.

– The lack of categorization at the lattice level usually means that information is unavailable or inconclusive. For example, studies restricted to low coverages at which extended domains are not observed cannot be categorized with respect to lattice level chirality.

4. Experimental methods and considerations

Our objectives require that the studies included in this review identify the phases of chiral adsorbates under conditions in which both enantiomers are present, although not necessarily as racemic mixtures. The adsorbate coverages range from low, in which case unoccupied space between adsorbates is readily observable in STM images, up to one monolayer. Unless otherwise stated, one monolayer means the saturation coverage achievable under the adsorption conditions. Very few studies determine absolute coverages in terms of molecules per unit area. For the most part, adsorbate phases have been identified using STM or LEED. By phase we mean the types of clusters formed and/or the periodicity of domains with long range order. More importantly, the studies included in this review also provide evidence for the enantiomer composition in these adsorbate phases. They must address the question of whether the phases are composed of molecules or clusters that are homochiral or heterochiral. In STM studies with sub-molecular resolution, homo- or heterochirality can be determined directly from examination of the STM images. In studies lacking sub-molecular resolution, the composition is determined based on the results of molecular simulations.

4.1 Preparation of chiral adsorbate layers

When STM is used to image chiral molecules at L–S interfaces, the chiral compound of interest is first dissolved into a non-conducting solvent and a drop of the solution is placed on the substrate of interest. The STM tip is then immersed into the drop and brought into tunneling range of the surface. In recent years, the effect of the solvent on chiral induction and self-assembly on surfaces has been studied.[154–158] There are several observations of solvent molecules co-adsorbing with the adsorbate of interest and thereby influencing the self-assembly process.[154–158] The use of solvents limits the accessible temperature range due to freezing at the low end and rapid evaporation at the high end. The use of solvent also allows tuning of surface chirality by co-adsorption of solvent in the chiral overlayer,[159,160] by inducing chirality in overlayers using chiral solvents[134,155,161] or by a variety of other means.[161,162] This ability to tune self-assembly has implications for enantioselective chemistry at interfaces.[155,156]

Chiral monolayers at G–S interfaces are commonly probed under ultra-high vacuum conditions (10^{-10} Torr). This allows direct visualization of adsorbate assembly on surfaces without the influence of solvent. One point to note about studies at G–S interfaces is that the adsorbates are typically deposited *via* sublimation onto the surface using Knudsen/effusion cells and this introduces a number of sample preparation issues. One caveat is that the sublimation temperature must be well below the decomposition temperature of the adsorbate. Sublimation of prochiral molecules will always lead to the deposition of a racemic mixture of enantiomers on the surface. However, the adsorption of a racemic mixture of chiral adsorbates can be non-trivial. For example, a simple equimolar physical mixture of two enantiomers of a chiral compound in the form of a crystalline powder can yield very different sublimation rates for the two enantiomers.[163,164]

If the two enantiomers are prepared by different routes, which is often the case, the powder morphologies can be quite different, resulting in enantiospecific differences in the net surface areas from which the enantiomers are subliming. Similarly, small deviations of the source material from a racemic composition can lead to substantial deviations in enantiomeric excess of the sublimating vapor. Sublimation of chiral compounds that form racemate crystals should yield a racemic vapor; however, experiments have shown that sublimation of enantiomer mixtures with as low as 5% ee can lead to amplification of the sublimate to ee = 10–30%.[163–167] This means that, if one wants to deposit an enantiomer mixture with a specific ee $\neq$ 0, this cannot be achieved by simply loading a sublimation source with material having that desired value of ee. Thus, we recommend sublimation of each enantiomer using separate sources whose sublimation rates can be calibrated and controlled independently.[168–171] One way of quantitatively calibrating enantiomer fluxes is to use mixtures in which one of the two enantiomers has been isotopically labelled allowing the gas phase ee to be determined using mass spectrometry. Fig. 10 shows that isotopic labeling of the L-enantiomers of amino acids such as alanine can be used to precisely calibrate the relative coverages of non-racemic adsorbed mixtures.[169] Even the fact that the source fluxes have a well-determined ee $\neq$ 0 does not mean that the adsorbed layer will have that ee. Non-linear enantiospecific effects in both adsorption sticking coefficients and in equilibrium adsorption isotherms will cause the surface ee to deviate from the gas phase ee.[172,173] This is obviously true for naturally chiral surfaces on which sticking coefficients and adsorption equilibrium constants must be enantiospecific, but is equally true for adsorption on achiral surfaces. Thus, determination of the ee of adsorbed enantiomer mixtures is both important and non-trivial.

Since the 1990's, STM has been the preferred method for study of surface chirality at both L–S and G–S interfaces.[174–176] However, other techniques such as electron diffraction have been used in several instances to probe chiral adlayers and determine the long range order of adsorbate lattices on periodic substrates. In the following section, we summarize some general considerations governing the choice of technique(s)

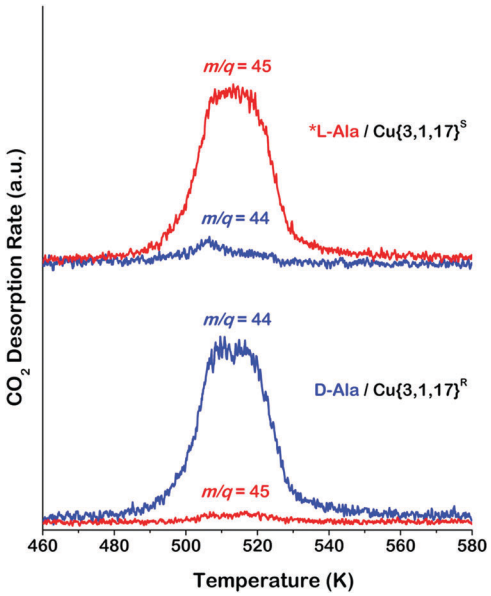

Fig. 10 TPRS of isotopically labelled L-alanine ($NH_2CH(CH_3)$*COOH) – * indicates (^{13}C) and unlabeled D-Ala on Cu(3,1,17)$^{R\&S}$. The areas under the CO_2 ($^{13}CO_2$) desorption signals at m/z = 44 and 45 for D- and L-Ala, respectively, precisely quantify the enantiomer composition. Reprinted with permission from ref. 169 Copyright 2014 American Chemical Society.

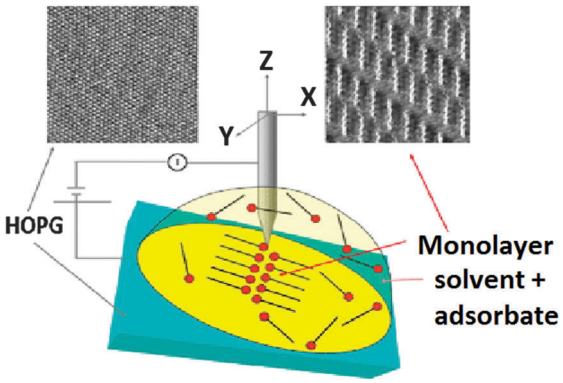

Fig. 11 Illustration of a STM experiment used to probe a monolayer on highly oriented pyrolytic graphite (HOPG) at the L–S interface using a solvent. For L–S interfaces, the adsorbate is dissolved in a non-conducting solvent. A drop of the solution is then deposited on the substrate and the surface is imaged using STM. Adapted from ref. 56 by permission of the Royal Society of Chemistry.

suitable to probe a given chiral adsorbate–surface system. We do not delve into the theory and operating principles of these techniques because they have been covered in detail by other authors.[177–179]

4.2 Scanning tunneling microscopy (STM)

At L–S interfaces, STM is the most widely applied method for study of chirality in 2D where it is used to record spatially resolved images of surfaces and adsorbed molecules. A schematic depicting STM operation at L–S interfaces is shown in Fig. 11. There are several features of the STM experiment that are of particular relevance to the study of chirality at surfaces. The first and most obvious is that, if STM is to be used to differentiate the chirality of the adsorbate, one must have sub-molecular resolution to be able to distinguish the left-enantiomer from the right-enantiomer. Not surprisingly, this is best achieved using relatively large molecules, as is reflected in the types of adsorbates used in many of the studies reviewed herein. Enantiodiscrimination of small chiral molecules such as D- and L-alanine (Ala), the smallest chiral amino acid, has not yet been achieved using STM. Relevant to molecular enantiodiscrimination using STM, it is important to point out that enantiodiscrimination of chiral adsorbates can be complicated by the fact that the tips used in STM can themselves be chiral.[180] The consequence of this is that the images of two enantiomers need not display perfect mirror symmetry with respect to one another. Another issue is that like all microscopy-based investigations, studies using STM require collection and analysis of statistically meaningful numbers of images. An additional complication is that electrons tunneling between tip and substrate have been observed to induce flipping of small prochiral adsorbates from one enantiomeric form to the other.[135] Thus, enantiodifferentiation of chiral adsorbates is non-trivial and often impossible based solely on the use of STM images.

4.3 Low energy electron diffraction (LEED)

In addition to STM, techniques such as low energy electron diffraction (LEED), reflection absorption infrared spectroscopy (RAIRS), X-ray photoelectron spectroscopy (XPS), photoelectron diffraction (PED) and near-edge extended absorption fine structure spectroscopy (NEXAFS) have been used to study the absolute chirality, bonding, long-range order and molecular orientation of chiral adsorbates at G–S interfaces.[64,181–183] Of these techniques, LEED has been used most widely to infer chiral aggregation in 2D. LEED is used at G–S interfaces under UHV conditions to determine the adsorbate unit cell structure and thus, serves to complement STM images. TA/Cu(110) was one of the first systems to be studied extensively using LEED.[70,184–186] Detecting chiral adsorbate overlayers on single crystal substrates using LEED is simply a matter of observing structures with unit cell vectors that break the mirror symmetry of the substrate. On achiral substrates such as low Miller index metal surfaces, racemic or achiral adsorbates that form chiral lattices will always form domains of both lattice enantiomorphs because they are energetically equivalent. Note that the LEED patterns generated by such chiral overlayers will appear to display mirror symmetry because they superimpose diffraction patterns from both enantiomorphous domains. It is interesting to speculate whether the chirality of adsorbate overlayers would have been noticed much earlier, if it were not for the fact that the LEED patterns superimposing both enantiomorph domains display mirror symmetry. In spite of the fact that the LEED patterns from each domain are chiral, superposition of the two yields a net LEED pattern that is achiral.

Using LEED to probe enantiomer segregation in adsorbate layers often involves comparing LEED patterns from enantiopure adsorbate layers with those from racemic adsorbate layers

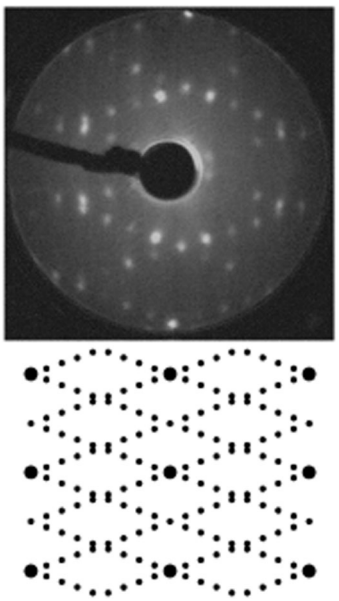

Fig. 12 Top: LEED pattern of racemic TA on Cu(110). Bottom: Schematic of the LEED pattern showing the superposition of (9 0, 1 2) and (9 0, −1 2) surface overlayers that form the LEED pattern. Adapted from ref. 186 Copyright 2005 with permission from John Wiley and Sons.

to determine whether domains are molecularly homochiral or heterochiral in composition.[187] An example of this is shown in Fig. 12 where racemic TA is deposited on Cu(110) and the diffraction pattern reveals two enantiomorphous domains on the surface. Each of these two domains corresponds to the domain formed by a monolayer of one of the two enantiomers of pure TA. This suggests that the racemic TA monolayer phase separates into domains that are enantiomerically pure or, in other words, molecular level homochiral. However, drawing conclusions from comparison of diffraction patterns of racemic and enantiopure layers is risky because they are inequivalent. In other words, if adsorption of pure enantiomers results in the formation of enantiomorphous lattices, the fact that the diffraction pattern of the racemic mixture exhibits a superposition of diffraction from both of those lattices does not mean that the adsorbed chiral species have separated in 2D into molecularly homochiral domains. For example, in the case of racemic heptahelicene/Cu(111), while the LEED pattern suggested the formation of enantiomorphous molecularly homochiral domains, STM revealed that the domains were molecularly heterochiral.[181,188]

Our survey reveals that with the advent of high-resolution STM and the increasing complexity of adsorbates, the use of LEED to detect chiral overlayers has become limited. There are also instances in which neither LEED nor STM can be used to detect enantiomer segregation due to the small size of the molecules and/or the lack of extended domains on the surface. For such instances, isotopically labelling one of the enantiomers and using TPRS can aid in precise determination of the ee of the adsorbed enantiomers which in turn, can be used to identify the tendency for homochiral or heterochiral aggregation.[170]

4.4 Computational modeling

Computational modeling and simulation methods have been used to augment or interpret many studies of chiral adsorbates.[189–194] Such modeling approaches include density functional theory (DFT), force field methods, molecular dynamics (MD) simulations and Monte Carlo methods.[195–198] DFT is often used in conjunction with STM to interpret observed images and predict adsorbate structures on surfaces.[199–202] A major challenge has been to account for enantiomer–enantiomer interactions.[59] A critical issue is that the enantiospecificity of the interaction energetics between chiral molecules and chiral surfaces or between enantiomers of chiral adsorbates is very small. These enantiospecificities are usually on the order of a few kJ mol^{-1} [104,203–207] and below the accuracy of DFT methods as applied to adsorbates on surfaces.[208] Overall, theoretical attempts fall short of capturing the full complexity of chiral aggregation and being able to predict the relative stabilities of chiral adsorbate complexes. As such, we have limited the scope of this review to experimental work and have not included studies that use computational techniques exclusively to predict enantiomer aggregation.

In the following four sections (5–8), we summarize findings for the propensity of chiral, prochiral, conformationally chiral and achiral adsorbates to aggregate into homochiral or heterochiral structures on surfaces. For each type of adsorbate, we have selected for detailed discussion a few studies whose findings are representative of common observations for that adsorbate type. After discussing those studies, a brief overview of the findings for that adsorbate type will provide an insight into their tendencies for enantiomer aggregation. This is followed by tables summarizing studies of that adsorbate type at L–S and G–S interfaces and categorizing each adsorbate–surface system as homochiral or heterochiral at the molecular and cluster level while also mentioning observations of lattice chirality. A variety of adsorbates with complex molecular structures have been mentioned in the following sections. To avoid inserting a large number of molecular structures into the text, Appendix A lists the molecular structures of all adsorbates included in this review for reference.

5. Enantiospecific aggregation of chiral adsorbates

This section discusses experimental studies of intrinsically chiral adsorbates, *i.e.* enantiomers in 3D, at L–S and G–S interfaces. It bears reiteration that only studies using enantiomer mixtures are included in this review; studies of enantiopure adsorbate layers are not directly relevant to our purpose. At L–S interfaces, the vast majority of studies use the HOPG surface, the exceptions being a few studies on Au(111) and Cu(111) surfaces.

Most studies at G–S interfaces have been performed on single crystal metal surfaces of Au and Cu. Studying the same adsorbate on Au and Cu probes the extent to which adsorbate–surface interactions affect enantiomer aggregation. One complicating feature of these surfaces is that the clean Au(111) surface undergoes reconstruction, adopting a herringbone pattern

that exposes both fcc(111)-like and hcp(111)-like regions.[209] On the other hand, clean Cu(111) remains unreconstructed. Cu is moderately reactive, allowing studies of many adsorbates at temperatures up to 450 K (in UHV) without decomposition. In recent years, Pt and Ag surfaces have also been studied to probe enantiomer aggregation.[153,172,201,210,211] In addition to the use of high symmetry, low Miller index surfaces, some studies have used naturally chiral surfaces, *i.e.* single crystal metal surfaces that are cut in low symmetry directions.[50,68,203] These surfaces expose kinked step edges that impart chirality to the surface because they are non-superimposable on their mirror images. Some naturally chiral surfaces have been shown to adsorb and decompose chiral species enantioselectively.[149,168,169,204,212,213] In addition to STM, LEED has been used to study the organization of chiral adsorbates at G–S interfaces.[181,183,186,187,214–217]

Many amphiphilic adsorbates with long alkyl chain have been studied on the HOPG surface because they form well-ordered monolayers with their aliphatic chains lying parallel to the surface.[175,176,218–221] HOPG is a convenient material for study because it is chemically inert and, therefore, it is easy to maintain clean surfaces that do not react with adsorbed species. Furthermore, HOPG is electrically conducting and amenable to imaging using STM. On Au and Cu surfaces, chiral adsorbates with aromatic rings and thiol end groups that interact with metal surfaces have been studied extensively.[222–224] Unlike L–S interfaces at which the use of solvent allows study of a wide variety of adsorbates, G–S interfaces are somewhat restricted in terms of adsorbates because they must be amenable to vapor deposition. As a result, some chiral adsorbates such as helicenes, amino acids and various 1,4-C_4-diacids have been studied with disproportionately high frequency at G–S interfaces. TA was one of the earliest molecules whose racemic mixtures were investigated at G–S interfaces.[60,225] The interest in TA arises from the fact that Ni and Cu surfaces modified by enantiomerically pure TA catalyze the enantioselective hydrogenation of methylacetoacetate with ee $\cong$ 90%.[226,227] Helicenes have been studied because of their emerging applications in fields such as molecular switches, non-linear optics, and chemo-sensing and are attractive experimentally because their large size allows easy determination of their absolute chirality when adsorbed on surfaces.[181,182,228,229] Amino acids also serve as a convenient choice for study of chiral surface chemistry because enantiomerically pure isotopomers of amino acids are readily available, thereby allowing use of mass spectrometry for quantitative enantiodiscrimination of species desorbing from a surface.[149] Also, given that there are many natural and non-natural α-amino acids, the influence of different chemical substituents on chiral packing can be studied when amino acids are used as adsorbates.[212,230,231] The molecular structures of the chiral adsorbates reviewed in this section are summarized in Table 6 in the appendix.

To probe L–S interfaces, STM has been the overwhelmingly popular choice for determining chiral packing of adsorbates. In many instances, the use of STM has been supplemented with other tools or methods. DFT and MD simulations have been used in conjunction with STM by many authors to determine overlayer structure.[218,220,232,233]

The papers selected for detailed discussion under this section on chiral adsorbates include two studies of helicenes using STM (one each at L–S and G–S interfaces), one study of an adsorbate containing a long alkyl chain adsorbed on HOPG and another one that utilizes a novel isotopic labelling technique to probe aggregation of aspartic acid enantiomers on Cu(111) in UHV. These examples serve to illustrate the complexity of enantiomer aggregation and assembly.

5.1 5-Amino-hexahelicene/Au(111) at L–S interface

Helicenes are a class of chiral molecules that have been studied on surfaces extensively because of their applications as helical ligands in asymmetric synthesis, as molecular switches and in dye synthesis.[229,234,235] Balandina *et al.* have use STM to study both enantiopure and racemic mixtures of 5-amino-hexahelicene (A[6]H, Fig. 13) adsorbed on Au(111) from 1,2,4-trichlorobenzene solution.[223] The enantiomers of A[6]H have helical shapes and are denoted *M*- and *P*-A[6]H respectively. The amine group removes the C_2 symmetry of the gas phase molecules and increases the adsorption energy of A[6]H over that of hexahelicene ([6]H) due to the interaction of the amine group with Au.

On deposition of racemic A[6]H on Au(111), two enantiomorphous domains consisting of trimers possessing p3 symmetry (Fig. 14) were observed. To determine the chirality of

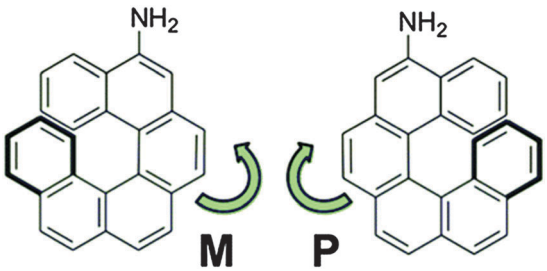

Fig. 13 Molecular structures of *M*- and *P*-5-amino-hexahelicene (A[6]H), with opposite directions of helicity from the highest ring (in bold) to the lowest ring. Adapted from ref. 223 by permission of the Royal Society of Chemistry.

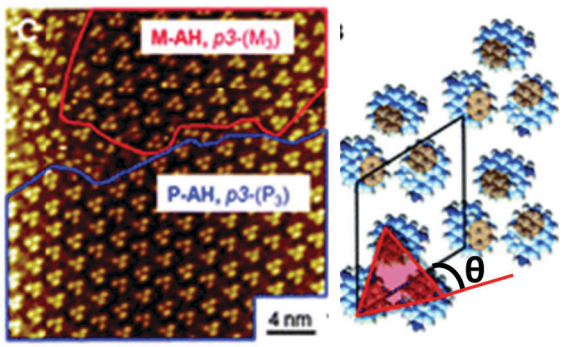

Fig. 14 Left: STM image showing enantiopure p3 domains formed by racemic A[6]H/Au(111). In the p3 domain, three molecules of A[6]H form a molecularly homochiral trimer which is repeated across the domain. Right: Schematic showing the arrangement of A[6]H molecules in trimers forming the p3 domain. The brown rings on each molecule indicates the highest part of the A[6]H molecule. Adapted from ref. 223 by permission of the Royal Society of Chemistry.

the A[6]H in the p3 domains, STM images of enantiopure *M*- and *P*-A[6]H on Au(111) were obtained. From those STM images, the angle θ (angle between the unit cell and the trimer) shown in the right panel of Fig. 14 was measured. The value of θ was found to be opposite for enantiopure *M*- and *P*-A[6]H on Au(111). Then, the angle θ was measured from the STM image of racemic A[6]H in the left panel of Fig. 14. By comparing the values for racemic A[6]H to those obtained for enantiopure *M*- and *P*-A[6]H on Au(111), it was found that the two p3 domains of the racemic A[6]H layer corresponded to enantiopure *M*- and *P*-A[6]H domains on the surface. Thus, by comparing STM images of enantiopure *vs.* racemic A[6]H, it was determined that racemic A[6]H forms molecularly homochiral domains on the surface.

From the STM images in Fig. 14, it can be seen that homochirality is expressed at the cluster-level. *M*- and *P*-A[6]H form trimers which are mirror images of each other, with the angle between the unit cell and the trimer (shown as θ in Fig. 14) being opposite for *M*- and *P*-A[6]H. At the lattice level, while the orientation of the trimers with respect to the high symmetry directions of the Au(111) substrate has not been indicated, it can be seen in the left panel of Fig. 14 that the two p3 domains have opposite angles θ between the unit cell and the trimer and thus, the domains are mirror images of each other.

Adsorption of racemic A[6]H/Au(111) is complicated by the formation of two phases on the surface. In addition to the two enantiomorphous p3 trimer domains, adsorption of racemic A[6]H/Au(111) results in the formation of domains with p6 symmetry as shown in Fig. 15. Roughly 62% of the domains are p3-type and 32% are p6-type. The p6 domain is a complex structure exhibiting supramolecular assembly at multiple levels as shown in the right panel of Fig. 15. At the lowest level, the p6 domain is comprised of A[6]H dimers that are believed to be molecularly heterochiral. Three of these dimers form a hexamer. The hexamers are chiral and exist homochirally in the p6 phase. At the highest level, pairs of these hexamers (total of 12 A[6]H molecules) assemble into the unit cells of a supramolecular hexagonal structure with p6 symmetry. As mentioned earlier, since it is not possible to ascertain the absolute chirality of individual A[6]H molecules, it cannot be concluded with certainty whether the p6 phase is homo- or hetero-chiral at the molecular level. The authors hypothesize that, if the p6 phase were molecularly homochiral, it would have been observed when enantiopure *M*- or *P*-A[6]H was deposited on Au(111) and, therefore, that the p6 phase formed by racemic A[6]H is molecularly heterochiral.

The coexistence of p3 and p6 domains for racemic A[6]H/Au(111) may result from kinetic barriers that hinder surface diffusion of A[6]H preventing the formation of the thermodynamically stable homochiral p3 domains. The evidence for kinetic trapping comes from the observation that on deposition of the racemic A[6]H–solvent mixture on Au(111) at ambient temperature, disordered regions are observed on the surface (top left corner of left panel in Fig. 15) hours after deposition. Alternatively, the presence of both p3 and p6 phases could be indicative of a thermodynamically stable two-phase system. However, since the local coverage of the molecularly homochiral p3 domain (0.72 molecules per nm^2) is higher than that of heterochiral p6 domain ($\sim$0.6 molecules per nm^2) and the DFT-calculated stabilization energy of homochiral A[6]H dimers is greater than that of heterochiral A[6]H dimers by $\sim$1.6 kcal mol^{-1}, it is suggested that molecularly homochiral domains are more stable than heterochiral domains.

In summary, domains with two different types of symmetry, p3 and p6 were observed on the racemic A[6]H/Au(111) surface. The p3 domains form molecularly homochiral trimers that, in turn exhibit cluster and lattice chirality. The molecular level chirality of the p6 domains cannot be determined with certainty although the authors suggest that they are heterochiral. A[6]H/Au(111) is an example of an adsorbate–surface system in which molecularly homochiral and heterochiral domains coexist on adsorption of a racemic mixture.

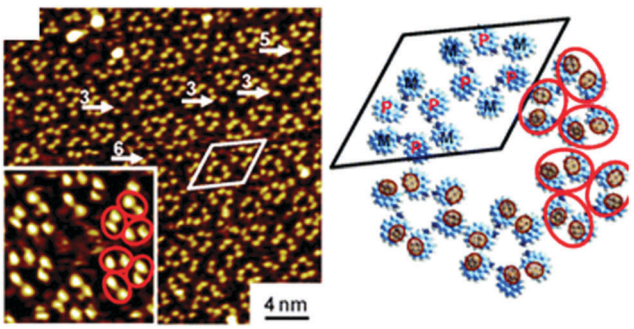

Fig. 15 Left: STM image of the molecularly heterochiral p6 domain that coexists with homochiral p3 domains of *M*- and *P*-A[6]H observed for the racemic A[6]H/Au(111) system. Right: Graphic of a hexagonal unit cell forming the p6 domain. Chirality is expressed at each level in this p6 domain, from the molecularly heterochiral dimers that assemble into hexamers which assemble as a supramolecular hexagonal structure, whose pores are chiral. The numbers in white on the left panel refer to the number of A[6]H molecules that can be accommodated in these pores. Adapted from ref. 223 by permission of the Royal Society of Chemistry.

5.2 MHPOBC/HOPG at L–S interface

This subsection describes an adsorbate–surface system exhibiting a transition from molecular heterochirality to homochirality as the ee of the adsorbed enantiomer mixture is varied.[220] The adsorbate, 4-[(1-methylheptyloxy)carbonyl]phenyl 4-octyloxy-4-biphenyl carboxylate (MHPOBC, Fig. 16) was dissolved in 1-octanol (7×10^{-3} M) and deposited on HOPG. Enantiopure MHPOBC deposited on HOPG forms an overlayer of MHPOBC molecules aligned along their long axes as shown in the bottom left and right panels of Fig. 16 (unit cell a = 2.2 nm; b = 2.6 nm). The overlayer is formed of very large domains with a local coverage of 0.352 molecules per nm^2 separated by large regions of uncovered HOPG. The submolecular resolution of the STM images allows the chirality of the adsorbed MHPOBC to be distinguished based on the orientations of the alkoxy chains relative to the polyphenyl core. The orientations suggest that the chiral methyl groups on the 1-methylheptyloxy chains are oriented away from the surface. However, there is one caveat to

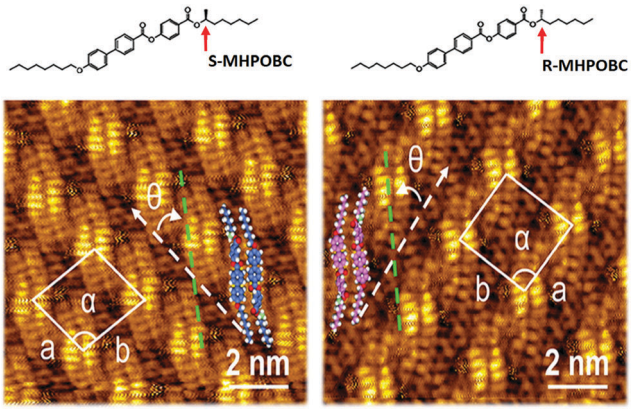

Fig. 16 Top: Molecular structures of *S*- and *R*-MHPOBC. The chiral center (red arrow) is formed by the methyl group on the 1-methylheptyloxy chain. Bottom: STM images of *S*- and *R*-MHPOBC monolayers on HOPG. The adsorbate molecular structure has been overlaid onto the image. The methyl groups (green) on the chiral center are marked with arrows. The molecular axis of the adsorbates and the unit cell vector form an angle θ. Adapted with permission from ref. 220 Copyright (2016) American Chemical Society.

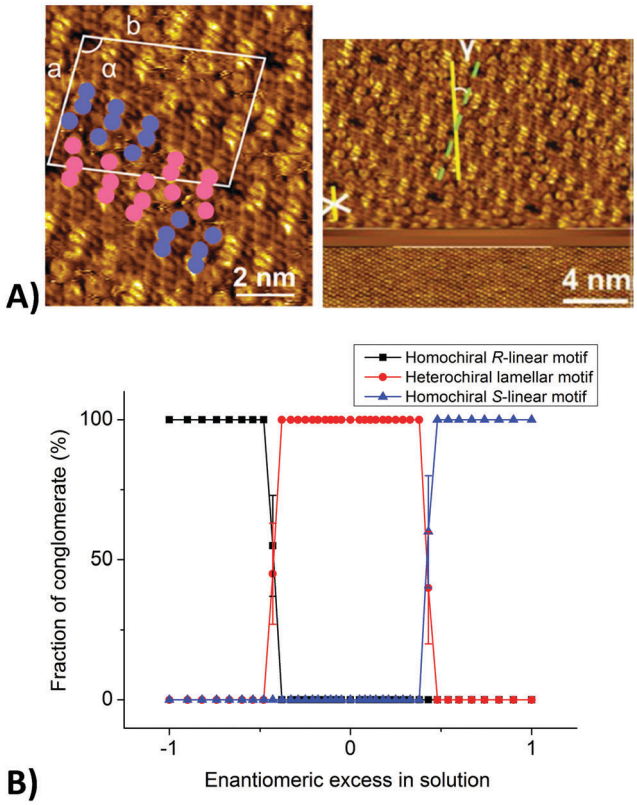

Fig. 17 (A) Left: STM of the two enantiomers of MHPOBC (blue and pink) arranged in a unit cell containing 10 molecules. The two joint bright dots represent the biphenyl ring of one molecule and the disjoined dot (of the same color) represents the phenyl ring separated by the ester group. Right: Composite STM image showing the racemic adlayer (top) making an angle of 22° with the HOPG substrate (imaged at bottom) with the yellow line indicating a HOPG lattice direction. (B) Plot showing how varying the ee_{sol} of the *R*- and *S*-MHPOBC mixture in solution affects the packing arrangement on the HOPG surface. For $-43\% < ee_{sol} < 43\%$, the overlayer adopts the lattice of the molecularly heterochiral overlayer shown in part (A) while for $|ee_{sol}| > 43\%$, the overlayer adopts the lattices of enantiopure MHPOBC on HOPG (Fig. 15). Adapted with permission from ref. 220 Copyright (2016) American Chemical Society.

the assignment of the chirality of MHPOBC based on STM images. The assignment of the molecular chirality of adsorbed MHPOBC is based on the assumption that the methyl group on the chiral center is oriented away from the surface. Flipping one enantiomer over would make it indistinguishable from the other. Having the methyl group oriented towards the surface would probably create an energy penalty but it is likely to be quite small relative to the molecular adsorption energy and intermolecular interactions. As a point of comparison, the structures of D- and L-alanine on $Cu(3,1,17)^S$ modeled using DFT calculations differ only in the orientation of the methyl group relative to the surface. D-Alanine with its methyl group point towards the $Cu(3,1,17)^S$ surface is only destabilized relative to L-alanine by 1 kJ mol^{-1}.[169]

When racemic MHPOBC (ee = 0) is deposited on HOPG, instead of observing two separate enantiopure domains, a single overlayer structure with a local coverage of 0.357 molecules per nm^2 is observed as shown in Fig. 17A (unit cell a = 4.5 nm; b = 6.3 nm). As assigned by the authors, both MHPOBC enantiomers are present in the same unit cell. The periodic unit cell contains 10 molecules, five of each enantiomer, hence, the overlayer of the racemic mixture is molecularly heterochiral at a surface enantiomeric excess of ee_s = 0. The overlayer unit cell vector makes an angle of 22° with the high-symmetry direction of the HOPG substrate shown in Fig. 17A, thus exhibiting lattice chirality. Substitution of the chiral methyl group in MHPOBC with a hydrogen atom renders the adsorbate prochiral. Its adsorption on HOPG results in an overlayer structure similar to that in Fig. 17A but with 12 molecules per unit cell. These are clearly molecularly heterochiral surface enantiomers.

The effect of varying the ee_{sol} of the MHPOBC solution on the structure of the HPOBC/HOPG monolayer was investigated by analyzing over 200 STM images obtained at ~40 different values of the solution phase ee_{sol}. When the HOPG was exposed to MHPOBC mixtures with $-43\% < ee_{sol} < 43\%$, the heterochiral 4.5 nm × 6.3 nm unit cell overlayer (Fig. 17A), was observed. However, when the MHPOBC solution exceeds $|ee_{sol}| > 43\%$, there is a sharp transition to the homochiral 2.2 nm × 2.6 nm unit cell overlayer seen in Fig. 16, suggesting that a molecularly homochiral phase is formed, as observed for the enantiopure MHPOBC. This transition between overlayer structures is revealed in Fig. 17B which plots the fraction of homochiral and heterochiral phases observed as a function of ee_{sol}. It is implied that the phase transition to global homochirality on the surface displaces the minority enantiomer into solution but this is neither demonstrated nor explicitly stated. The interpretation of these images relies on the assumption that the chiral methyl group on the 1-methylheptyloxy chain is always oriented away from the surface. If this were not the case, simply flipping the *R*-MHPOBC over would give it the same apparent footprint as *S*-MHPOBC and one could not quantify

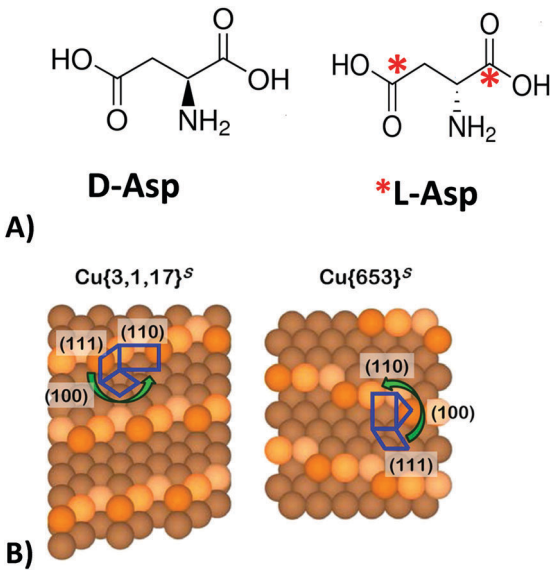

Fig. 18 (A) Molecular structures of D- and L-Asp. To distinguish between the two enantiomers, the carboxylate carbons have been isotopically labelled with ^{13}C (marked *). (B) Ball model of the naturally chiral Cu(3,1,17)^{S} and Cu(653)^{S} surfaces. The different color of the atoms along the step edges represent different coordination numbers, with the highest being of lightest color and the lowest being of darkest color. Adapted with permission from ref. 213 Copyright 2016 American Chemical Society.

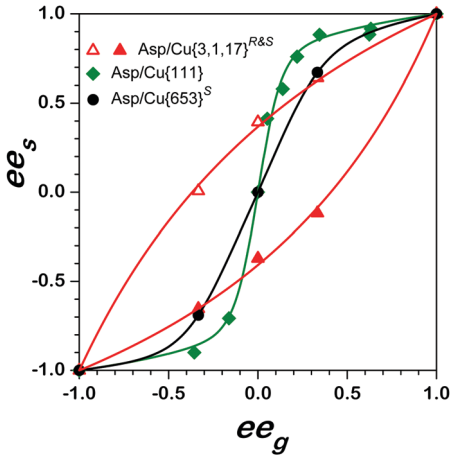

Fig. 19 Plots of ee_s *vs.* ee_g isotherms for Asp/Cu(111) (green diamonds), Asp/Cu(653)^{S} (black circles) and Asp/Cu(3,1,17)$^{R\&S}$ (red hollow and filled triangles). Cu(3,1,17)$^{R\&S}$ surfaces are chiral and show classic enantiospecific adsorption behavior without any evidence of homo/hetero-chiral aggregation. In contrast, Asp enantiomers tend to aggregate homochirally on the Cu(111) and Cu(653)^{S} surfaces. This behavior manifests itself through the slope being >1 at ee_g = 0 revealing amplification of chirality on the surface. Adapted with permission from ref. 213 Copyright 2016 American Chemical Society.

the molecular ee of the overlayer simply based on the STM images of the ordered overlayers. It is possible that an excess of one MHPOBC enantiomer on the surface is sufficient to force the long range order of the overlayer into an apparently homochiral structure with the 2.2 nm × 2.6 nm unit cell but that these unit cells contain both molecular enantiomers with the minority enantiomer flipped over to adopt the footprint of the majority enantiomer. Similarly, it is not clear that the molecular contents of the 4.5 nm × 6.3 nm unit cell remains racemic as ee_{sol} deviates from racemic.

5.3 Aspartic acid/Cu(111) at G–S interface

A novel equilibrium adsorption method using isotopically labelled enantiomers probes enantiomer interactions in amino acid (**R**-CH(NH_2)COOH) monolayers without the use of STM. Mixtures of amino acid enantiomers including alanine (Ala, **R** = CH_3), aspartic acid (Asp, **R** = CH_2COOH), serine (Ser, **R** = CH_2OH) and phenylalanine (Phe, **R** = $CH_2C_6H_5$) have been studied on several single crystal Cu surfaces using this technique.[168,171,213] Of these adsorbates, Asp (Fig. 18A) has been most widely studied using achiral Cu(111) and Cu(100) and the chiral Cu(3,1,17)$^{R\&S}$ and Cu(653)$^{R\&S}$ surfaces.[213] In this section, we will specifically discuss the Asp/Cu(111) system in which enantiomer aggregation has been studied at saturation coverage using the equilibrium adsorption method.[170]

The equilibrium adsorption method relies on discriminating between Asp enantiomers by isotopically labelling the carboxyl carbons of *L-Asp (Fig. 18A) with ^{13}C while leaving the carboxyl carbons of D-Asp unlabeled. When temperature programmed reaction spectroscopy is performed with *L- and D-Asp co-adsorbed on the surface, the decomposition of Asp leads to the desorption of $^{13}CO_2$ and CO_2 from *L-Asp and D-Asp, respectively.[149] The desorption yields of $^{13}CO_2$ and CO_2 are recorded independently using mass spectrometer signals at m/z = 45 ($^{13}CO_2$) and m/z = 44 (CO_2). The ratio of the two signals allows accurate determination of the coverage ratio of *L- and D-Asp enantiomers that are in equilibrium with any given enantiomer ratio in the gas phase. Using this technique, enantiospecific interactions of adsorbed Asp enantiomers have been studied on achiral Cu(111) and on naturally chiral Cu(3,1,17)$^{R\&S}$ and Cu(653)^{S} surfaces.[170,213]

Under equilibrium adsorption conditions, the relationship between the enantiomeric excess of Asp on the surface, ee_s, and that in the gas phase, ee_g, provides insight into the interactions between adsorbed enantiomers. Fig. 19 shows ee_s *vs.* ee_g for mixtures of D- and *L-Asp exposed to Cu(111), Cu(3,1,17)$^{R\&S}$, and Cu(653)$^{R\&S}$ surfaces at temperatures of ~450 K in the presence of gas fluxes that were sufficient to yield coverages very close to that of the saturated monolayer. Exposure of a racemic mixture, ee_g = 0, of Asp to the Cu(3,1,17)$^{R\&S}$ surfaces reveals enantiospecific adsorption, $ee_s \neq 0$, driven by the chirality of the surfaces, with a preference for adsorption of D-Asp on the Cu(3,1,17)^{R} surface. Equilibrium adsorption on Cu(111) and Cu(653)^{S}, however, reveals ee_s = 0 at ee_g = 0 and therefore, no evidence of enantiospecific adsorption. This must be the case for Cu(111) because it is achiral, however, it need not have been the case for adsorption on Cu(653)^{S}. More importantly, the data on Cu(111) and Cu(653)^{S} show that $ee_s \neq ee_g$ except when ee_g = 0 or ±1, revealing some form of enantiospecific interactions between adsorbates. These adsorption isotherms can be reproduced *via* a Langmuir-like model, which has been modified to account for homochiral/heterochiral aggregation

of enantiomers.[213] The model enables direct determination of enantiospecific adsorption equilibrium constants of homochiral/heterochiral cluster formation in two-dimensions. For the cases of D- and L-Asp adsorption on Cu(111) and Cu(653)^S, the fact that $|ee_s| > |ee_g|$ indicates that homochiral aggregation dominates over heterochiral aggregation and thus, that these systems are molecularly homochiral. Note that $|ee_s| < |ee_g|$ would have indicated a tendency towards molecular heterochirality, *i.e.* a tendency to form a racemate phase.

While the equilibrium adsorption isotherms provide insight into the enantiospecific interactions of chiral adsorbates and the tendency of enantiomer mixtures to interact homochirally or heterochirally at the molecular level, they do not provide any of the structural insight of the STM experiment. One cannot explore the formation of structures that are chiral at the cluster or lattice level using this method. However, the adsorption isotherm method allows direct insight into enantiospecific interactions at the molecular level, without the need for sub-molecular STM imaging.

5.4 Heptahelicene/Ag(100) at G–S interface

Section 5.2 discussed MHPOBC/HOPG wherein a chiral phase transition was observed as a function of varying ee_{sol}.[220] In this section, we will discuss the heptahelicene ([7]H)/Ag(100) system which exhibits a phase transition from molecularly homochiral to heterochiral packing over the coverage range 0.05–1 ML.[153] [7]H consists of seven benzene rings arranged in a helical structure. It thus exhibits helical chirality and has two enantiomers as shown in Fig. 20. Given their large size, the absolute chirality of individual [7]H molecules is easily determined using STM based on the direction of increasing brightness of the feature imaged. [7]H has been observed to form molecularly homochiral or heterochiral phases on single crystal surfaces including Ag(111), Au(111), Cu(111) and Cu(100).[188,236–238]

STM images obtained for racemic 7[H]/Ag(100) at coverages of 0.05 ML, 0.33 ML, 0.5 ML and 1.0 ML relative to saturation coverage are shown in Fig. 21. On the Ag(100) surface, homochiral tetramer clusters are observed at coverages <0.05 ML as shown in Fig. 21A. When the coverage increases above 0.05 ML, heterochiral clusters begin to form on the surface. These heterochiral clusters consist of two molecules each of *P*-[7]H and *M*-[7]H. When coverages of 0.33 and 0.5 ML are reached, only the heterochiral tetramers remain and no homochiral clusters are observed. The heterochiral tetramers shown in Fig. 21C are non-superimposable mirror images of each other, thus also exhibiting cluster-level heterochirality. Thus, in contrast to its behavior on Cu(100) and Cu(111), [7]H on Ag(100) does not form molecularly homochiral overlayers at intermediate or high coverage.[239,240]

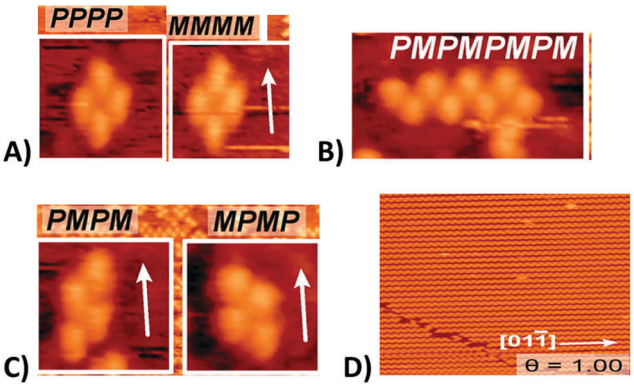

Fig. 21 STM images of racemic [7]H on Ag(100) shown for four different coverages: (A) 0.05 ML (B) 0.33 ML (C) 0.50 ML and (D) 1.0 ML. At 0.05 ML, only isolated homochiral *PPPP* and *MMMM* tetramers are observed but as the coverage increases to 0.33 ML, these homochiral tetramers disappear and heterochiral zigzag rows appear to dominate. When the coverage increases to 0.5 ML, some heterochiral tetramers appear but at saturation coverage, the heterochiral zigzag rows are long enough to form domains. Adapted from ref. 153 Copyright 2015 ACS AuthorChoice American Chemical Society.

As the racemic [7]H coverage increases past 0.5 ML tending towards saturation, the tetramers gradually arrange into zigzag rows which in turn aggregate into larger domains (Fig. 21D). Each zigzag row has *M*- and *P*-[7]H molecules arranged in the *PMPMPM* arrangement shown in Fig. 22, thus exhibiting molecular-level heterochirality. This zigzag row domain is aligned parallel to the [0,−1,−1] substrate lattice; however, an enantiomorphous domain exists with the opposite arrangement of enantiomers (Fig. 22). Hence, this overlayer exhibits lattice chirality. This zigzag row structure contains both [7]H enantiomers in each unit cell and forms a (4 0, 0 7) lattice relative to the substrate with a packing density of 0.85 molecules per nm^2. The density of this molecular-level heterochiral overlayer, is lower than the density of 0.91 molecules per nm^2 exhibited by enantiopure [7]H adsorbed on Ag(100). The fact that the stable heterochiral domain has a lower density than the enantiopure domain contradicts Wallach's rule which states that heterochiral domains (racemates) tend to be more stable because they are more dense than homochiral (conglomerate) domains.[110,111]

To investigate the origin of this apparent contradiction, the binding energies of homochiral and heterochiral clusters of *M*- and *P*-[7]H with varying cluster sizes was calculated using MD simulations. When the cluster size is >6, molecularly heterochiral clusters were found to be more stable than homochiral clusters by 0.63 kJ mol^{-1} while homochiral clusters were favored for dimers and tetramers. This inversion in stability with increasing cluster size was attributed to lattice mismatch of the homochiral clusters with the Ag(100) substrate.

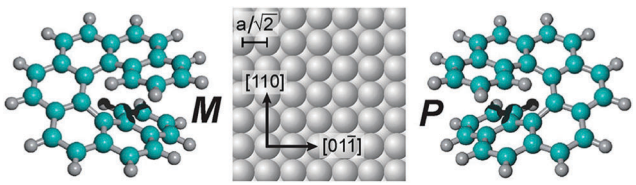

Fig. 20 Ball and stick models of the two enantiomers, *M*- and *P*-[7]H and the structure of the Ag(100) surface in the middle. [7]H consists of seven benzene rings and the direction of helicity determines the molecular handedness. Adapted from ref. 153 Copyright 2015 ACS AuthorChoice American Chemical Society.

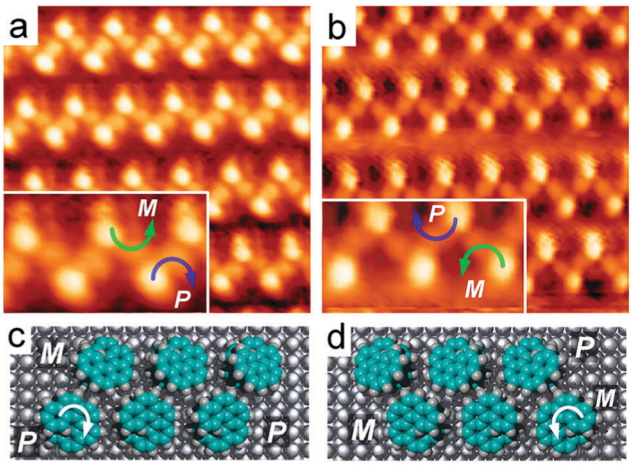

Fig. 22 STM images of zigzag rows of [7]H/Ag(100) forming domains at saturation coverage. (A and B) Two different domains formed when racemic [7]H is deposited on Ag(100). These domains are mirror images of one another, thus exhibiting lattice heterochirality while each domain contains both *M*- and *P*-[7]H and thus, is molecularly heterochiral. (C and D) Structural models of these domains showing a zigzag row that contains *M* and *P* enantiomers arranged alternately. The white arrow indicates the handedness of the molecule. Adapted from ref. 153 Copyright 2015 ACS AuthorChoice American Chemical Society.

5.5 Overview of chiral adsorbate mixtures in 2D

We conclude this section on chiral adsorbates by reviewing the numbers of entries under each of the categories (homo- or hetero-chirality at the molecular, cluster or lattice level) and highlighting studies that reveal factors influencing enantiomer aggregation on surfaces. Table 1 lists all of the adsorbate–surface systems in which mixtures of chiral adsorbates have been studied. The row at the bottom totals the numbers in each category.

Table 1 categorizes the behavior of mixtures of chiral adsorbates on various surfaces. However, for any given adsorbate–surface system, enantiomer aggregation in 2D is a function of parameters including: adsorbate coverage (θ), enantiomeric excess (ee) and temperature (T). Ideally, enantiomer aggregation and the structures formed on a surface would be fully described in the form of a phase diagram spanning (θ, ee, T). Unfortunately, no study of which we are aware comes close to providing this level of detail for any adsorbate–surface system exhibiting chirality. Most such studies are limited to a narrow range of (θ, ee, T); for example, very few explore enantiomer mixtures with ee $\neq$ 0, $\pm$1. Thus, for most systems, we do not know whether types of packing other than those listed in our tables can occur in regions of (θ, ee, T) other than those examined. Nevertheless, we have endeavored to account for all known studies and hence, our analysis adequately summarizes the current state of knowledge.

For chiral adsorbates, our literature survey found 16 unique adsorbate–surface systems studied at the L–S interface and 35 unique adsorbate–surface systems studied at the G–S interface. In many cases, individual systems are described in multiple publications. Eight of the 16 systems studied at the L–S interface use the HOPG surface while the rest use Au(111) or Cu(111). At G–S interfaces, 22 studies used Cu, 4 studies used Au surfaces and the remaining studies were conducted on Ag, Pt & TiO_2 surfaces. While the adsorbates studied at L–S interfaces are relatively large molecules such as carboxylic acids having long alkyl chains, most of the adsorbates studied at G–S interfaces are smaller and of three types; 1,4-C_4 diacids such as TA, various types of helicenes and various amino acids.

Overall, for chiral molecules at L–S and G–S interfaces, there are 21 entries exhibiting homochirality at the molecular-level and 22 entries exhibiting heterochirality at the molecular-level. At the cluster level, there are 6 entries exhibiting homochirality and 5 exhibiting heterochirality. There are 9 systems in L–S and 11 systems in G–S interfaces that exhibit lattice chirality. There is no significant difference in the trends between L–S and G–S interfaces; at both molecular-level and cluster-level, both types of interfaces have more systems exhibiting homochiral than heterochiral packing.

From Table 1, it can be seen that for mixtures of chiral molecules deposited on surfaces, roughly equal number of systems tend to aggregate homochirally *vs.* heterochirally at both the molecular and cluster-levels. This behavior is clearly distinct from 3D enantiomer aggregation where most compounds have been found to aggregate heterochirally (racemates).[58] It is also interesting to note that there are a substantial number of adsorbate systems exhibiting heterochirality at the molecular- and cluster-levels The probability of finding heterochirality in adsorbed monolayers is significantly higher than in 3D.[59] This is the first exhaustive study of the available literature conducted to test that hypothesis. Our review has comprehensively assessed the available data and arrived at the conclusion that there is no evidence of a strong preference for either homochiral or heterochiral aggregation in enantiomer mixtures on surfaces.

Some studies listed in Table 1 deserve to be highlighted to illustrate some of the variables that influence enantiomer aggregation and our ability to detect it. Most of the studies listed in Table 1 have relied on the use of STM to distinguish enantiomers. However, it is important to point out that enantiodiscrimination using STM is not always straightforward. For example, the –OH functional group on long chain alcohols used to identify the chiral configuration of the adsorbed alcohols, is imaged at very different bias voltages (400–700 mV for triacontanol *vs.* −1200 to −1500 mV for nonacosan-10-ol) when located at different positions on the alkyl chain.[241] This dependence adds a layer of complexity to accurately identifying adsorbate chirality.

A study by Ernst *et al.* illustrates the limitations of LEED for probing chiral organization of the racemic [7]H/Cu(111) system.[181] In an early study using LEED, the diffraction pattern of racemic [7]H/Cu(111) revealed the presence of two chiral domains on the surface. Furthermore, enantiopure *M*- and *P*-[7]H each exhibited enantiomorphous diffraction patterns revealing single enantiomer overlayers with the same periodicity as those produced by racemic [7]H. Not surprisingly, those results were interpreted to suggest that spontaneous resolution of [7]H enantiomers occurs on Cu(111), suggesting molecular-level

Table 1 Aggregation in chiral adsorbate–surface systems

Surface	Adsorbate	Mol-homo	Mol-hetero	Clust-homo	Clust-hetero	Lattice chiral	RSS	No organ.	Ref.
At L–S interfaces									
Au(111)	1,1′-Binaphthalene-2,2′-dithiol	✓		✓		✓			248
Au(111)	2-Butanethiol		✓						233
Au(111)	5-Amino[6]helicene	✓	✓	✓	✓	✓			223
Au(111)	Chiral trigonal prism molecule	✓				✓			222
I/Au(111)	BINAC		✓						224
Cu(111)	QUINAP	✓				✓			249
Cu(111)	Tyrosine	✓				✓			250
HOPG	1,2–Dihydroxyoctadecane		✓						251
HOPG	OPA	✓				✓			219
HOPG	9,10-Diiodooctadecan-1-ol		✓			✓			221
HOPG	Formamide with ester		✓				✓		252
HOPG	MHPOBC	✓	✓			✓			220
HOPG	Nonacosane-10-ol								241
HOPG	Oleic acid diiodide		✓			✓			253
HOPG	OPV 3I		✓		✓				254
Pt(111)	1-(1-Naphthyl)ethylamine		✓						210
Total for liquid–solid interfaces		**7**	**10**	**2**	**2**	**9**	**1**	**0**	

Surface	Adsorbate	Mol-homo	Mol-hetero	Clust-homo	Clust-hetero	Lattice chiral	RSS	No organ.	Ref.
At G–S interfaces									
Ag(100)	Heptahelicene	✓	✓		✓	✓			153
Ag(111)	Heptahelicene		✓						236
Ag(111)	Tartaric acid		✓			✓			201 and 255
Au(110)	Cysteine		✓		✓				230 and 256
Au(110)	Thia[11]heterohelicene							✓	257
Au(111)	Heptahelicene		✓						236
Au(111)	Thia[11]heterohelicene						✓		258
Calcite(1,0,−1,4)	Heptahelicene-2-carboxylic acid		✓						259
Cu(100)	5-Amino[6]helicene	✓	✓				✓		245
Cu(100)	Heptahelicene	✓		✓		✓			238
Cu(100)	Alanine	✓				✓			260, 214 and 261
Cu(110)	3-Pyrroline-2-carboxylic acid						✓		247
Cu(110)	Alanine							✓	217
Cu(110)	Di-phenylalanine	✓							262
Cu(110)	Malic acid		✓			✓			263
Cu(110)	Phenylglycine	✓				✓			187
Cu(110)	Proline						✓		264
Cu(110)	Resorcinol ether derivative							✓	243
Cu(110)	Serine	✓			✓				183
Cu(110)	Tartaric acid	✓				✓			265, 266, 186 and 267
Cu(111)	Heptahelicene		✓			✓	✓		188, 181, 237 and 268
Cu(111)	Alanine	✓		✓					269
Cu(111)	Aspartic acid	✓		✓					170
Cu(111)	Cyano-heptahelicene	✓		✓		✓			240
Cu(3,1,17)	Alanine							✓	169
Cu(3,1,17)	Aspartic acid							✓	171
Cu(3,1,17)	Phenylalanine							✓	168

Table 1 (*continued*)

Surface	Adsorbate	Mol-homo	Mol-hetero	Clust-homo	Clust-hetero	Lattice chiral	RSS	No organ.	Ref.
Cu(3,1,17)	Serine							✓	168
Cu(311)	Alanine	✓							270
InSb(001)	[11]Anthrahelicene		✓						202
Ni(111)	Heptahelicene							✓	242
Pt(111)	Propylene oxide	✓	✓						172, 210 and 271
Sn/Cu(100)	5-Amino[6]helicene		✓			✓			245
TiO_2(011)–2 × 1	[11]Anthrahelicene							✓	244
TiO_2(110)–1 × 1	[11]Anthrahelicene	✓				✓			244
Total for gas–solid interfaces		**14**	**12**	**4**	**3**	**11**	**5**	**9**	

Abbreviations: BINAC, 1,1′-binaphthyl-2,2′-dicarboxylic acid; QUINAP, 1-(2-diphenylphosphino-1-naphthyl)isoquinoline; OPA, 2-(3-(octadecyloxy)phenoxy)propanoic acid; MHPOBC, 4-[(1-methylheptyloxy)carbonyl]phenyl 4′-octyloxy-4-biphenylcarboxylate; OPV3I, oligo(*p*-phenylenevinylene) phenylglycinamide. Structures of all molecules listed in Table 6 are available in Appendix A.

homochiral (conglomerate) aggregation. Later, however, STM images of [7]H/Cu(111) contradicted the earlier conclusions drawn from LEED.[188,237] Although two non-superimposable chiral lattices were observed after adsorption of racemic [7]H, those domains are heterochiral at the molecular level and different from the homochiral lattices of the same periodicity formed by enantiopure [7]H. The fact that the enantiopure monolayers of [7]H/Cu(111) adopt the same overlayer lattices as racemic [7]H/Cu(111) is coincidental.

The interplay between kinetic barriers and thermodynamic driving forces dictating enantiomer aggregation has also been observed in studies of [7]H/Ni(111) and a resorcinol ether derivative/Cu(110) (see Appendix A for figure).[242,243] On Ni(111), [7]H molecules were not observed to form any chiral structures due to low surface mobility. When the racemic resorcinol-derivative ($(HOOCCHCH_3)_2C_6H_6O_2$) was deposited on Cu(110), Robin *et al.* observed an adsorbed overlayer that could be categorized as a RSS. The growth of homochiral clusters of tens of molecules is inhibited because they are surrounded by the opposite enantiomer. These examples reveal the presence of kinetic barriers to enantiomer separation that result in neither spontaneous resolution into homochiral domains nor a well-ordered heterochiral layer.

The adsorption protocol used to prepare enantiomer monolayers on surfaces can influence the resulting structure, providing clear evidence that thermodynamics is not always dictating the outcome. Santagata *et al.* have studied the effect of two different types of deposition protocols for TA/Ag(111); one in which *S*-TA was first deposited followed by *R*-TA (sequential deposition) and the other in which a racemic mixture of *S*- and *R*-TA was deposited (co-deposition).[201] Not surprisingly, the study found that depositing *R*- and *S*-TA sequentially resulted in segregation on the surface with two separate homochiral domains being formed while co-deposition resulted in a molecularly heterochiral domain (racemate). It is known that when an enantiomer is present in excess, it can steer the chirality of the entire adsorbate layer to one type of enantiomorph. Thus, during sequential deposition, when an *S*-TA overlayer is exposed to *R*-TA vapor, the *R*-TA must have displaced some of the *S*-TA and formed *R*-TA domains.

Among those chiral adsorbate–surface systems considered in this work, a total of 15 adsorbate–surface systems have been categorized as forming random solutions on the surface (marked "RSS") or exhibiting a no organization state of no chiral organization (marked "no organization"). All but one of these systems were reported on G–S interfaces. Of these 15 systems, 40% of the systems report evidence of RSS on the surface while the rest suggest no specific organization on the surface. This latter group consists mostly of amino acids and helicene adsorbates on TiO_2 and naturally chiral Cu surfaces.[168,244,245] While RSS are rare in 3D, it is expected that a few instances in 2D would be uncovered by our survey. Proline (Pro, **R** = $(CH_2)_4NH$) and its derivative, 3-pyrroline-2-carboxylic acid (PCA, C_4H_7NCOOH) on Cu(110) are the only species to have been shown using STM to form a RSS in 2D.[246,247] That study introduced the concept of handedness (molecular chirality) *vs.* footedness (adsorption footprint

chirality) of an adsorbate on a surface. In essence this creates diastereomerism, much like that observed in TA which can have *RR*-, *SS*-, *RS*- and *SR*-forms. In the case of adsorbate–surface diastereomers this results in two inequivalent pairs of enantiomers; *i.e.* if the subscripts 'h-' and 'f-' refer to handedness and footedness, then $R_hR_f \equiv S_hS_f \neq R_hS_f \equiv S_hR_f$. While the (4 × 2) overlayer formed by PCA/Cu(110) was found to be a RSS at both the handedness and footedness level, Pro/Cu(110) forms an ordered (4 × 2) overlayer which was a RSS at the molecular level but heterochiral at the footedness level. Even the overlayer formed in the case of resorcinol/Cu(110) discussed earlier can be considered to be a RSS.[243]

Some entries under the 'no organization' category include systems in which no evidence of enantiomer aggregation has been observed. These include equilibrium adsorption studies of the amino acids Ala, Ser and Phe on chiral Cu(3,1,17)$^{R\&S}$.[168,169,171,212] Those studies suggest that enantiomers of these three amino acids, far from showing any evidence of homo- or hetero-chiral aggregation, do not even demonstrate enantiospecific adsorption on chiral Cu(3,1,17)$^{R\&S}$. In contrast, Asp demonstrates enantiospecific adsorption on Cu(3,1,17)$^{R\&S}$ and molecularly homochiral aggregation on Cu(111) and Cu(653)$^{R\&S}$.[168,169,171] This comparison of different amino acids highlights how even small differences in functional groups can lead to differences in enantiomer aggregation.

The papers discussed above provide a glimpse into the multiple factors that influence enantiomer aggregation and assembly on surfaces. Detecting these requires selection of the appropriate probing technique and understanding the subtle competition between kinetic and thermodynamic forces that determine enantiomer aggregation. It is challenging to account for all of these factors when making theoretical predictions of how chiral molecules will assemble when deposited on surfaces.

6. Enantiospecific aggregation of prochiral adsorbates

This section reviews adsorbate–surface systems of prochiral adsorbates at L–S and G–S interfaces. Prochiral molecules are achiral in 3D (no enantiomers) but are rendered chiral by adsorption. For our purposes we consider prochiral to mean molecules with a finite number of mirror planes. Thus, even on a featureless surface, adsorption breaks mirror symmetry, unless one of those planes is oriented normal to the surface. Such molecules can form surface enantiomers by adsorption in isolation onto a flat featureless surface; *i.e.* species σ_v^0 and $\bar{\sigma}_v^0$ in Fig. 6A. The achiral molecules that are non-prochiral are those with multiple mirror planes, such as atoms (zero-dimensional) or truly linear molecules (one-dimensional), that cannot form enantiomers by adsorption in isolation onto a flat featureless surface; *i.e.* species σ_v^n and σ_v^∞ in Fig. 6A. One of the simplest examples of a prochiral molecule is Gly, which adsorbs on Cu(110) in two enantiomorphous forms, as shown in Fig. 5.[135,272] In the terminology invoking 'handedness' and 'footedness', the origin of chirality in adsorbed prochiral species (on an featureless surface) is purely in their footedness.[231] Because they are only rendered chiral by the process of adsorption, overlayers of prochiral molecules must yield racemic mixtures of surface enantiomers when adsorbed on an achiral surface unless there is some chiral bias imposed on the adsorption process. Among other things, this means that the issues associated with the preparation of truly racemic fluxes of a chiral vapor for adsorption under UHV conditions, are moot. Adsorption on an intrinsically chiral surface should result in some enantiomeric bias in the chirality of the adsorbate population. One of the other important distinctions between chiral and prochiral adsorbates is that prochiral adsorbates can switch their chirality by 'flipping' over. This then serves as a mechanism for interconversion between homochiral and heterochiral phases. The molecular structures of the prochiral adsorbates reviewed in this section are summarized in Table 7 in the appendix.

We have examined 23 studies of prochiral adsorbate–surface systems at L–S interfaces and 34 prochiral adsorbate–surface systems at G–S interfaces. At L–S interfaces, the most commonly studied prochiral adsorbates are compounds with carboxylic acid functional groups and long alkyl chains. All studies at L–S interfaces have used HOPG surfaces. At G–S interfaces, the adsorbates are much more diverse, ranging from Gly to nitronaphthalene. Most studies at G–S interfaces have been performed on Au and Cu single crystal surfaces with (111) and (100) orientations. A few studies have used Ag and Pt surfaces. These metal surfaces differ in the strength of their interactions with adsorbates. Cu tends to chemisorb a given adsorbate more strongly than Au.[273] Ag(111) is unreconstructed while Au(111) adopts the herringbone reconstruction, leading to larger surface diffusion barriers on Au(111) than on Ag(111).[209] Adsorption on Ag tends to be stronger than on Au but substantially weaker than on Cu.[273] Studying the same adsorbate on these surfaces enables understanding of the effect of adsorbate–surface interaction on chiral adsorbate organization. STM is the most widely used technique to probe the structures formed by prochiral adsorbates at the G–S interface. LEED has also been a valuable tool.

Three prochiral adsorbate–surface systems are discussed in detail in this section. The first is a study of prochiral anthracene derivatives on HOPG and demonstrates the effect on surface chirality of having odd and even numbers of carbon atoms in pendant alkyl chains. Another is a study of prochiral 4-[*trans*-2-(pyrid-4-yl-vinyl)]benzoic acid (PVBA) on metal surfaces. Our discussion reviews the behavior of PVBA on a number of surfaces (Au, Cu, Bi *etc.*) and illustrates the effects on enantiomer aggregation of adsorbate–surface interaction strength.

6.1 Anthracene derivatives/HOPG at L–S interface

Wei *et al.* have studied two anthracene derivatives (Fig. 23), namely 1,5-bis-(3′-thiaalkyl)anthracene (BTAA), on HOPG.[274] Each molecule possesses C_{2h} symmetry and consists of two 3′-thiaalkyl chains attached to the first and fifth carbon atoms of an anthracene core. The difference between the two molecules is that their thiaalkyl chains differ in length by a single $-CH_2$ group. One has two odd-numbered $C_{11}H_{23}$ (undecyl) chains (BTAA-11), while the other has two even-numbered $C_{12}H_{25}$ (dodecyl) chains (BTAA-12).[274] Both molecules are prochiral because adsorption

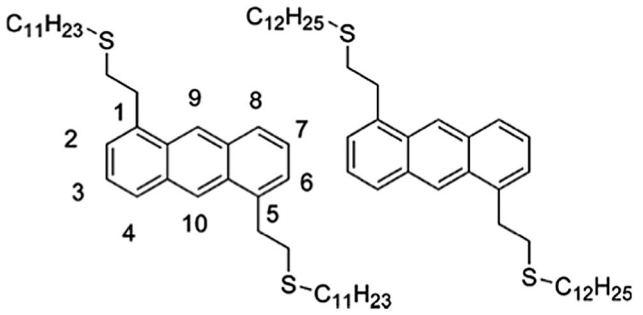

Fig. 23 Molecular structures of the two anthracene molecules studied by Wei *et al.* The difference between the two molecules is the lengths of their alkyl chains. Both molecules are prochiral *i.e.* they can adsorb in enantiomorphous configurations. Adapted from ref. 274 Copyright 2004 American Chemical Society.

on the two sides of the anthracene core results in 3′-thiaalkyl chains oriented in different directions and the formation of species that are nonsuperimposable mirror images of one another. The authors have observed significant differences in enantiomer aggregation of BTAA-11 and BTAA-12 on HOPG. Wei *et al.* have not indicated the absolute coverage at which these experiments were conducted; however, the molecules are close-packed indicating that the coverage must be close to saturation.

The presence of chemical markers such as sulfur atoms and the aromatic anthracene groups makes it easy to visualize BTAA using STM and to differentiate between surface enantiomers. The top panels of Fig. 24 show STM images of BTAA-11 and BTAA-12 on HOPG. In the STM images in Fig. 24, each of the two straight black lines in the ''N'' shape represent the distance between the two sulfur atoms of a single molecule. In the STM image of BTAA-11 (Fig. 24 top left panel), rows of bright areas are interspersed with dark areas. In the bright areas, the repeating pattern is a set of eight spots (outlined in one molecule), six of them arranged in two rows and two on the periphery. The spots on the periphery are the sulfur atoms and the six spots arise from the anthracene core. The length of the blue line shown in the figure matches the length of the molecule (3.98 nm), thus indicating the position of the molecules in the parallel rows. The dark areas between the bright rows are attributed to interdigitated alkyl chains. Furthermore, in the top left panel of Fig. 24, alternate rows have different arrangements as indicated by the backward and forward N's (shown in black) superimposed on the top right corner of the image. This means that molecules in a given row are adsorbed in one enantiomeric form but that molecules in adjacent rows adopt the opposite enantiomorphous form. This molecular arrangement adopted by the BTAA-11 in adjacent rows is illustrated by the schematic model shown in Fig. 24 bottom left panel. The BTAA-11 overlayer is molecularly heterochiral.

The STM image of BTAA-12 (Fig. 24 top right panel) reveals bright rows interspersed with dark areas. However, unlike the overlayer formed by BTAA-11, all the rows contain BTAA-12 in one enantiomorphous form. This is easily observed in the repeating pattern of the bright dots in adjacent rows. This molecular arrangement adopted by BTAA-12 in adjacent rows is illustrated by the schematic model shown in Fig. 24 bottom right panel. Thus, while the overlayer formed by BTAA-11 is molecularly heterochiral, the overlayer formed by BTAA-12 is molecularly homochiral.

The heterochiral *vs.* homochiral packing adopted by BTAA-11 and BTAA-12, respectively, is intriguing given that the only difference between the two molecules is one $-CH_2$ group in the 3′-thiaalkyl chain. However, the difference in packing can be explained on the basis of interdigitation of the 3′-thiaalkyl chains. The bottom left and right panels of Fig. 24 show schematics of the 3′-thiaalkyl chain arrangements for BTAA-11 and BTAA-12, respectively. In BTAA-12 the terminal CH_2–CH_3 bond (marked in dashed green arrow) is parallel to the aryl–C1′ bond (marked in dashed blue arrow) in the same molecule. This means that, the terminal CH_2–CH_3 bonds in adsorbed BTAA-12 will be parallel to the aryl–C1′ bonds in adjacent rows, if the BTAA-12 in adjacent rows are of the same enantiomer. However, for BTAA-11 the terminal CH_2–CH_3 bonds would be rotated by 110° with respect to the aryl–C1′ bond of the molecules in the adjacent row, if the BTAA-11 in adjacent rows were the same enantiomer. As the molecular model in Fig. 24 bottom left shows, to obtain a close-packed overlayer of BTAA-11 with CH_2–CH_3 bonds in one row parallel aryl–C1′ bonds in the adjacent row requires that molecules in adjacent rows be different surface enantiomers. Thus, the observation of homochiral *vs.* heterochiral packing for even- and odd-numbered alkyl chain molecules can be explained on the basis of which arrangement leads to a close-packed monolayer.

No details have been given on how the BTAA overlayers are oriented with respect to the high symmetry directions of the HOPG lattice, making it difficult to ascertain the existence of lattice chirality. The authors do not mention whether they conducted analyses of multiple domains before arriving at the conclusion that all the surface domains for each BTAA molecule were packed in the same arrangement (homo- or hetero-chiral). Thus, there is no report of additional domains related by rotational or mirror symmetry to those shown in Fig. 24.

Odd–even chain length effects in long-chain organic adsorbates on surfaces have been widely studied.[275–279] The interdigitation of alkyl chains and its influence on the formation of self-assembled monolayers that is described by Wei *et al.* has also been observed for other alkyl and alkanol monolayers on HOPG.[280,281] There are also similarities between BTAA/HOPG and monolayers of odd/even chain length fatty acids on HOPG studied by Hibino *et al.*[275] For these fatty acids/HOPG, instead of van der Waals forces, hydrogen bonding between –COOH groups was deemed to be the dominant interaction between adsorbates. Odd chain length fatty acids were observed to form molecularly heterochiral domains while even chain length fatty acids formed molecularly homochiral domains.

6.2 PVBA on metal surfaces at G–S interface

The prochiral molecule 4-[*trans*-2-(pyrid-4-yl-vinyl)]benzoic acid (PVBA) has been studied on several different metal surfaces.[282] Fig. 25 shows the molecular structure of PVBA, which consists of benzoic acid connected to a pyridine group *via* a vinyl bridge.

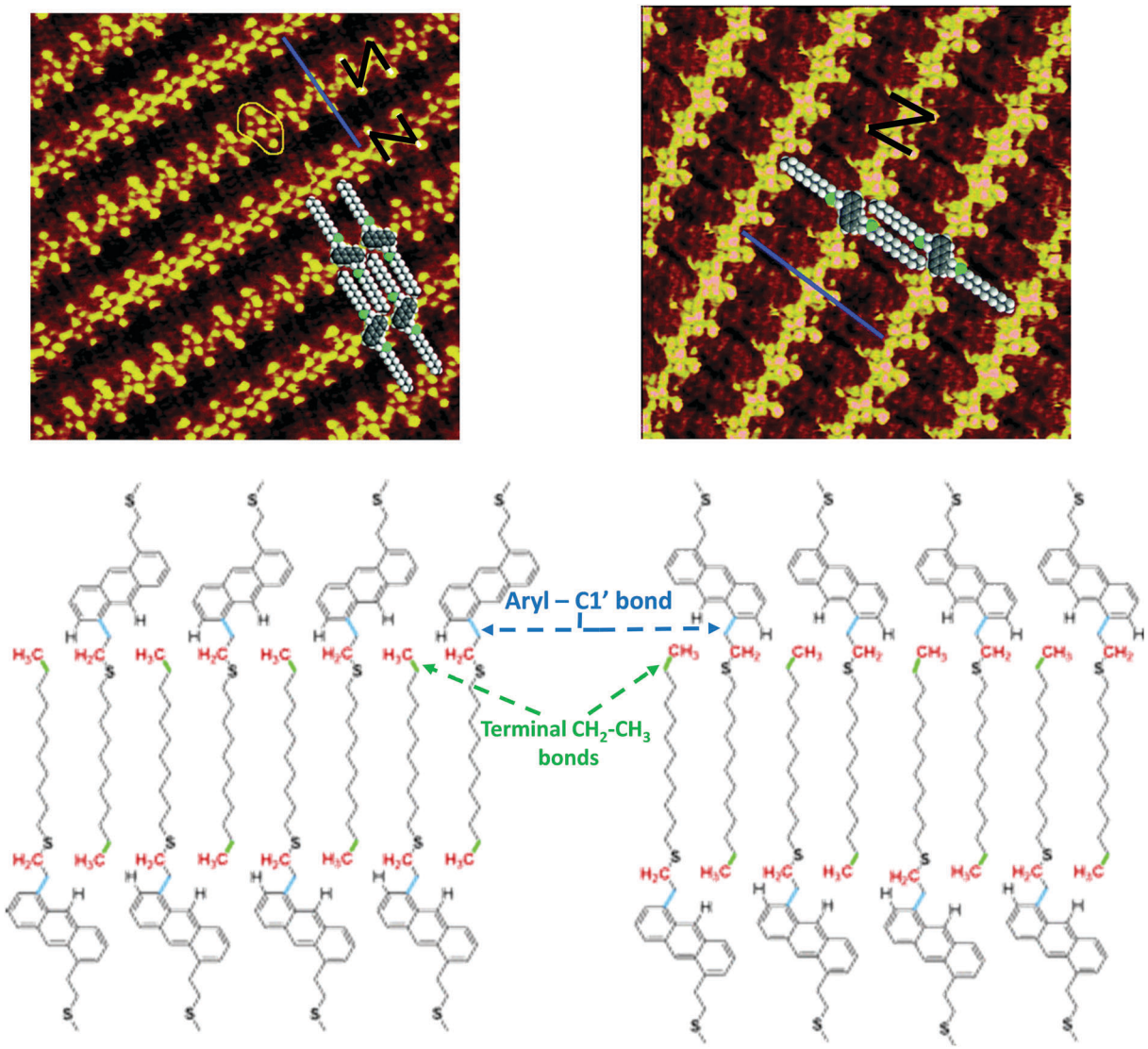

Fig. 24 Left top and bottom panels show an STM image and molecular model of BTAA-11 on HOPG. To ensure a close-packed arrangement, the C_{aryl}–C1 bonds (indicated by the dashed blue arrow in bottom panel) of adjacent molecules must be parallel, which is only possible, if opposite surface-enantiomers are present in adjacent adsorbate rows since the number of carbon atoms in the undecyl chain is odd. This leads to a molecular-level heterochiral layer. Right top and bottom panels show STM image and molecular model of BTAA-12 adsorbed on HOPG. To ensure close-packed arrangement, the aryl–C1′ bonds (indicated by the dashed blue arrow in bottom panel) of adjacent BTAA-12 molecules must be parallel, which is only possible if only one surface-enantiomer is present in the domain. This leads to a molecular-level homochiral layer. Adapted from ref. 274 Copyright 2004 American Chemical Society.

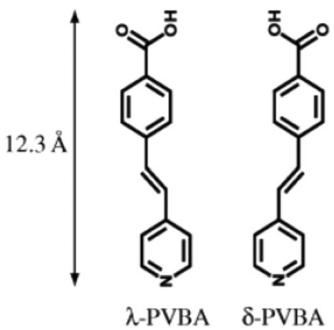

Fig. 25 Molecular structure of prochiral PVBA surface enantiomers, δ- and λ-PVBA. Adapted from ref. 284 Copyright 2005 American Chemical Society.

Prochiral PVBA adsorbed in 2D on its two faces forms surface enantiomers referred to as δ- and λ-PVBA. In this section, we focus on studies of PVBA adsorbed on Au, Ag, Cu and Pd surfaces.[138,283–285]

6.2.1 PVBA on Ag(111) and Au(111). Studies of PVBA adsorbed at coverages in the range 0.1–0.6 ML (relative to saturation coverage) on Au(111) and Ag(111) have shown that PVBA behaves similarly on both surfaces.[138,283,286] PVBA/Au(111) forms enantiomorphous domains, having parallel double rows of aligned PVBA, as shown in Fig. 26A. The spacing between the double rows in both domains decreases with increasing PVBA coverage as seen by comparing the images in the left (θ = 0.3 ML) and the right (θ = 0.6 ML) panels of Fig. 26A.

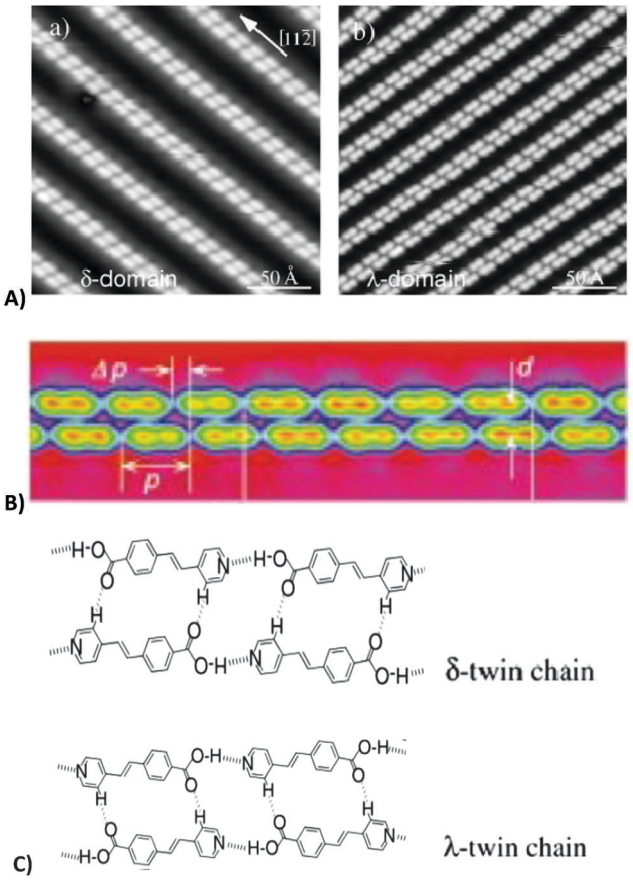

Fig. 26 (A) STM images of PVBA/Ag(111) at 0.3 ML and 0.6 ML showing two types of molecularly homochiral domains. δ-(left) and λ-(right), each consisting of PVBA molecules attached end-to-end forming long double rows. Adapted from ref. 283 Copyright 2002 American Chemical Society. (B) High-resolution STM image of PVBA/Ag(111) showing a double row of PVBA molecules in head–tail arrangement in each row and the corresponding molecules in the two rows in an anti-parallel arrangement. Adapted from ref. 283 Copyright 2000 with permission from John Wiley and Sons. (C) Molecular model of double row arrangement for δ-(left) and λ-(right) domains, schematically depicting hydrogen bonding between PVBA molecules in the same row (head–tail arrangement) and with PVBA molecules in the neighboring row. Adapted from ref. 138 Copyright 2001 American Chemical Society.

To identify the orientation of PVBA molecules in the double rows, high resolution STM images were obtained (Fig. 26B).[286] The repeating oval features in both rows were identified as single λ-PVBA molecules. The right lobe in the upper row of Fig. 26B is deemed to be the benzoic acid moiety. Although the STM images are not sufficiently resolved to make this determination directly, the staggering of molecules is consistent with the structure shown in Fig. 26C. PVBA molecules in double rows adopt a head–tail arrangement, with hydrogen bonds formed between the pyridyl N atoms and the carboxylic acid groups of adjacent PVBA molecules in the same row. The staggering of molecules in parallel rows arises from hydrogen bonding between pyridyl C–H bonds and the C═O groups in molecules on opposite sides of the chain. Further, the authors interpret the somewhat extended left lobe of the molecule in the lower row compared to the circular left lobe in the upper row as indication that the PVBA molecules in the two rows are aligned in an anti-parallel arrangement. This suggests that hydrogen bonding is possible only, if the molecules in the upper and lower row are the same surface-enantiomers *i.e.* the double rows are molecularly homochiral. MD simulations further suggest that homochiral PVBA double rows are more energetically stable than heterochiral double rows. The domains shown in the left and right panels of Fig. 26A are mirror images of each other and hence, PVBA/Ag(111) also exhibits lattice chirality.

6.2.2 PVBA on Pd(111). PVBA/Pd(111) has been studied using STM at a coverage of 0.1 ML by Kim *et al.*[285] Roughly 85% of the clusters observed on the surface are dimers and the remainder are trimers, tetramers and hexamers. Further discussion has been restricted to the dimers. The PVBA dimers were found to be of two types; linear dimers and bent dimers shown in Fig. 27A and C, respectively. These two types were distinguished from one another based on the symmetry across the long axis of the dimer. The two PVBA molecules forming the linear dimer are related by C_2 symmetry around the midpoint of the dimer axis while the two PVBA molecules forming the bent dimer are related *via* mirror symmetry through a plane perpendicular to the dimer axis. Thus, the linear dimers are molecularly homochiral; both PVBA molecules are the same surface-enantiomer (δ–δ or λ–λ). The bent dimers are molecularly heterochiral (δ–λ).

An analysis of 93 dimers images revealed that statistically equivalent numbers of linear and bent dimers are present. Hence, PVBA/Pd(111) has been categorized as both molecular-level homo- and heterochiral. The authors suggest that stronger PVBA bonding to Pd(111) than to either Ag(111) or Au(111)

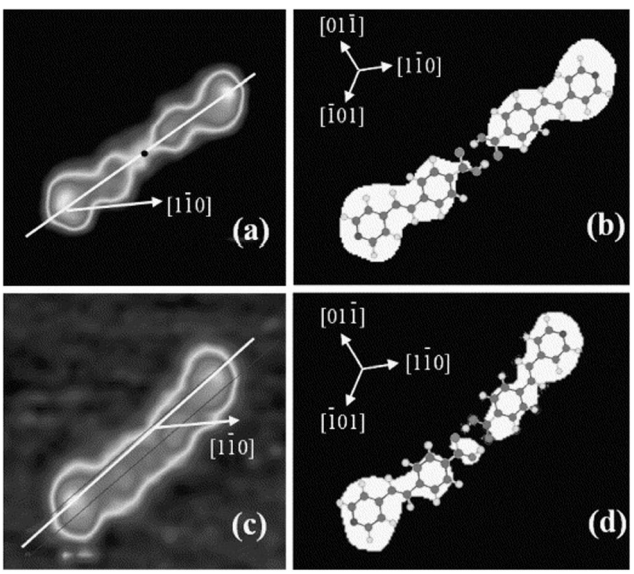

Fig. 27 High resolution STM images of PVBA/Pd(111) showing two types of dimers: (a) linear and (c) bent. (b and d) Show molecular models of PVBA overlaid on the STM images of linear and bent dimers, respectively. The linear dimers are molecularly homochiral while bent dimers are molecularly heterochiral. Reprinted from ref. 285 Copyright 2003 with permission from Elsevier.

precludes the formation of extended supramolecular domains. However, since studies at coverages >0.1 ML have not been reported, it is possible that the lack of extended domains is attributable to low coverage. This also obviates the expression of lattice chirality for PVBA/Pd(111).

6.2.3 PVBA on Cu(100). PVBA forms a more diverse set of surface structures on Cu(100) than on any of the other surfaces on which it has been studied. On Cu(100), PVBA undergoes a coverage-dependent phase transition from molecular-level homochirality to molecularly heterochirality at a critical coverage of θ_c = 0.05 ML.[284] The absolute monolayer coverage is defined as one PVBA molecule per surface Cu atom and was determined, in this case, using STM. At a coverage of 0.02 ML, well below the critical coverage θ_c, two enantiomorphous domains, rotated by $\pm 11^\circ$ with respect to the [001] substrate lattice direction, are observed on the Cu(100) surface as shown in Fig. 28a. Thus, chirality is expressed at the lattice level in PVBA/Cu(100). Each of these enantiomorphous domains has two kinds of molecular arrangements; molecules arranged in a parquet pattern (domain A in Fig. 28a) which consists of square voids and molecules arranged in a rectangular pattern (domain B in Fig. 28a) which is more close-packed than domain A. High-resolution STM images of the PVBA molecules in these domains are shown in Fig. 28c and reveal a dumbbell-shaped image for each individual molecule. Based on comparison with Fe–PVBA lattices studied on Cu(100), the dumbbell shape was attributed to a single PVBA molecule with the flat end assigned to the pyridyl moiety.[287] A molecular model of the dumbbell shape is shown in Fig. 28d. DFT calculations show that all the dumbbell dimers forming the domain shown in Fig. 28b are molecularly homochiral. In Fig. 28b, they are all δ–δ PVBA.

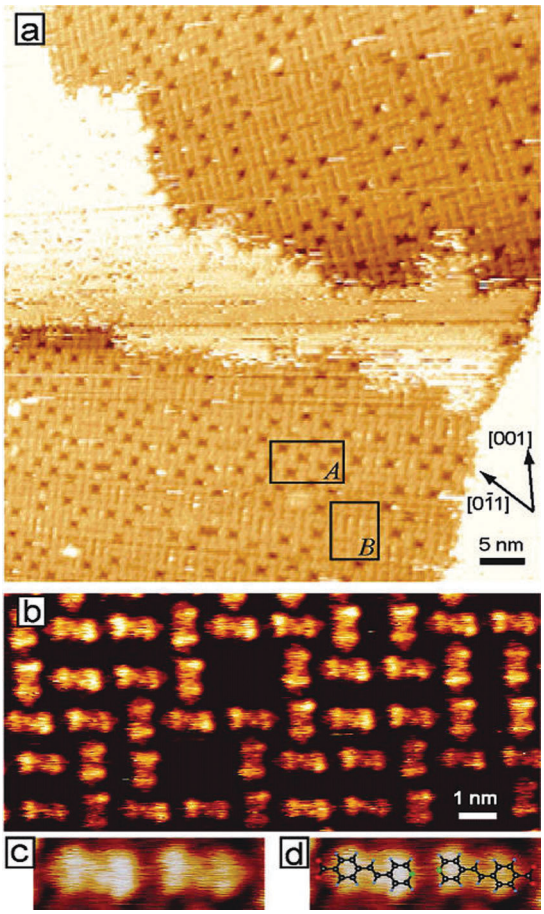

Fig. 28 (a) STM image of PVBA/Cu(100) at 0.02 ML showing two enantiomorphous domains. Areas marked A and B are the parquet and rectangular domain, respectively. (b) High-resolution STM image of the parquet domain A showing the individual molecules and the characteristic square voids. (c) High-resolution STM image of two PVBA molecules forming a dimer. (d) Molecular model of homochiral PVBA molecules forming the dumbbell. Adapted from ref. 284 Copyright 2005 American Chemical Society.

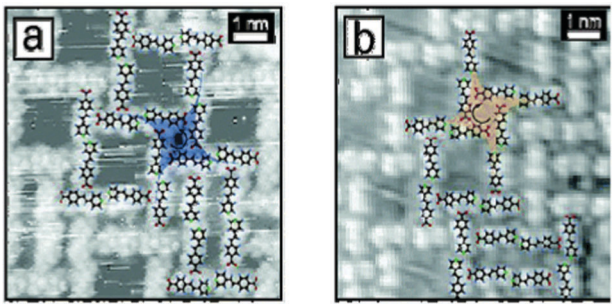

Fig. 29 STM images of two homochiral parquet domains (δ- and λ-PVBA domains in a and b respectively) with clockwise and counter-clockwise orientations formed by PVBA/Cu(100) at a coverage of θ = 0.018. The molecular arrangements of PVBA molecules that comprise the domains are overlaid on the images. Adapted from ref. 284 Copyright 2005 American Chemical Society.

Fig. 29(a and b) shows schematic molecular models of parquet domains formed by δ- and λ-PVBA molecules on Cu(100) overlaid on STM images. In the δ- and λ-domains, the center of the junction formed by the squares (shaded in blue and green respectively for δ- and λ-) is rotated either in CW or CCW orientation, expressing homochirality at the cluster level. Thus, at lower than critical coverage (θ = 0.018), PVBA/Cu(100) exhibits both molecular- and cluster-level homochirality while also being chiral at the lattice level.

When the coverage of PVBA/Cu(100) exceeds θ = 0.05, the parquet pattern shown in Fig. 28 begins to disappear and is replaced with domains comprised of butterfly-shaped structures (''butterfly domain'', Fig. 30). At a coverage of θ = 0.055, the parquet pattern completely disappears and only the butterfly domain is observed on the surface. Fig. 30A shows a high-resolution STM image of the butterfly domain. Each of the units seen on the image represents one PVBA molecule. The authors recognize that this image has a lower resolution than Fig. 27; nevertheless, they are able to distinguish between δ and λ PVBA molecules based on the protrusion of the vinyl bridge of the PVBA molecule, marked with the white arrow on Fig. 30A. Based on this, they conclude that the domain shown in Fig. 30A contains both δ and λ PVBA molecules and is molecularly heterochiral. A model to represent this molecularly heterochiral domain is shown in Fig. 30B in which it is suggested that the four PVBA molecules forming a tetramer are the same

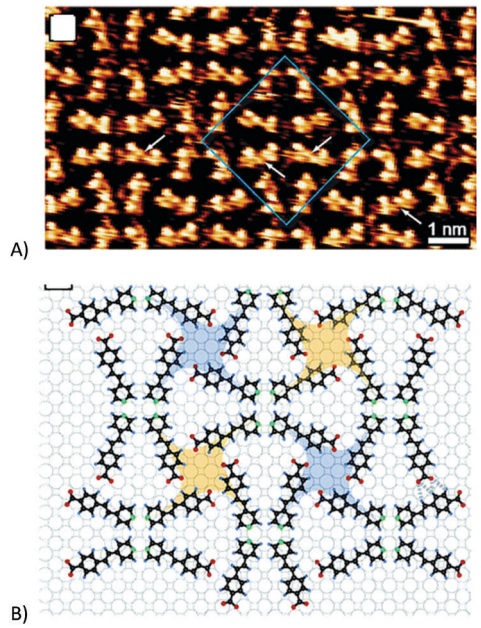

Fig. 30 (A) STM image of the butterfly phase of PVBA/Cu(100) at θ = 0.55. The square outlines the unit cell and arrows point to vinyl bridges of each PVBA molecule. (B) Molecular model of the butterfly phase clockwise and counter-clockwise tetramers of λ- and δ-PVBA clusters in the same domain. Adapted from ref. 284 Copyright 2005 American Chemical Society.

surface enantiomer; the tetramers are colored in blue or green depending on whether the four molecules are δ or λ PVBA molecules, respectively. Also, the tetramer itself can have either clockwise or counterclockwise orientation and both types exist in the same domain. Thus, it is also cluster-level heterochiral. The square unit cell of this butterfly domain is oriented along the (001) direction of the Cu(100) and hence, lattice chirality is not exhibited by this phase.

The transition from a molecularly homochiral (parquet domain) to a heterochiral phase (butterfly domain) when θ_c = 0.05 is exceeded is attributed by Vidal *et al.* to the need for a closely-packed overlayer which overcomes steric repulsion between the N and H atoms of adjacent pyridyl groups in the parquet phase. This leads to an abrupt phase transition from a homochiral to heterochiral overlayer.

6.3 Overview of prochiral adsorbates in 2D

From the studies discussed above, it is clear that organization of prochiral molecules on surfaces is sensitive to multiple parameters including coverage and molecular structure. In this section, we will review our findings on the type of enantiomer aggregation preferred by prochiral adsorbates and then mention a few studies that serve to illustrate the variety of possibilities for prochiral adsorbate organization.

Table 2 lists all prochiral adsorbate–surface systems that have been reviewed herein and categorizes each. It must be repeated that non-superimposable configurations of adsorbed prochiral molecules are not usually referred to as enantiomers, in the sense that once they desorb they are no longer chiral. For the purposes of this review, we are referring to the two enantiomorphs of prochiral adsorbates as surface enantiomers. Using this definition, we have categorized aggregates of prochiral adsorbates as molecularly homochiral or heterochiral.

The totals in the bottom rows of Table 2 for L–S and G–S interfaces suggest that at both the molecular- and cluster-level, there is a slight preference for homochirality over heterochirality. There are a total of 32 and 24 entries that were categorized as molecularly homochiral and heterochiral, respectively, while 14 and 9 entries were designated as cluster-level homochiral and heterochiral, respectively. A total of 36 systems, more than half of all the prochiral adsorbate systems reviewed, expressed chirality at the lattice level. While there are more molecular- and cluster-level homochiral adsorbate–surface systems, a significant number (~40%) of prochiral adsorbate–surface systems were found to exhibit heterochiral packing at the molecule- and cluster-level. The fraction of adsorbate–surface systems exhibiting homochiral aggregation at the molecule- and cluster-level suggests that adsorption decreases (relative to 3D) the tendency of racemic mixtures to aggregate heterochirally. In the remainder of this section, we will deliberate on some key studies that seek to illustrate this point.

Glycine (the achiral amino acid with R = H), has been studied as a simple prochiral molecule using STM, LEED and DFT simulations on Cu(110), Cu(100) and Cu(111).[193,272,288–294] The structures formed by Gly on Cu(110) and Cu(100) have been a source of debate.[211] On Cu(110), although it has been proposed that Gly packs heterochirally, there is some ambiguity to the interpretation of results from photoelectron diffraction, STM, and DFT simulations. The 1-nitronaphthalene/Au(111) system shows a transition from molecular-level homochirality to heterochirality as the coverage increases above 0.25 ML.[272,295,296] It is also the only system that we have encountered wherein the surface enantiomers in the molecular-level heterochiral decamer clusters that it forms are observed to be present in an unequal rather than racemic ratio (*i.e.* 4 : 1 instead of a 1 : 1). This asymmetry in molecular composition makes the decamers themselves chiral leading to chiral expression at both the molecular and cluster level.

The enantiospecific adsorption properties of chiral molecules on chiral surfaces, discussed earlier for the Asp/Cu(3,1,17)$^{R\&S}$ system[212] also extends to prochiral molecules on chiral surfaces. When prochiral 9-ethynylphenanthrene ($C_{16}H_{10}$) is deposited on the PdGa(111) surface, which is naturally chiral owing to its non-centrosymmetric structure, a very high ee (94–98%) of either the *R*- or *S*-surface enantiomer is observed depending on the chirality of the naturally chiral PdGa surface.[297]

The metastable nature of chiral organization is evident from the number of studies in Table 2 wherein a transition from one type of packing to another is observed. The transition occurs due to either a small change in coverage, as in the cases of PVBA/Cu(100) and quinacridone derivatives/Au(111), or by simply annealing the surface at a higher temperature as in the case of guanine/Au(111), DBAQ (2,6-dibromoanthraquinone)/Au(111) and dioxaborine derivatives(DOB)/HOPG.[284,298–301]

Table 2 List of prochiral adsorbate–surface systems at L–S and G–S interfaces

Surface	Adsorbate	Mol-homo	Mol-hetero	Clus-homo	Clus-hetero	Lattice chiral	RSS	No organ.	Ref.
At L–S interfaces									
HOPG	BTAA-11		✓						274
HOPG	BTAA-12	✓							274
HOPG	Adenine	✓		✓	✓	✓			174 and 302
HOPG	AOPV			✓		✓			134
HOPG	DOB					✓			301
HOPG	18-18HSQ		✓						303
HOPG	Fatty acid (even)	✓				✓			275
HOPG	Fatty acid (odd)		✓						275
HOPG	Formamide derivative			✓		✓			304
HOPG	Furan oligomer	✓				✓	✓		305
HOPG	Heptadecanoic Acid		✓						306
HOPG	HPOBC		✓			✓			220
HOPG	DMHA	✓				✓			307
HOPG	OPV C5							✓	308
HOPG	OPV3-CHO			✓		✓			308
HOPG	OPV4-CHO			✓		✓			309
HOPG	OPV 2	✓				✓			310
HOPG	Tetraacid 3a	✓	✓						311
HOPG	Tetraacid 4a	✓							311
HOPG	Tetraester 3b	✓		✓					311
HOPG	Tetraester 4b	✓							311
HOPG	Eladeic acid diiodide		✓			✓			253
MoS_2	Adenine	✓				✓			174
Total for liquid–solid interfaces		**11**	**7**	**6**	**1**	**13**	**1**	**1**	

Surface	Adsorbate	Mol-homo	Mol-hetero	Clus-homo	Clus-hetero	Lattice chiral	RSS	No organ.	Ref.
At G–S interfaces									
Ag(111)	PVBA	✓				✓			138
Au(111)	1-Nitronaphthalene		✓		✓				296
Au(111)	1-Nitronaphthalene	✓	✓			✓			295
Au(111)	TPTZ	✓				✓			312
Au(111)	PVBA	✓				✓			138
Au(111)	Adenine	✓	✓	✓		✓			313
Au(111)	B		✓		✓				62
Au(111)	BA			✓		✓			62
Au(111)	BH		✓		✓	✓	✓		62
Au(111)	BHA		✓	✓	✓	✓	✓		62
Au(111)	2,6-Dibromoanthraquinone	✓	✓			✓			299
Au(111)	Guanine	✓	✓	✓	✓	✓			300 and 314
Au(111)	Naphtho[2,3-*a*]pyrene	✓				✓			315
Au(111)	*N*,*N*′-Dihexadecylquinacridone	✓	✓			✓			298
Au(111)	Xanthine	✓		✓		✓			200
Au(111)	α-Sexithiophene	✓				✓			316
Cu(100)	1,2,4-Benzene tricarboxylic acid	✓				✓			317

Table 2 (*continued*)

Surface	Adsorbate	Mol-homo	Mol-hetero	Clus-homo	Clus-hetero	Lattice chiral	RSS	No organ.	Ref.
Cu(100)	Stilbene dicarboxylic acid	✓				✓			318
Cu(100)	Glycine		✓						272, 288 and 289
Cu(100)	PVBA	✓	✓	✓	✓	✓			284
Cu(110)	Stilbene dicarboxylic acid	✓	✓			✓			319
Cu(110)	Adenine	✓				✓			320
Cu(110)	Fluorene-1-carboxylic acid		✓						321
Cu(110)	Glycine	✓	✓						290, 291 and 288
Cu(110)	*N*,*N*′-Dihexadecylquinacridone	✓				✓			322
Cu(111)	2,5-Dichlorothiophenol		✓		✓				323
Cu(111)	Glycine	✓		✓					324 and 292
Cu(111)	Indigo	✓				✓			325
Cu(111)	Naphtho[2,3-*a*]pyrene			✓	✓	✓			326
Cu(211)	Propene		✓						135
Cu(311)	Glycine					✓			270
Ge(100)	Styrene		✓						327
Pd(111)	PVBA						✓		285
PdGa(111)	9-Ethynylphenanthrene	✓						✓	297
Total for gas–solid interfaces		**21**	**17**	**8**	**8**	**23**	**3**	**1**	

Abbreviations: BTAA-11, 1,5-bis-(3′-thia-tetradecyl)anthracene; BTAA-12, 1,5-bis-(3′-thia-pentadecyl)anthracene; AOPV, oligo(*p*-phenylenevinylene)ureido-triazine derivative; BIC, 5-(benzyloxy)-isophthalic acid derivative; DOB, bis(4,4′-(*m*,*m*′-di(dodecyloxy)phenyl)-2,2′-difluoro-1,3,2-dioxaborin); 18-18HSQ, bis(4-dioctadecylamino-phenyl)squaraine; HPOBC, 4-[(1-heptyloxy)carbonyl]-phenyl-4′-octyloxy-4-biphenylcarboxylate; DMHA, *N*,*N*′-dodecanomethylenebishexanoamide; OPV3-CHO, oligo(*p*-phenylenevinylene)3-aldehyde; OPV4-CHO, oligo(*p*-phenylenevinylene)4-aldehyde; PVBA, 4-[*trans*-2-(pyrid-4-yl-vinyl)]benzoic acid; TPTZ, 2,4,6-tris(2-pyridyl)-1,3,5-triazine; B, 1,4-bis((3-*tert*-butyl-phenyl-)ethynyl)benzene; BA, 1,4-bis((5-*tert*-butyl-3-formyl-4-methoxy-phenyl)ethynyl)benzene; BH, 1,4-bis((2-*tert*-butyl-4-hydroxy)ethynyl)benzene; BHA, 1,4-bis((5-*tert*-butyl-4-hydroxy-3-formylphenyl)ethynyl)benzene; ONE, oligo(naphthylene–ethynylene) derivative. Structures of all molecules listed in Table 7 are available in Appendix A.

7. Enantiospecific aggregation of conformationally chiral adsorbates

This section is devoted to studies of conformationally chiral adsorbates whose 3D structures have two or more perpendicular mirror planes. These are not prochiral in the sense that adsorption with one mirror plane parallel to a featureless flat surface does not engender chirality; the perpendicular mirror planes remain a symmetry element of the adsorbate–substrate system. However, if the adsorbate can adopt conformations that break the perpendicular mirror symmetry, it is then chiral. This is quite possible for molecules with the flexibility to adopt multiple conformations at the ambient temperature; *i.e.* conformations that are within a few k_BT in energy of the achiral ground state conformation (Fig. 4).

We have identified 32 studies of conformationally chiral adsorbate–surface systems. Of these, 14 systems are on L–S interfaces while 18 are on G–S interfaces. As expected, most of the adsorbates studied at L–S interfaces are molecules with long alkyl chains which can easily adopt metastable conformations. At G–S interfaces, rubrene has been studied extensively. HOPG has been the substrate of choice for all the studies on L–S interfaces while single crystal surfaces of Ag, Au and Cu have been used for studies at G–S interfaces. The molecular structures of the conformationally chiral adsorbates reviewed in this section are summarized in Table 8 in the appendix.

For detailed discussion of conformationally chiral adsorbates, we have chosen two adsorbate–surface systems. First is the adsorption of Frechet-type dendron molecules on HOPG where interdigitation of conformational flexible alkyl chains influences 2D self-assembly.[328] The other study focused on rubrene adsorbed on various metal surfaces.[305,312,316,326,332–334]

7.1 Long alkyl chain molecules on HOPG at L–S interfaces

Merz *et al.* have studied two similar molecules containing octyl sidechains on HOPG: 3,5-bis[(3,5-bisoctyloxyphenyl)-methyloxy]benzaldehyde (BBOMB) and 3,5-bis[(3,5-bisoctyloxy-phenyl)-methyloxy]benzyl alcohol (BBOMA) (structures in Fig. 31).[328] The molecules only differ in the type of functional group (R = CH═O or CH_2OH). Both molecules have two perpendicular mirror planes in the conformation shown in Fig. 31 and are achiral in 3D. However, rotations about the many single bonds results in enantiomorphous conformations, albeit with low barriers between them. In 2D, packing of these molecules is complicated by interdigitation of the alkyl chains of neighboring molecules leading to conformations that are chiral or prochiral. Thus, we have categorized these molecules as conformationally chiral adsorbates. The alkyl chains of these molecules make them suitable for the formation of various self-assembly motifs.[329,330] Furthermore, the aromatic groups act as chemical markers allowing easy visualization in 2D using high-resolution STM. Both BBOMB and BBOMA form similar overlayers on HOPG. When monolayers of BBOMB and BBOMA are prepared by deposition from solution onto HOPG followed by evaporation of the solvent, a ''flower'' pattern is observed for both adsorbates (Fig. 32). The difference in contrast between the aromatic and alkyl moieties results from higher tunneling current (brighter contrast) through the aromatic groups than through the alkyl groups.

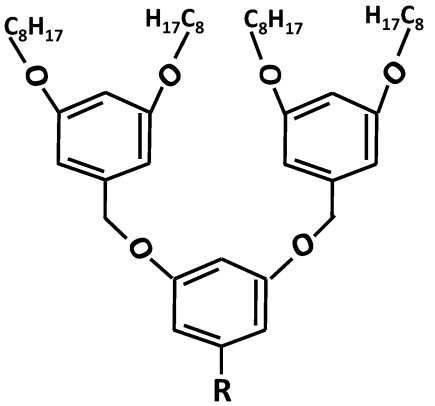

Fig. 31 Molecular structure of 3,5-bis[3,5-bis(octyloxy)-phenyl-methyloxy]-benzyl alcohol (R = CH_2OH) (BBOMB) and 3,5-bis[3,5-bis-(octyloxy)-phenyl-methyloxy]benzaldehyde (R = CHO) (BBOMA). Although achiral in the conformation drawn they can become chiral by rotation about any of the C–O or C–C bonds.

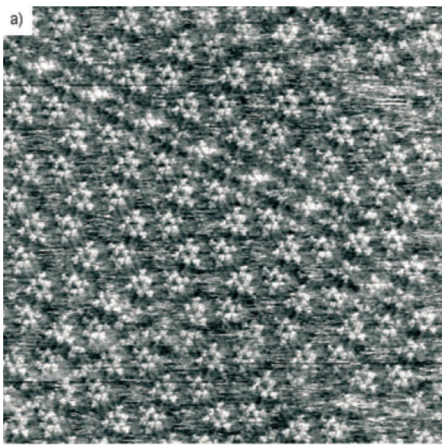

Fig. 32 STM image of a monolayer of BBOMB on HOPG, showing a domain with trimers and a row of dimers. Adapted from ref. 328 Copyright 2005 with permission from John Wiley and Sons.

Fig. 33a is a high-resolution image of the hexagonal flower domain shown in Fig. 32 showing six clusters, each of which is a trimer of BBOMB molecules. To elucidate the ordering of the BBOMB molecules in this hexagonal structure, Merz *et al.* have referred to simulations by Fisher *et al.* that predict the ordering and simulate the STM images of benzene on HOPG substrates.[331] According to those calculations, benzene adopts a configuration with three protrusions imaged *via* STM, thus displaying three-fold symmetry. In Fig. 33a, these three protrusions are circled in the top right cluster of the hexagon. Each of the objects with three protrusions in cluster represents one aromatic ring. Thus, after analysis of ~20 STM images, Merz *et al.* concluded that each of the individual clusters shown in Fig. 33a contains three BBOMB molecules. Using this as a basis, a schematic of the molecular organization forming the hexagonal superstructure was deduced and is shown in Fig. 33b.

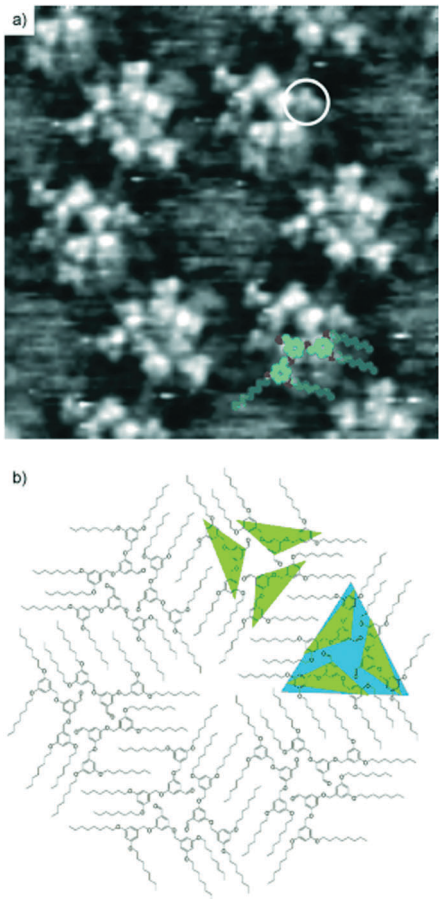

Fig. 33 (a) STM image showing a hexagonal superstructure of six BBOMB trimer clusters. The three protrusions of a single aromatic group are visible in the circle and a ball model of the BBOMB molecule is overlaid on the image. (b) Model of the BBOMB molecules forming the trimer and showing how each trimer is arranged in a hexagonal superstructure. Adapted from ref. 328 Copyright 2005 with permission from John Wiley and Sons.

Each of the individual clusters is a trimer made of three BBOMB molecules and the trimers further organize themselves in to the hexagonal superstructure.

Chirality is exhibited at the molecular level in BBOMB/HOPG. Note that the conformations shown in Fig. 33b and 34 are conformationally chiral as a result of several rotations about C–O and C–C bonds relative to the achiral structure shown in Fig. 31. The BBOMB/HOPG overlayer shown in Fig. 32 is molecularly homochiral.

Chirality is exhibited at the cluster-level by BBOMB/HOPG. Fig. 34 shows a schematic model of the two types of hexagonal superstructures formed by the trimers. All of the six trimers (shown by shaded blue triangles) forming a given hexagonal superstructure have the same orientation and thus, lend a handedness to the hexagonal superstructure. Note that in neither of the trimer assemblies do the triangles point towards the center, rendering the trimers chiral. Since each hexagonal superstructure is made up of only trimers with just one orientation, the system is homochiral at the cluster-level, both in terms of the hexagonal superstructure and the trimers that make up the superstructure. Thus, two levels of cluster-level chirality (at the trimer and the hexagonal level) are observed.

Interdigitation of alkyl chains is observed in many molecules with alkyl side groups. The study by Merz *et al.* illustrates a case in which interdigitation of alkyl chains in conformationally chiral adsorbates leads to adoption of chiral conformations and homochirality at the molecular and cluster levels.

7.2 Rubrene on metal surfaces at G–S interface

Another molecule that has been studied at several G–S interfaces is rubrene (Fig. 35), a polycyclic aromatic hydrocarbon.[332–338] Rubrene consists of a tetracene backbone with two phenyl groups attached to both of the central rings. In the gas phase, rubrene is an axially chiral molecule due to twisting of the tetracene backbone and rotation of the phenyl groups.[335] In spite of its axial chirality, we did not find any references to enantiomers of rubrene existing in the gas phase; probably because the barrier to interconversion between enantiomers is very low in 3D. However, when rubrene is adsorbed on surfaces, it adopts two enantiomorphous configurations. Thus, in our review, rubrene has been included among the conformationally chiral adsorbates. Like PVBA, rubrene has been studied on

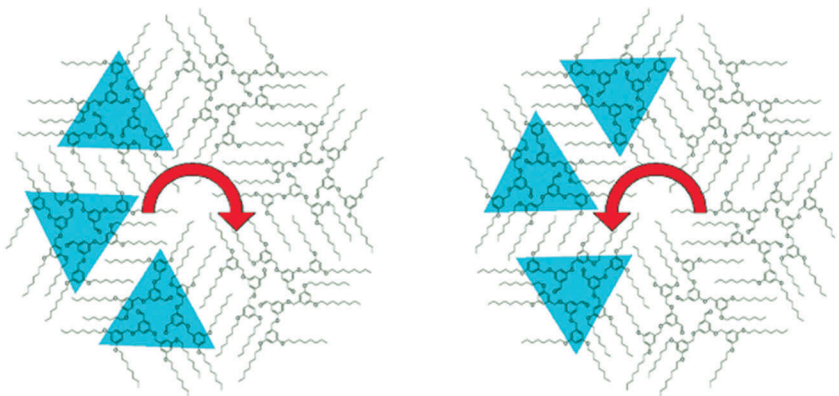

Fig. 34 Mirror image domains formed by BBOMB/HOPG. Each hexagonal structure is comprised of six trimers. The triangles formed by the trimers (colored) do not point to the center of the hexagon thus lending a handedness (CW or CCW) to the hexagonal structure, thereby exhibiting cluster-level chirality. Adapted from ref. 328 Copyright 2005 with permission from John Wiley and Sons.

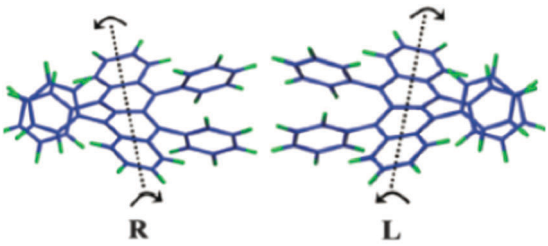

Fig. 35 Molecular structure of rubrene showing *R*- and L-rubrene. In the gas phase, rubrene molecules have their tetracene backbones twisted and phenyl groups rotated out of plane. Reproduced from ref. 332 with permission from the PCCP Owner Societies.

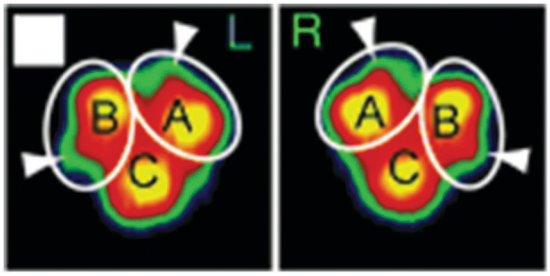

Fig. 36 STM images of isolated rubrene molecules (dimensions of the order of ~1 nm) on Au(111) with the "shoulder" marked by the white arrows used to distinguish between L- and *R*-enantiomers. Adapted from ref. 335 Copyright 2010 with permission from John Wiley and Sons.

several different metal surfaces. In the following sections, we review the chiral overlayers formed by rubrene on Au(111), Ag(111), Ag(100) and Bi(111).

7.2.1 Rubrene on Au(111). Rubrene has been studied on Au(111) by Pivetta *et al.* using coverages ranging from 0.01 ML to saturation.[335,339] The absolute chirality of rubrene adsorbed on both Au(111) and Ag(111) surfaces can be determined by noting the positions of the shoulders on the STM images of isolated rubrene molecules, as shown in Fig. 36. It is not stated how the molecular structure of rubrene explains the appearance of a shoulder. At rubrene/Au(111) coverages in the range 0.01–0.1 ML, one observes isolated rubrene molecules and dimers, trimers and pentamers, (Fig. 37). These clusters are found to be molecularly homochiral *i.e.* they are aggregates of either L- or *R*-rubrene.[339] No heterochiral clusters are observed.

When the coverage of rubrene/Au(111) increases to 0.1–0.15 ML, molecularly homochiral honeycomb islands made up of hexamer rings were observed which gradually disappear as the coverage increases to 0.2 ML and are replaced by 1D pentagon chains.

At coverages above 0.3 ML, islands of rubrene start to appear on the surface (Fig. 38). The circles in Fig. 38 top panel encompass single rubrene molecules. At this stage, when closely-packed islands are observed on the surface, the authors suggest that the individual rubrene molecules can now adopt four different chiral surface conformations, each having two enantiomorphs. These conformers are distinguished from one another based on the positioning of the three lobes (Fig. 36) with respect to each other. However, no insight is provided into what causes rubrene to adopt four different conformations at

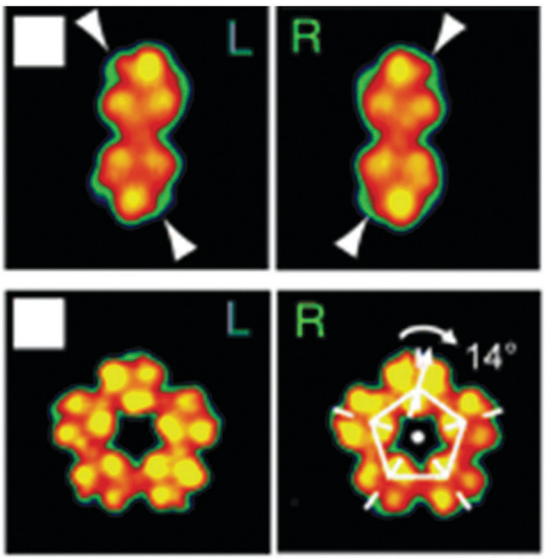

Fig. 37 STM images of different supramolecular clusters of rubrene/Au(111). Top: Dimers of rubrene with L- or *R*-orientation at the cluster level (depending on the placement of the shoulder shown by arrows). Bottom: L- and *R*-pentamers of rubrene. Adapted from ref. 335 Copyright 2010 with permission from John Wiley and Sons.

an intermediate coverage of around 0.3 ML, apart from the suggestion that intermolecular interaction and interaction of monomers with existing supramolecular assemblies (like pentamers) may be responsible.

Fig. 38 bottom left panels show the so called 'D' conformation adopted by rubrene at >0.3 ML coverage. This 'D' conformation is different from the 'A' conformation that was adopted by rubrene at low coverages of (0.01–0.2 ML) as shown in Fig. 36. Similarly, there are 'B' and 'C' conformations. Since both L- and

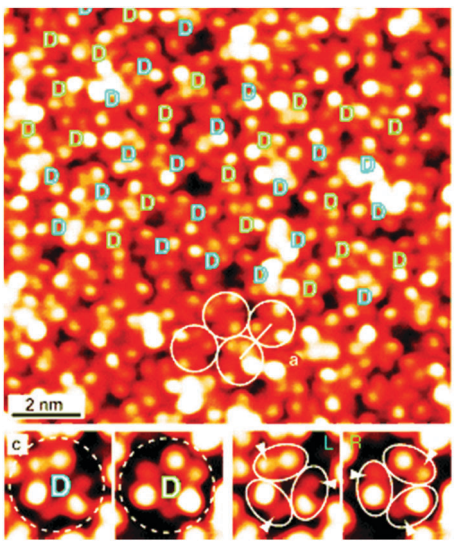

Fig. 38 Top: STM images of close-packed domain of rubrene/Au(111) showing only D conformers in the domain. Different colors represent the two surface enantiomers of rubrene. Bottom: L- and *R*-enantiomers of the D conformer. Adapted from ref. 335 Copyright 2010 with permission from John Wiley and Sons.

R-rubrene adopts the so called "D" conformation, enantiomers of this conformation are possible as shown in the bottom panel of Fig. 38. The top panel of Fig. 38 shows a 2D island formed by adsorbed rubrene. The chirality of the individual rubrene molecules shown in Fig. 38 (top panel) has been determined based on the notation described for the "D" adsorbate conformation shown in the bottom panel of the same figure. The authors claim that Fig. 38 top panel has resolution high enough to reveal that it is molecularly heterochiral *i.e.* both L- and *R*-rubrene molecules are observed in the same domain. The two enantiomers of rubrene, both of which are present in the "D" conformation, are indicated by different colors in Fig. 38 (blue "D" refers to L-rubrene and green "D" refers to *R*-rubrene). There is no mention of how these 2D islands are oriented or registered with respect to the underlying Au(111) lattice and, therefore, lattice chirality could not be determined.

7.2.2 Rubrene on Ag(111) and Ag(100). Compared to the Au(111) surface where several different supramolecular structures of rubrene were observed at low coverages (Fig. 37), there is much less diversity in the self-assembled structures formed by rubrene on the Ag(111) and Ag(100) surfaces.[335] Unlike rubrene/Au(111), rubrene does not form isolated clusters on Ag(100) or Ag(111) surfaces, even at low coverages of ~0.2 ML. Instead, domains are observed that grow in size as the coverage increases. Fig. 39A shows sub-molecular resolution STM images of such domains on Ag(100). These domains are molecularly heterochiral and the enantiomers are distinguished as L- and *R*-rubrene by color in the bottom panel of Fig. 39. A key difference between the domains on Ag(100) and on Au(111) is that the domains on Ag(100) have well-defined long range periodicity and the rubrene surface enantiomers are arranged in a well-ordered fashion. As shown schematically in Fig. 39B, the domain consists of heterochiral rows (direction of row marked with arrow) with molecules in adjacent rows rotated by 180°. The overlayers formed by rubrene on Ag(111) are very similar to those described for Ag(100).

Significant differences in the behavior of rubrene on Au and Ag surfaces at low coverages have been noted; namely the propensity to form isolated clusters on Au(111) in contrast with a tendency for island formation on Ag(100). This difference was attributed to weaker adsorbate–surface interactions on Au(111) than on Ag(100). Also, charge transfer from the rubrene to the Au surface and the higher work function of Au(111) than Ag(100) (~5.2 eV *vs.* 4.5 eV) were hypothesized to lead to dipole formation and repulsion between rubrene molecules on Au(111), hindering island formation at low coverages.

7.2.3 Rubrene on Bi(111). Rubrene was also studied on the Bi(111) surface.[332] Bi exhibits weak adsorbate–surface interactions and is being studied increasingly due to the feasibility of epitaxial growth of organic films.[340] On the Bi(111) surface, isolated rubrene molecules display a chiral image with three-lobes (labeled A, B, C in order of decreasing brightness) shown in Fig. 40. The dimensions of the images (~1 nm) are roughly those of isolated rubrene molecules on Au and Ag surfaces.[335] In one configuration, there is a clockwise arrangement of ABC (*R*-rubrene) while in the other, a counterclockwise arrangement of ABC (L-rubrene). This is similar to the images of isolated rubrene shown in Fig. 36 for Au(111) but without the characteristic shoulder.

When rubrene is deposited on Bi(111) surfaces, it tends to aggregate into 2D islands which grow in size as coverage increases. High-resolution STM images of such islands are shown in the top panels of Fig. 41. Using the designation of absolute chirality shown in Fig. 40, these islands were found to be molecularly homochiral *i.e.* two mirror domains each comprising of just one molecular enantiomorph. The molecular models of the enantiomorphous rubrene adsorption conformations are overlaid on the STM images in the insets of the top panels of Fig. 41. The bottom panel of Fig. 41 illustrates the orientation of rubrene molecules in a (4 × 3) ordered overlayer.

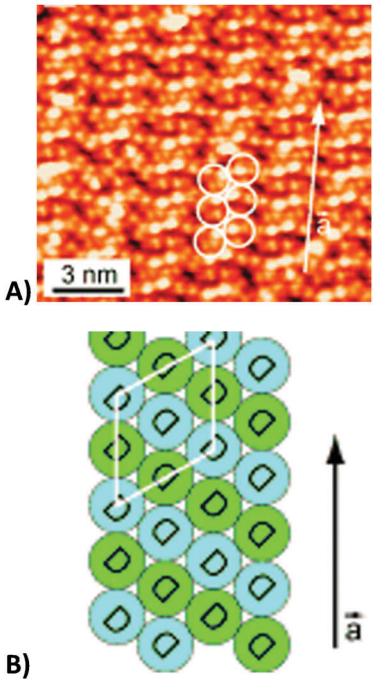

Fig. 39 (A) STM image of rubrene/Ag(100) showing ordered domain. (B) Molecular model of arrangement of rubrene enantiomers in the D conformation in the domain. The domain is molecularly heterochiral containing both L-rubrene (blue) and *R*-rubrene (green). Adapted from ref. 335 Copyright 2010 with permission from John Wiley and Sons.

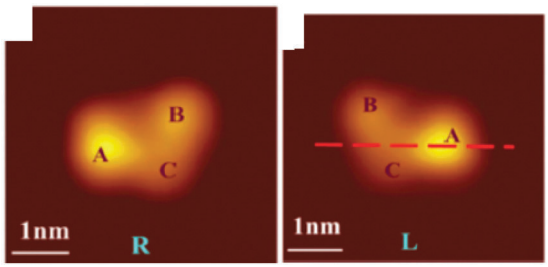

Fig. 40 STM images of isolated rubrene molecules on Bi(111) showing non-superimposable adsorbate conformations. Reproduced from ref. 332 with permission from the PCCP Owner Societies.

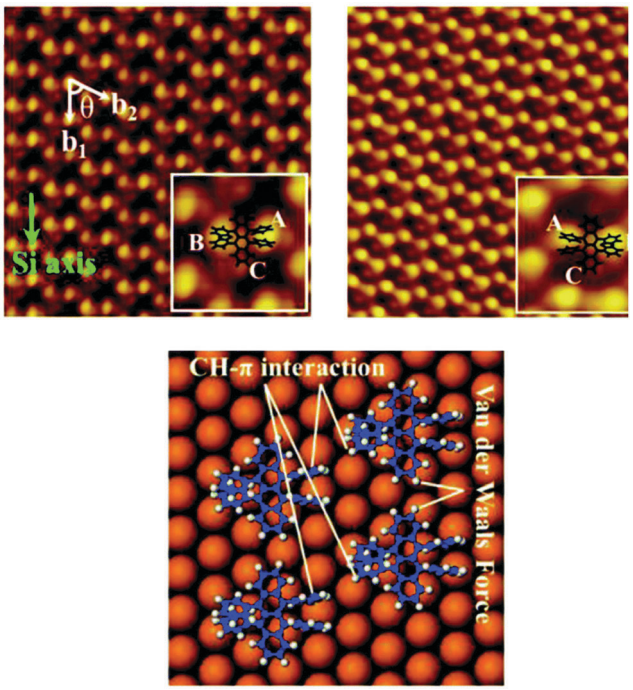

Fig. 41 Top left and right: High-resolution STM images of L- and *R*-domains of rubrene/Bi(111) with the adsorption geometry of rubrene shown in the inset. The substrate lattice direction is marked as SI axis. Bottom: Molecular model of rubrene adsorbed on Bi(111) showing interactions responsible for domain formation like CH–π interaction and van der Waals forces. Reproduced from ref. 323 with permission from the PCCP Owner Societies.

When the Bi(111) surface is annealed at 350 K after depositing rubrene, a new ordered overlayer with a 33.9 Å × 33.4 Å lattice appears that is made up of triangular-shaped clusters of rubrene molecules. This new overlayer also exists in two enantiomorphous domains, as shown in Fig. 42 left and right panels. These domains impart lattice-level chirality while simultaneously exhibiting cluster-level homochirality in that the individual domains are formed only of right- or left-tilted clusters. However, these domains and the clusters of which they are formed are heterochiral at the molecular level, *i.e.* the six rubrene molecules that form each cluster include three molecules of each enantiomer.

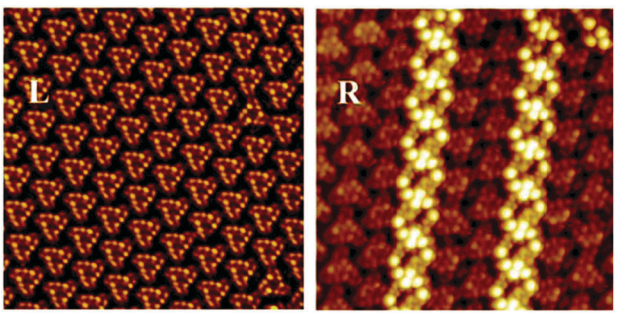

Fig. 42 STM images of L- and *R*-hexamer domains after annealing rubrene/Bi(111) at 350 K. The domains form adjacent to the domains shown in Fig. 41. Reproduced from ref. 332 with permission from the PCCP Owner Societies.

Sun *et al.* suggest that due to weak adsorbate–surface interactions, some of the surface enantiomers in the (4 × 3) ordered homochiral domains flip their chirality during annealing to yield the heterochiral 33.9 Å × 33.4 Å lattice.

7.3 Overview of conformationally chiral adsorbates

In this section, we review our findings on the type of chiral aggregation observed in the case of conformationally chiral adsorbates. Table 3 lists all the systems categorized as conformationally chiral adsorbates. On L–S interfaces, we find only 4 instances of molecular chirality being expressed on the surface while all but one of the systems express cluster-level chirality, with a clear preference for homochirality at the cluster level (11 systems with homochirality *vs.* only 2 reporting heterochirality at the cluster-level). Almost all systems exhibit lattice-level chirality. Given that most of the conformationally chiral adsorbates studied at L–S interfaces are not conventionally chiral, *i.e.* do not exist as stable enantiomers in 3D, molecular homochirality is not expected to feature prominently in this group. The only system at L–S interfaces where no lattice- or cluster-level chirality was observed was the MMOMC/HOPG system, in which the enantiomorphous domains were found to be related by six-fold symmetry with respect to the HOPG lattice direction.

For conformationally chiral adsorbates at G–S interfaces, there were a significantly higher number of instances of molecular level chirality than observed at L–S interfaces (17 *versus* 4) with 11 out of those 16 systems reporting molecular-level heterochirality and the remaining 6 reporting homochirality. A large contribution to these numbers comes from rubrene and oligophenylene derivatives, which were observed to adopt non-superimposable mirror-image configurations on metal surfaces. In addition to molecular-level chirality, more than half the systems showed cluster- and lattice-level chirality. We now mention some specific systems.

In their study of bis-dehydrobenzo[12]annulene derivatives on HOPG, Tahara *et al.* found that self-assembly on surfaces can be tuned by carefully controlling the concentration of the adsorbate in the solution.[341] A number of different homochiral and heterochiral structures were observed on the surface as the concentration and the alkyl chain length were varied.

Our survey also revealed systems where the overlayer structures of conformationally chiral adsorbates are kinetically hindered. For example, Jiang *et al.* deposited boron subphthalocyanine on Au(111) and found that depending on the deposition temperature, different types of ordered surface structures, ranging from honeycomb to diamond pattern, along with different levels of chiral expression can be observed.[342] In a study by Cheng *et al.*, a temperature driven transition from achiral structures into enantiomorphous structures was observed for biphenyl triazine molecules on HOPG.[343] When deposited on HOPG, initially only achiral structures are formed but when heated to 55–60 °C, the monolayer self-assembles into large domains that are made up of chiral clusters with only one enantiomorph present in each domain, thus leading to a cluster-level homochiral and lattice-level chiral overlayer.

Table 3 List of conformationally chiral adsorbate–surface systems at L–S and G–S interfaces

Surface	Adsorbate	Mol-homo	Mol-hetero	Clus-homo	Clus-hetero	Lattice chiral	RSS	No organiz.	Ref.
At L–S interfaces									
HOPG	BBOMA	✓		✓		✓			328
HOPG	BBOMB	✓		✓		✓			328
HOPG	BTD			✓		✓			343
HOPG	TTD			✓		✓			343
HOPG	DBA-decyl			✓		✓			341
HOPG	DBA-undecyl			✓		✓			341
HOPG	DBA-tetradecyl			✓	✓	✓			341
HOPG	DBA-hexadecyl			✓	✓	✓			341
HOPG	DBA-decyloxy			✓		✓			341
HOPG	DBA-nonyloxy			✓		✓			341
HOPG	TOPE					✓			277
HOPG	MMOMC	✓							232
HOPG	Arachidic anhydride	✓				✓			346
HOPG	BIC			✓		✓			347
Total for liquid–solid interfaces		**4**	**0**	**11**	**2**	**13**	**0**	**0**	
Surface	Adsorbate	Mol-homo	Mol-hetero	Clus-homo	Clus-hetero	Lattice chiral	RSS	No organiz.	Ref.
At G–S interfaces									
Ag(100)	Rubrene		✓						335
Ag(111)	CpCB					✓			348
Ag(111)	Rubrene		✓						335
Ag(111)	Tetrapyridyl-porphyrin			✓		✓			349
Au(100)	Rubrene	✓	✓			✓			335
Au(111)	6-Nitrospiropyran		✓				✓		345
Au(111)	8-Nitrospiropyran		✓	✓		✓			215
Au(111)	CpCB			✓		✓			342
Au(111)	*m*OPE		✓		✓				344
Au(111)	ONE		✓			✓			350
Au(111)	*p*OPE	✓	✓	✓	✓	✓			344
Au(111)	Rubrene	✓	✓						335
Au(111)	sOPE	✓	✓	✓	✓				344
Bi(111)	Rubrene	✓	✓	✓		✓			332
Cu(100)	Lander molecule	✓				✓			351
Cu(100)	Rubrene			✓		✓			336
Cu(111)	Rubrene			✓		✓			337
Total for gas–solid interfaces		**6**	**11**	**8**	**3**	**11**	**1**	**0**	

Abbreviations: BBOMA, 3,5-bis[3,5-bis(octyloxy)phenylmethyloxy]benzyl alcohol; BBOMB, 3,5-bis[3,5-bis-(octyloxy)phenylmethyloxy]benzaldehyde; BTD, biphenyl 1,3,5-triazine-2,4-diamine; TTD, triphenyl 1,3,5-triazine-2,4-diamine; DBA-decyl, decyl-substituted bis-dehydrobenzo[12]annulene; DBA-undecyl, undecyl-substituted bis-dehydrobenzo[12]annulene; DBA-tetradecyl, tetradecyl bis-dehydrobenzo[12]annulene; DBA-hexadecyl, hexadecyl bis-dehydrobenzo[12]annulene; DBA-decyloxy, decyloxy bis-dehydrobenzo[12]annulene; DBA-nonyloxy, nonyloxy bis-dehydrobenzo[12]annulene; CpCB, chloro[subphthalocyaninato]boron(III); BIC, 5-(benzyloxy)-isophthalic acid derivative; TOPE, *t*-oligo(*p*-phenylene vinylene) derivative; ONE, oligo(naphthylene–ethynylene)derivative; MMOMC, 1-[5′-(5″-methylthien-2″-yl)-2′-methylthien-3′-yl]-2-[5′-(5″-octadecylthien-2″-yl)-2′-methylthien-3′-yl]cyclopentene; *m*OPE, *meta*-oligo-phenylene-ethynylene; *p*OPE, *para*-oligo-phenylene-ethynylene; *s*OPE, *spoke*-oligo-phenylene-ethynylene. Structures of all molecules listed in Table 8 are available in Appendix A.

In many cases, STM data has been supplemented by DFT simulation. For example, enantiomers of the adsorbed dithienylethene derivative (MMOMC, shown in Appendix A) cannot be distinguished easily on HOPG using STM. Therefore, MD calculations of its homochiral/heterochiral dimers were used to show that the homochiral dimer is more stable than the heterochiral dimer on the HOPG surface.[232] One of the barriers to forming long range ordered domains of chiral adsorbates with molecular-level homochirality is low surface diffusion; either as a result of large molecular size or adsorbate–surface interaction.[242] Busse *et al.* have shown that for large conformationally chiral molecules like oligo-phenylene-ethynylene derivatives (OPE), molecules can switch chirality in order to form molecular-level homochiral domains without the need for enantiomer diffusion. In the specific case of OPE's, this switching has been demonstrated using STM and is interpreted to occur when the end group around a molecular spoke of the OPE molecule rotates leading to the *tert*-butyl groups orienting in the opposite direction.[344] Another molecule, 6-nitrospiropyran demonstrates the opposite behavior on Au(111), *i.e.* heterochirality at the handedness level while forming a RSS at the footedness level.[345] This is opposite to what was observed in the proline/Cu(110) system.[264]

8. Enantiospecific aggregation of achiral adsorbates

This section is devoted to studies of achiral adsorbates that are neither prochiral nor conformationally prochiral in 3D. As illustrated in Fig. 6–9, achiral adsorbates can form chiral structures on surfaces and exhibit chirality at the cluster- and lattice-level. They do not exhibit molecular chirality as adsorbates but they can be considered surface enantiomers, if they adsorb on a surface in such a way that they break the underlying symmetry of the substrate. In that sense they can exhibit molecular-level chirality.

In our survey, we have found 16 achiral adsorbate–surface systems exhibiting some level of chirality at G–S interfaces. The number of achiral adsorbate–surface systems reviewed is lower than the numbers of adsorbate–surface systems surveyed in Sections 5–7. This is because we include only those studies in which the expression of chirality by achiral adsorbates has been explicitly discussed by the authors. There are undoubtedly, many other examples in the literature of achiral adsorbates having been probed on surfaces but the chiral aspects of such systems were not discussed. We did not find any relevant examples of achiral adsorbates on L–S interfaces to include in this review. The molecular structures of the achiral adsorbates reviewed in this section are summarized in Table 9 in the appendix.

At G–S interfaces, ~75% of all studies were conducted on single crystal Au and Cu surfaces with the remainder on single crystal Ag and Bi surfaces. The adsorbates studied include phthalocyanines, porphyrins and succinic acid ($HO_2C(CH_2)_2CO_2H$).

For detailed discussion, we have chosen the Ni-tetramethyl-tetraaza[14]annulene/Au(111) system that demonstrates that coverage-driven transitions from heterochiral to homochiral packing can be observed for achiral adsorbates.[352]

8.1 Ni-Tetramethyl-tetraazaannulene/Au(111) at G–S interface

The last system we will discuss is the adsorption of achiral Ni-tetramethyl-tetraazaannulene (Ni-TMTAA, Fig. 43) on Au(111).[352] This molecule is not planar but does have two perpendicular mirror planes. It forms chiral overlayers and exhibits a coverage-driven transition at the cluster level from heterochiral to homochiral assembly over the coverage range 0.2–0.8 ML. The structure of Ni-TMTAA is shown in the Fig. 43. Simulations of the electron density distribution of adsorbed Ni-TMTAA were

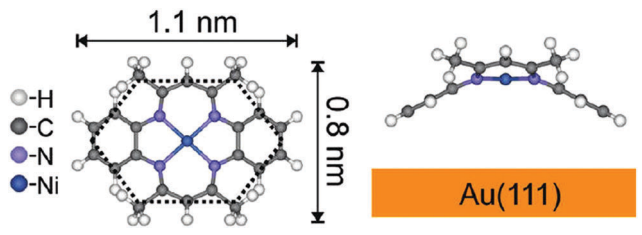

Fig. 43 Left: Molecular structure Ni-tetramethyl-tetraazaannulene (Ni-TMTAA). Right: Adsorption of Ni-TMTAA in a saddle shape on Au(111) is shown with the benzene rings pointing downwards. Adapted with permission from ref. 352 copyright 2010 American Chemical Society.

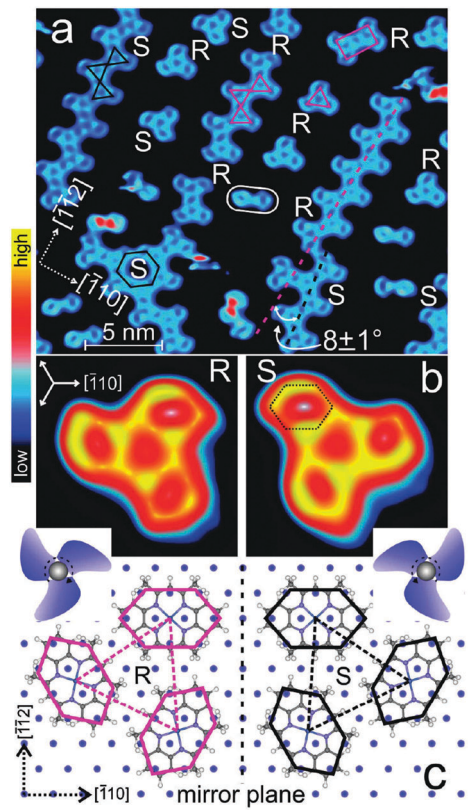

Fig. 44 Top: Ni-TMTAA on Au(111) at 0.3 ML showing *R* and *S* shaped isolated trimers and trimers arranged in linearly attached end to end. Middle: Pseudo-3D representation of the STM image of the *R*- and *S*-trimer. Bottom: Molecular model of *R*- and *S*-trimer showing the arrangement of methyl groups whose orientation minimizes steric repulsion. Adapted with permission from ref. 352 Copyright 2010 American Chemical Society.

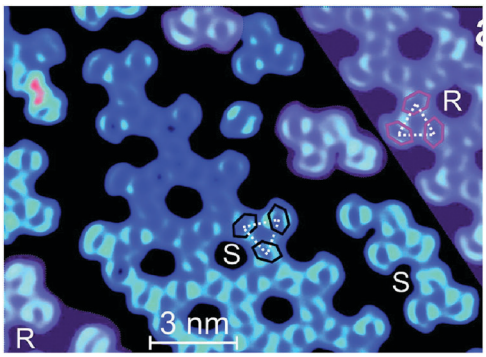

Fig. 45 STM image of Ni-TMTAA/Au(111) showing honeycomb shaped islands of *S*- and *R*-domains at 0.5 ML. Adapted with permission from ref. 352 Copyright 2010 American Chemical Society.

compared with STM images to deduce that Ni-TMTAA adsorbs with the terminal benzene rings pointed towards the surface as shown in the right panel of Fig. 43.

In STM images, a single Ni-TMTAA molecule is shaped like an elongated hexagon. The dimensions match those of the Ni-TMTAA molecule shown in Fig. 43 left panel. Fig. 44A shows an STM image of Ni-TMTAA/Au(111) at a coverage of 0.3 ML. Triangular structures marked *R* and *S* as well as rows comprised of multiple triangular structures are observed. These triangular structures are trimers of Ni-TMTAA. Fig. 44B is a representation of this structure showing two types of trimers forming a hexagonal structure marked with dotted line on the *S*-trimer. The orientation of the Ni-TMTAA molecules in the trimers renders these clusters chiral. Thus, cluster-level chirality (at the level of trimers) is expressed. At a coverage of 0.3 ML, both *R* and *S* trimers are observed in close proximity; hence Ni-TMTAA/Au(111) is categorized as cluster-level heterochiral. As the coverage of Ni-TMTAA increased from 0.3 ML to 0.8 ML, the trimers were observed to aggregate and form honeycomb shaped domains as shown in Fig. 45. These domains are comprised of either *R*- or *S*-trimers and are, hence, cluster-level homochiral.

To understand why chiral trimers (and not symmetric achiral trimers) are formed from achiral Ni-TMTAA/Au(111), the binding energies of chiral and achiral trimers were calculated using force field simulations.[352] The interaction energies of chiral trimers were found to be 5 times stronger than those of achiral trimers (10 *vs.* 2 kJ mol^{-1}). This, coupled with the weak adsorbate–surface interaction of Au(111) contributed to the formation and stabilization of chiral structures. As further evidence of the influence of adsorbate–surface interactions on chiral aggregation, Ni-TMTAA/Cu(111) was not found to show any chiral ordering. This was attributed by the authors to strong adsorbate–surface interaction on Cu(111) as compared to Ni(111).[353]

8.2 Overview of achiral adsorbates in 2D

Table 4 summarizes the achiral adsorbate–surface systems reviewed. It is interesting to note that most of the adsorbates in this group are fairly large molecules (with the exception of succinic acid). The totals at the end of Table 4 show that at the cluster-level, there is a very clear preference for homochiral over heterochiral aggregation. At the cluster level, there are 12 examples of homochiral *vs.* 4 examples of heterochiral. 14 systems were categorized as exhibiting lattice chirality.

A few systems demonstrate molecular level chirality following adsorption of achiral molecules. This has been observed when succinic acid ($C_4H_6O_4$) and coronene derivatives have been deposited on Cu(110).[70,354,355] When succinic acid was deposited on Cu(110), chiral lattices (Fig. 46A) were observed. This chirality was interpreted to arise from a combination of Cu surface reconstruction and distortion of the adsorbed

Table 4 List of achiral adsorbate–surface systems at G–S interfaces

Surface	Adsorbate	Mol-homo	Mol-hetero	Clus-homo	Clus-hetero	Lattice chiral	RSS	No organiz.	Ref.
At G–S interfaces									
Ag(100)	Copper phthalocyanine	✓	✓	✓	✓	✓			356
Ag(111)	Dicarbonitrile-penta(phenyl)			✓		✓			357
Ag(111)	Dicarbonitrile-quart(phenyl)			✓		✓			357
Au(111)	CPBPB			✓		✓			358
Au(111)	4,4′-Biphenyldicarboxylic acid			✓		✓			145
Au(111)	PhDAT			✓	✓	✓			359
Au(111)	Ni-TMTAA			✓	✓				352
Bi(111)	Pentacene			✓		✓			360
Cu(110)	Co(II)-Tetraphenylporphyrin			✓		✓			361
Cu(110)	Corannulene					✓			362
Cu(110)	HtB-HBC			✓		✓			355
Cu(110)	Succinic acid	✓	✓			✓			354 and 70
Cu(111)	TPCA			✓		✓			363
Cu(111)	CBC			✓		✓			364
Cu(100)	Zinc phthalocyanine	✓	✓		✓				365
Cu(110)	(*R*,*S*)-Tartaric acid	✓				✓			184
Total for gas–solid interfaces		**4**	**3**	**12**	**4**	**14**	**0**	**0**	

Abbreviations: CPBPB, 1,3,5-trikis(4′-carboxylphenyl)-2,4,6-trikis(4′-*tert*-butylphenyl)-benzene; PhDAT, 6-phenyl-2,4-diamino-1,3,5-triazine; Ni-TMTAA, nickel tetramethyl-tetraazaannulene; HtB-HBC, 2,5,8,11,14,17-hexa-*tert*-butylhexabenzo[*bc*,*ef*,*hi*,*kl*,*no*,*qr*]coronene; TPCA, 2,2′:6′,2″-terpyridine-4′-carboxylic acid; CBC, hexa-cata-hexabenzocoronene. Structures of all molecules listed in Table 6 are available in Appendix A.

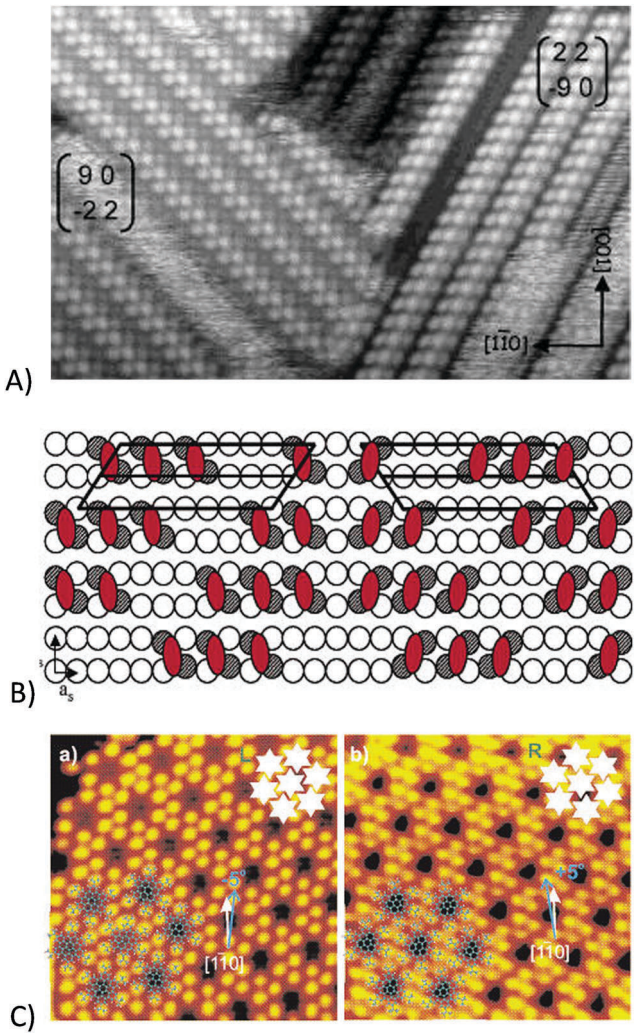

Fig. 46 (A) STM images of succinic acid deposited on Cu(110) with the two mirror image domains (9 0; −2 2) and (2 2; −9 0) shown. (B) Model showing succinate molecules (red ovals) adsorbed on Cu substrate (white circles) with the locally reconstructed Cu atoms (grey circles). Adapted with permission from ref. 70 Copyright 2004 American Chemical Society. (C) STM image of HtB-HBC molecules on Cu(110). The star shape model of the molecule is superimposed on the STM image to show that clusters form two mirror image domains on Cu(110) (shown in the left and right panel), with each domains rotated by ±5° with respect to the underlying Cu(110) lattice. Reprinted with permission from ref. 355 Copyright (2006) American Chemical Society.

succinate, a molecular model of which is shown in Fig. 46B. In case of the coronene derivative hexa-*tert*-butyl-hexabenzocoronene (HtB-HBC) adsorbed on Cu(110) shown in Fig. 46C, formation of a close-packed adlayer forces the star-shaped molecule to adopt two enantiomorphous lattices with respect to the substrate lattice.[70,354,355]

Mugarza *et al.* reported the interesting observation of achiral Cu-phthalocyanine (Cu-PC) ($CuC_{32}H_{18}N_8$, structure in appendix A) adopting chiral conformations as a function of STM bias when deposited on Ag(111).[356] Cu-PC is achiral but on the surface, when imaged *via* negative STM bias, individual molecules appear to have chiral structures. When the bias is changed to positive, the chiral structure is replaced by an achiral structure. The authors suggest that distortion of the highest occupied molecular orbital (HOMO) as a result of the interaction of the benzyne groups of the adsorbate with the surface leads to an asymmetry between the HOMO lobes. This asymmetry results in a chiral image of the adsorbate at negative STM bias. Interestingly, even though the observed chirality is of electronic origin, a coverage dependent transition at the cluster-level from heterochiral to a globally homochiral overlayer is observed for Cu-PC/Ag(111). This transition is facilitated by easy switching of surface-induced chirality given the achiral nature of the molecule.

In conclusion, this section has described chiral expression by achiral adsorbates. The available information suggests that homochirality is strongly favored at the cluster-level while lattice chirality is expressed by all 16 systems considered.

9. Conclusion and outlook

We have made the first attempt to review comprehensively all studies of chiral molecular adsorbates on surfaces and to probe their tendency towards homochiral or heterochiral aggregation in 2D. Given the large number of studies dealing with a variety of adsorbates, the adsorbate–surface systems covered by this review have been arranged into four different groups depending on the structure of the adsorbate; chiral, prochiral, conformationally chiral or achiral. All adsorbate–surface systems belonging to these four groups have been categorized based on their tendency to exhibit homochiral or heterochiral aggregation at the molecular level, homochiral or heterochiral aggregation at the cluster level, and whether they exhibit long range order in lattices that are chiral.

One of the primary goals of this review has been to determine whether there is a propensity for chiral adsorbate systems to adopt homochiral over heterochiral structures. As discussed in the introduction section, this fundamental question regarding the nature aggregation of chiral species on surfaces is relevant to utility of surface chirality in enantioselective chemical processing. In the late 19th century, it was suggested that racemic mixtures of chiral molecules in 3D prefer to crystallize as racemates because heterochiral packing has higher density and hence thermodynamic stability, a hypothesis whose validity is in doubt given the large number of observations that deviate from this behavior. It was later hypothesized that on surfaces, molecules would favor conglomerate (homochiral) packing due to the reduced symmetry of the surface environment. The summary in Table 5 represents the first systematic attempt to test this general hypothesis.

One key finding of this review is that based on the current state of knowledge, there is no evidence of a strong preference of chiral, prochiral or conformationally prochiral adsorbates to aggregate either homochirally or heterochirally at the molecular level. The numbers tabulated at the end of Table 5, indicate a roughly 50% probability for molecular level homochiral aggregation. This observation does indicate a difference between the behavior of chiral adsorbates on surface and the

Table 5 Summary of adsorbate aggregation behavior

Table	Adsorbate type	# Systems	Mol-homo	Mol-hetero	Cluster-homo	Clus-hetero	Lattice chiral	RSS	No organization
1	Chiral	51	21	22	6	5	20	6	9
2	Prochiral	56	32	24	14	9	36	4	2
3	Conf. chiral	31	10	11	19	5	24	1	0
4	Achiral	16	4	3	12	4	14	0	0
	All	**154**	**67**	**59**	**51**	**23**	**93**	**11**	**11**

known propensity of chiral molecules to crystalize in 3D into racemate rather than conglomerate structures. In contrast, when adsorbates form chiral clusters there does seem to be a $\sim 2:1$ tendency of those clusters to favor homochiral aggregation over heterochiral aggregation (Table 5).

Based on the data assimilated and analyzed in this review, it is clear that chiral assembly on surfaces is a very complex phenomena, with multiple parameters affecting the packing of chiral overlayers. For example, temperature has been observed to have a marked effect on overlayer chirality in many cases.[299,308,313,332,343] Changing the coverage of chiral adsorbate mixtures has been observed to lead to transitions in chirality expressed in adsorbed species.[153,188,220,284,298,335] Given these observations, we believe that the complexity of chiral aggregation on surfaces cannot be captured by hypotheses based on single criteria (*e.g.* surface packing density) and that a more holistic understanding of the energetics of adsorbate–surface systems will be needed to predict their tendencies towards homochiral or heterochiral aggregation.

One common suggestion from the studies spanning all four groups of adsorbates is that hydrogen bonding and van der Waals interactions are the dominant forces responsible for chiral aggregation. In many cases, it was suggested that a subtle balance between the various forces leads to transitions in phase and behavior when macroscopic parameters such as coverage, ee, or temperature are varied.

We conclude by taking a look at challenges yet to be tackled in the field of adsorbate-induced surface chirality. The stability of self-assembled structures is critical for their application in devices like organic transistors and bio-sensors and has been discussed in the general context by many researchers.[366–370] If an application involves enantiospecific properties of chiral overlayers, then the stability of the chirality manifested by organic overlayers will be critical. In most of the studies that we have reviewed, we did not find that stability of the homo- or hetero-chiral overlayer has yet emerged as an area of focus. We attribute this to the focus on deciphering the fundamentals of chiral aggregation. However, understanding stability issues will be crucial, if chiral structures are to be incorporated into functional devices or processes. Yet another challenge is the controlling and tuning of chiral self-assembly to obtain desired surface structures. On this front, attempts are continually being made to determine how parameters including ee and temperature play a role in determining chirality. What is needed are systematic attempts to determine full chiral phase diagrams as a function of coverage, ee, and temperature that will yield insights into the parameters that dictate surface chirality and need to be included in models of these phenomena. Some progress has been made in the use of theoretical methods and simulations to predict self-assembly; however, first principles-based calculations have not yet been able to resolve the subtle differences in enantiospecific adsorption energies and other surface reaction energetics that have been observed experimentally. These limitations in the accuracy of molecular simulation hinder the prediction and rational design of chiral self-assembled structures.

Abbreviations

[7]H	heptahelicene
2D	Two-dimension
3D	Three-dimension
A[6]H	5-Amino-hexahelicene
Ala	alanine
Asp	aspartic acid
BBOMA	3,5-Bis[(3,5-bisoctyloxyphenyl)-methyloxy]benzyl alcohol
BBOMB	3,5-Bis[(3,5-bisoctyloxyphenyl)methyloxy]-benzaldehyde
BTAA - 11	1,5-Bis-(3′-thia-tetradecyl)anthracene
BTAA - 12	1,5-Bis-(3′-thia-pentadecyl)anthracene
D-/L-	dextro-/levo-(enantiomer designation based on Fischer convention)
DFT	Density functional theory
ee	Enantiomeric excess
Gly	glycine
G–S	Gas–solid
HOPG	Highly oriented pyrolytic graphite
L–B	Langmuir–Blodgett
LEED	Low energy electron diffraction
L–S	Liquid–solid
M-/*P*-	minus-/plus-(enantiomer designation for helically chiral molecules)
MD	Molecular dynamics
MHPOBC	4-[(1-Methylheptyloxy)carbonyl]phenyl 4-octyloxy-4-biphenylcarboxylate
ML	Monolayer (maximum value is 1 ML representing saturation coverage)
NEXAFS	Near-edge extended absorption fine structure spectroscopy
Ni-TMTAA	Ni-Tetramethyl-tetraazaannulene
PED	Photoelectron diffraction
Phe	phenylalanine
Pro	proline

PVBA	4-[*trans*-2-(Pyrid-4-yl-vinyl)]benzoic acid
R-/*S*-	rectus-/sinister-(enantiomer designation based on the Cahn–Ingold–Prelog convention)
RAIRS	Reflection absorption infrared spectroscopy
RSS	Random solid solution
Ser	serine
STM	Scanning tunneling microscopy
TA	tartaric acid
UHV	Ultra-high vacuum
XPS	X-ray photoelectron spectroscopy
θ	Fractional coverage

Conflicts of interest

There are no conflicts to declare.

Appendix A

Table 6 Chiral adsorbates

1-(1-Naphthyl) ethylamine	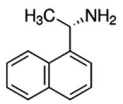
1,1′-Binaphthalene-2,2′-dithiol	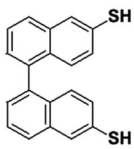
1,2 Dihydroxy-octadecane	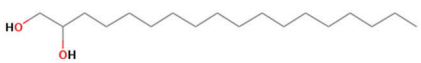
[11]Anthrahelicene	
2-Butanethiol	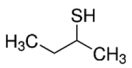
3-Pyrroline-2-carboxylic acid	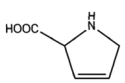
5-Amino[6]helicene	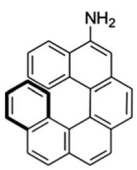
9,10-Diiodo-octadecan-1-ol	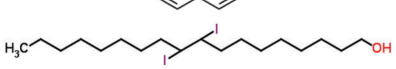
Alanine	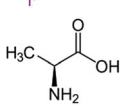
Aspartic acid	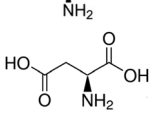

Table 6 (*continued*)

BINAC	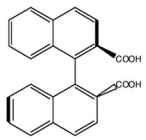
Chiral trigonal prism molecule	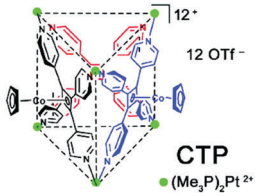
Cyano-heptahelicene	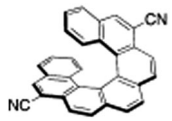
Cysteine	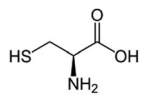
Di-phenylalanine	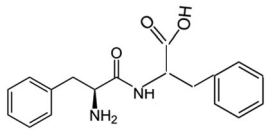
Formamide with ester	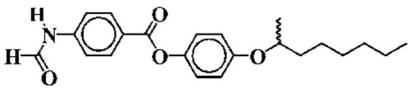
Heptahelicene	
Heptahelicene-2-carboxylic acid	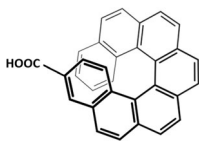
Malic acid	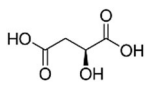
MHPOBC	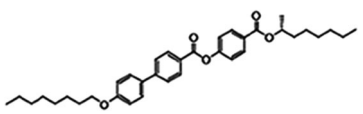
Nonacosane-10-ol	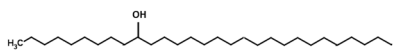
Oleic acid diiodide	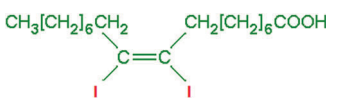
OPA	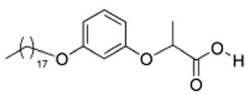

Table 6 (*continued*)

OPV 3I	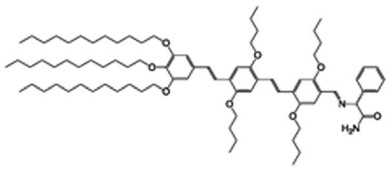
Phenylalanine	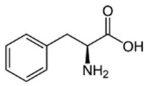
Phenylglycine	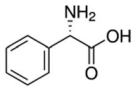
Proline	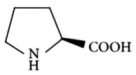
Propylene oxide	
QUINAP	
Resorcinol ether derivative	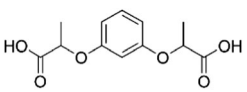
Serine	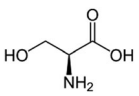
Tartaric acid	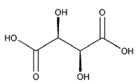
Thia[11]heterohelicene	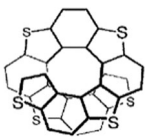
Tryptophan	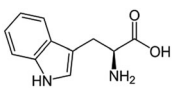
Tyrosine	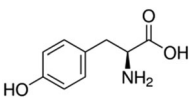

Note: some molecular structures of intrinsically chiral molecules, especially those listed in Table 6, only show one enantiomer. This is not meant to suggest that this was the only enantiomer studied. Both enantiomers were adsorbed as a racemic/non-racemic mixture. Only one enantiomer has been shown because the primary purpose of the table is to serve as a reference for the adsorbate molecular structure.

Table 7 Prochiral adsorbates

1,2,4-Benzenetricarboxylic acid	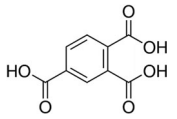
18-18HSQ	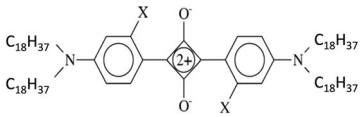
1-Nitronaphthalene	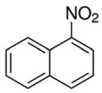
2,5-Dichlorothiophenol	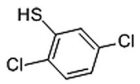
2,6-Dibromo-anthraquinone	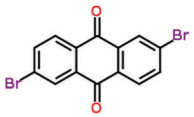
9-Ethynylphenanthrene	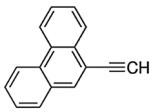
Adenine	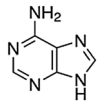
AOPV	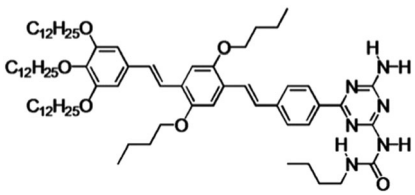
B	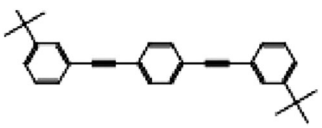
BA	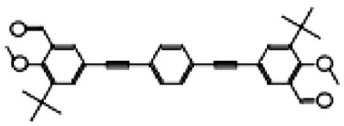
BH	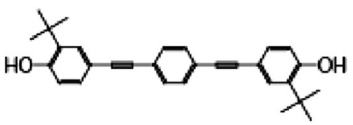
BHA	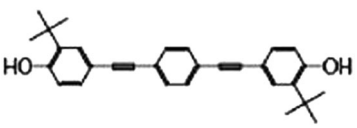
BTAA-11	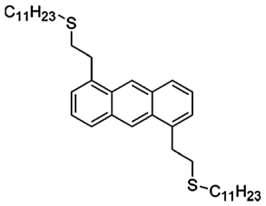

Table 7 (*continued*)

BTAA-12	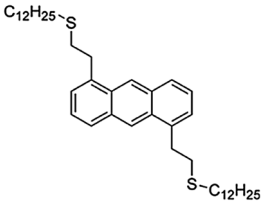
DMHA	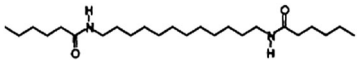
DOB	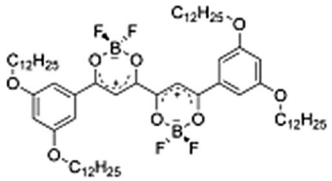
Eladeic acid iodide	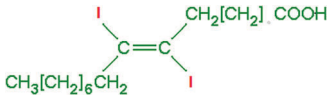
Fluorene-1-carboxylic acid	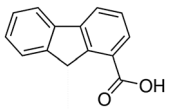
Formamide derivative	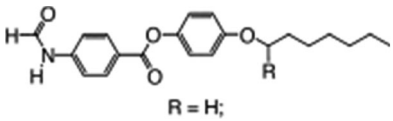
Furan oligomer	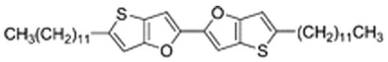
Glycine	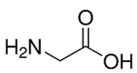
Heptadecanoic Acid	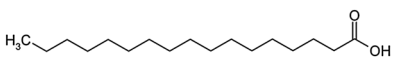
HPOBC	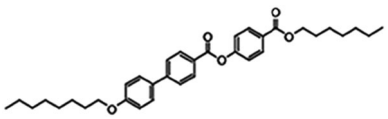
Indigo	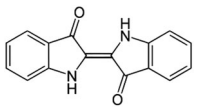
N,*N*′-Dihexadecylquinacridone	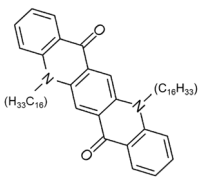
Naphtho[2,3-*a*]pyrene	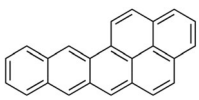
OPV 2	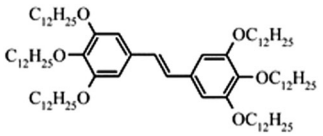

Table 7 (*continued*)

OPV C5	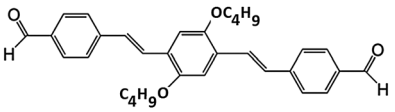
OPV3-CHO	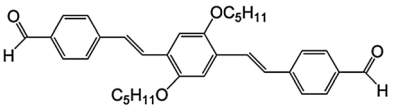
OPV4-CHO	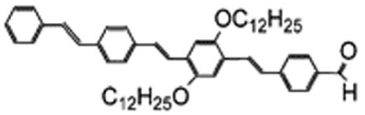
Propene	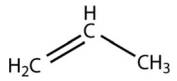
PVBA	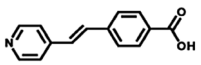
Stilbene dicarboxylic acid	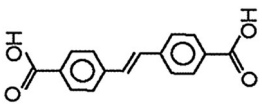
Styrene	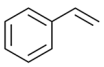
Tetraacid 3A	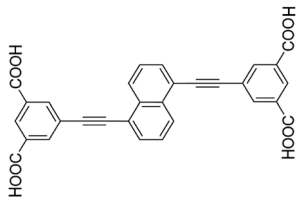
Tetraacid 4A	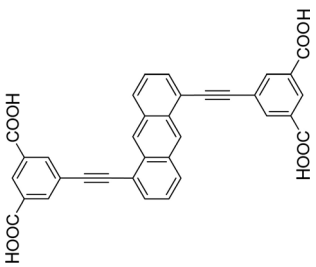
Tetraester 3b	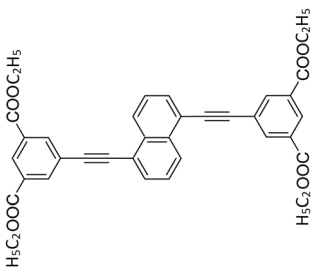
Tetraester 4b	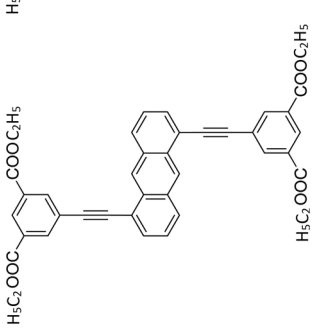

Table 7 (*continued*)

TPTZ	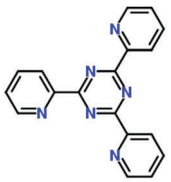
Xanthine	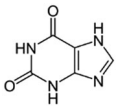
α-Sexithiophene	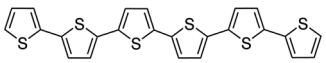

Note: some molecular structures of intrinsically chiral molecules, especially those listed in Table 6, only show one enantiomer. This is not meant to suggest that this was the only enantiomer studied. Both enantiomers were adsorbed as a racemic/non-racemic mixture. Only one enantiomer has been shown because the primary purpose of the table is to serve as a reference for the adsorbate molecular structure.

Table 8 Conformationally chiral (CC) adsorbates

6-Nitrospiropyran	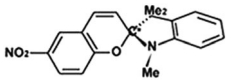
8-Nitrospiropyran	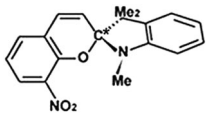
Arachidic anhydride	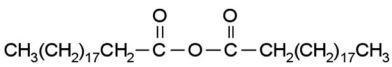
BBOMA	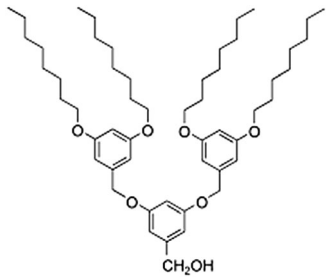
BBOMB	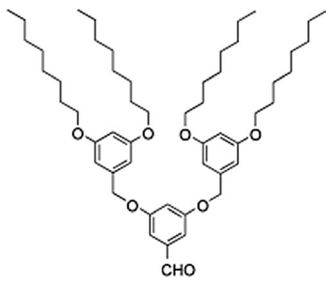
BIC	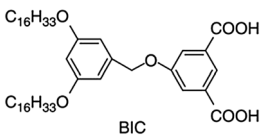
BTD	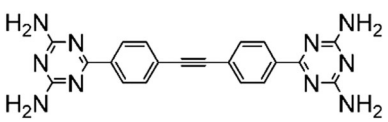

Table 8 (*continued*)

CpCB	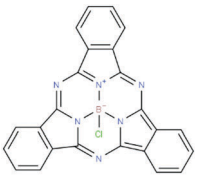
DBA-decyl	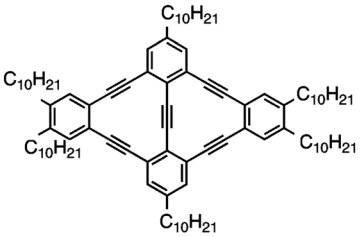
DBA-undecyl	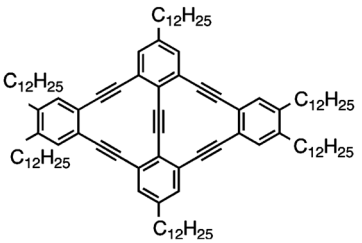
	1b
DBA-tetradecyl	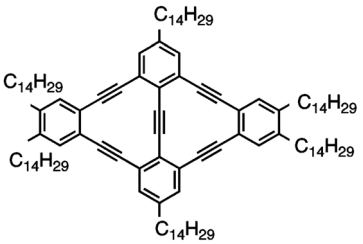
DBA-hexadecyl	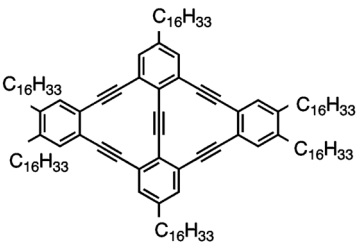
DBA-decyloxy	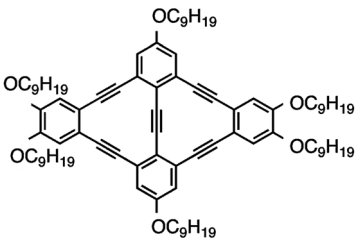
DBA-nonyloxy	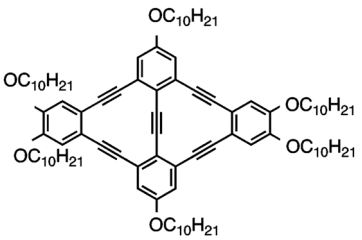

Table 8 (*continued*)

Lander molecule	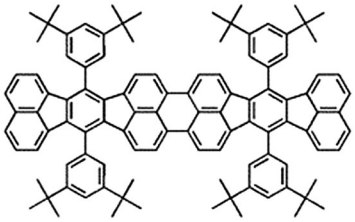
MMOMC	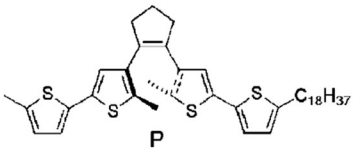
*m*OPE	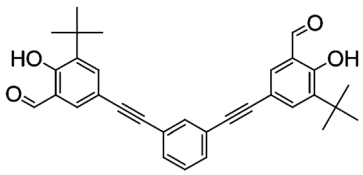
ONE	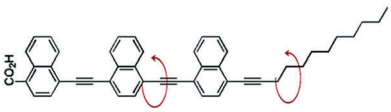
*p*OPE	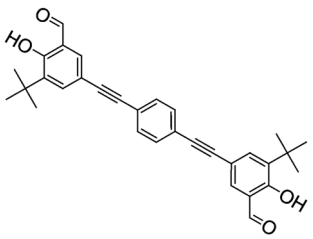
Rubrene	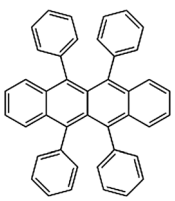
*s*OPE	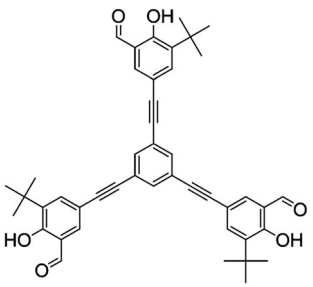
Tetrapyridyl-porphyrin	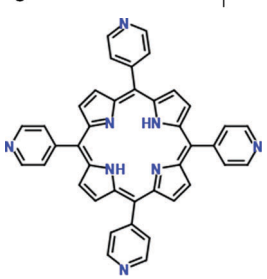

Table 8 (*continued*)

TOPE	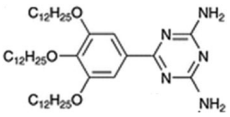
TTD	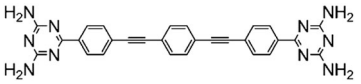

Note: some molecular structures of intrinsically chiral molecules, especially those listed in Table 6, only show one enantiomer. This is not meant to suggest that this was the only enantiomer studied. Both enantiomers were adsorbed as a racemic/non-racemic mixture. Only one enantiomer has been shown because the primary purpose of the table is to serve as a reference for the adsorbate molecular structure.

Table 9 Achiral adsorbates

CPBPB	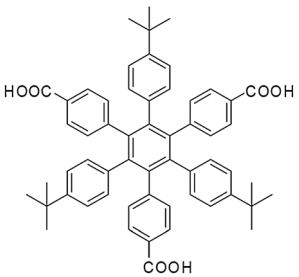
PhDAT	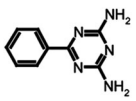
Ni-TMTAA	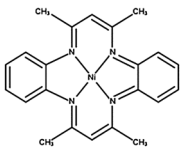
Pentacene	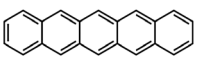
Co(II)-Tetraphenylporphyrin	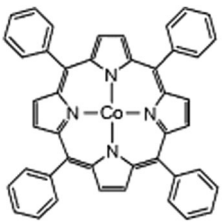
Corannulene	
HTB-HBC	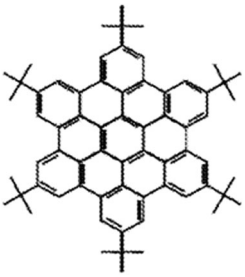

Table 9 (*continued*)

Succinic acid	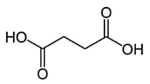
TPCA	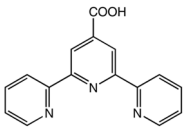
CBC	
Dicarbonitrile-penta(phenyl)	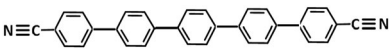
Dicarbonitrile-tetra(phenyl)	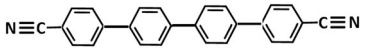
Zinc phthalocyanine	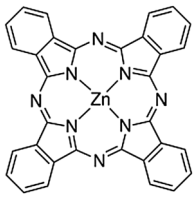
(*R*,*S*)-Tartaric acid	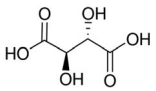
Copper phthalocyanine	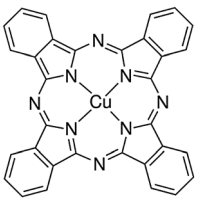
4,4′-Biphenyldicarboxylic acid	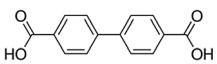

Note: some molecular structures of intrinsically chiral molecules, especially those listed in Table 6, only show one enantiomer. This is not meant to suggest that this was the only enantiomer studied. Both enantiomers were adsorbed as a racemic/non-racemic mixture. Only one enantiomer has been shown because the primary purpose of the table is to serve as a reference for the adsorbate molecular structure.

Acknowledgements

The authors work in the field of chiral surface science and enantioselective adsorption has been supported by DOE Grant No. DE-SC0008703.

References

1 L. Kelvin, *Oxford Univ. Jr. Sci. Club*, 1894, **18**, 3–57.
2 J. Kwon, M. Tamura, P. W. Lucas, J. Hashimoto, N. Kusakabe, R. Kandori, Y. Nakajima, T. Nagayama, T. Nagata and J. H. Hough, *Astrophys. J., Lett.*, 2013, **765**, L6.
3 W. A. Bonner, *Chirality*, 2000, **12**, 114–126.
4 R. A. Hegstrom and D. K. Kondepudi, *Sci. Am.*, 1990, **262**, 108–115.
5 K. Manchester, *Endeavour*, 2001, **25**, 148–152.
6 E. Ben-Jacob and H. Levine, *Nature*, 2001, **409**, 985–986.
7 C. Grande and N. H. Patel, *Nature*, 2009, **457**, 1007–1011.
8 Y. Wang, J. Xu, Y. Wang and H. Chen, *Chem. Soc. Rev.*, 2013, **42**, 2930–2962.
9 K. Hermann, *Crystallography and Surface Structure: An Introduction for Surface Scientists and Nanoscientists*, Wiley-VCH Verlag GmbH & Co., Weinheim, Germany, 2016.
10 S. Mauskopf, in *Chiral Analysis*, ed. K. Busch and M. Busch, Elsevier, Amsterdam, 2006, pp. 3–24.
11 J. Gal, *Helv. Chim. Acta*, 2013, **96**, 1617–1657.
12 L. Pasteur, *C. R. Acad. Sci.*, 1848, **26**, 535–538.
13 B. Kahr and A. G. Shtukenberg, *Isr. J. Chem.*, 2017, **57**, 31–38.
14 D. Kondepudi and K. Asakura, in *Chiral Analysis*, ed. K. Busch and M. Busch, Elsevier, Amsterdam, 2006, pp. 25–45.
15 F. W. Lichtenthaler, *Angew. Chem., Int. Ed.*, 1995, **33**, 2364–2374.
16 M. Rosanoff, *J. Am. Chem. Soc.*, 1906, **28**, 114–121.
17 A. Wohl and K. Freudenberg, *Eur. J. Inorg. Chem.*, 1923, 309–313.
18 G.-Q. Lin, Q.-D. You and J.-F. Cheng, *Chiral drugs: Chemistry and biological action*, John Wiley & Sons, Hoboken, NJ, 2011.
19 J. Hornback, *Organic Chemistry Brooks Cole*, Pacific Grove, CA, 1998.
20 J. Bijvoet, A. Peerdeman and A. Van Bommel, *Nature*, 1951, **168**, 271–272.
21 M. Šámal, S. Chercheja, J. í. Rybáček, J. Vacek Chocholoušová, J. Vacek, L. Bednárová, D. Šaman, I. G. Stará and I. Stary, *J. Am. Chem. Soc.*, 2015, **137**, 8469–8474.
22 A. D. McNaught, *Compendium of chemical terminology*, Blackwell Science Oxford, Oxford, 1997.
23 G. Bringmann, A. J. Price Mortimer, P. A. Keller, M. J. Gresser, J. Garner and M. Breuning, *Angew. Chem., Int. Ed.*, 2005, **44**, 5384–5427.
24 J. L. Bada, *Nature*, 1995, **374**, 594–595.
25 W. A. Bonner, *Origins Life Evol. Biospheres*, 1991, **21**, 59–111.
26 L. Keszthelyi, *BioSystems*, 1987, **20**, 15–19.
27 V. A. Avetisov, V. I. Goldanskii and V. V. Kuz'min, *Phys. Today*, 1991, **44**, 33.
28 D. G. Blackmond, *Cold Spring Harbor Perspect. Biol.*, 2010, **2**, a002147.
29 A. Guijarro and M. Yus, *The origin of chirality in the molecules of life: a revision from awareness to the current theories and perspectives of this unsolved problem*, RSC Publishing, Cambridge, UK, 2008.
30 M. Avalos, R. Babiano, P. Cintas, J. L. Jimenez and J. C. Palacios, *Tetrahedron: Asymmetry*, 2010, **21**, 1030–1040.
31 M. Quack, *Angew. Chem., Int. Ed.*, 2002, **41**, 4618–4630.
32 R. Plasson, D. K. Kondepudi, H. Bersini, A. Commeyras and K. Asakura, *Chirality*, 2007, **19**, 589–600.
33 D. G. Fraser, D. Fitz, T. Jakschitz and B. M. Rode, *Phys. Chem. Chem. Phys.*, 2011, **13**, 831–838.

34 S. Mane, *Anal. Methods*, 2016, **8**, 7567–7586.
35 F. O. Kelsey, *Teratology*, 1988, **38**, 221–226.
36 J. Tomaszewski and M. M. Rumore, *Drug Dev. Ind. Pharm.*, 1994, **20**, 119–139.
37 C. Sahajwalla, ed. I. K. Reddy and R. Mehvar, *Chirality in Drug Design and Development*, CRC Press, Boca Raton, FL, 2004.
38 I. Agranat, S. R. Wainschtein and E. Z. Zusman, *Nat. Rev. Drug Discovery*, 2012, **11**, 972–973.
39 H. Caner, E. Groner, L. Levy and I. Agranat, *Drug Discovery Today*, 2004, **9**, 105–110.
40 H. Murakami, in *Novel Optical Resolution Technologies*, ed. K. Sakai, N. Hirayama and R. Tamura, Springer, Berlin, Germany, 2007, pp. 273–299.
41 S. Erb, *Pharm. Technol.*, 2006, **30**, 14–18.
42 R. Technologies, Chiral Chemicals Market Research Report, 2017.
43 C. Challener, *Pharm. Technol.*, 2016, **40**, 28–29.
44 G. I. Analysts, Chiral Technology – A global strategic business report, 2016.
45 R. Noyori, *Angew. Chem., Int. Ed.*, 2002, **41**, 2008–2022.
46 K. B. Sharpless, *Angew. Chem., Int. Ed.*, 2002, **41**, 2024–2032.
47 W. S. Knowles, *Angew. Chem., Int. Ed.*, 2002, **41**, 1998–2007.
48 J. Kumar, K. G. Thomas and L. M. Liz-Marzán, *Chem. Commun.*, 2016, **52**, 12555–12569.
49 F. Zaera, *J. Phys. Chem. C*, 2008, **112**, 16196–16203.
50 A. J. Gellman, J. D. Horvath and M. T. Buelow, *J. Mol. Catal. A: Chem.*, 2001, **167**, 3–11.
51 K.-H. Ernst, *Phys. Status Solidi B*, 2012, **249**, 2057–2088.
52 J. Wang and B. L. Feringa, *Science*, 2011, **331**, 1429–1432.
53 B. L. Feringa, *Acc. Chem. Res.*, 2001, **34**, 504–513.
54 C. A. Schalley, K. Beizai and F. Vögtle, *Acc. Chem. Res.*, 2001, **34**, 465–476.
55 R. Naaman and D. H. Waldeck, *Annu. Rev. Phys. Chem.*, 2015, **66**, 263–281.
56 J. Elemans, I. De Cat, H. Xu and S. De Feyter, *Chem. Soc. Rev.*, 2009, **38**, 722–736.
57 M. Liu, L. Zhang and T. Wang, *Chem. Rev.*, 2015, **115**, 7304–7397.
58 J. Jacques, A. Collet and S. H. Wilen, *Enantiomers, racemates, and resolutions*, J. Wiley & Sons, Inc., New York, 1981.
59 I. Kuzmenko, I. Weissbuch, E. Gurovich, L. Leiserowitz and M. Lahav, *Chirality*, 1998, **10**, 415–424.
60 M. O. Lorenzo, S. Haq, T. Bertrams, P. Murray, R. Raval and C. Baddeley, *J. Phys. Chem. B*, 1999, **103**, 10661–10669.
61 A. M. Berg and D. L. Patrick, *Angew. Chem., Int. Ed.*, 2005, **44**, 1821–1823.
62 C. Bombis, S. Weigelt, M. M. Knudsen, M. Norgaard, C. Busse, E. Laegsgaard, F. Besenbacher, K. V. Gothelf and T. R. Linderoth, *ACS Nano*, 2010, **4**, 297–311.
63 R. Raval, *Chem. Soc. Rev.*, 2009, **38**, 707–721.
64 S. M. Barlow and R. Raval, *Surf. Sci. Rep.*, 2003, **50**, 201–341.
65 I. Weissbuch, M. Berfeld, W. Bouwman, K. Kjaer, J. AlsNielsen, M. Lahav and L. Leiserowitz, *J. Am. Chem. Soc.*, 1997, **119**, 933–942.
66 R. M. Hazen and D. S. Sholl, *Nat. Mater.*, 2003, **2**, 367–374.
67 C. Orme, A. Noy, A. Wierzbicki, M. McBride, M. Grantham, H. Teng, P. Dove and J. DeYoreo, *Nature*, 2001, **411**, 775–779.
68 J. D. Horvath and A. J. Gellman, *Top. Catal.*, 2003, **25**, 9–15.
69 C. F. McFadden, P. S. Cremer and A. J. Gellman, *Langmuir*, 1996, **12**, 2483–2487.
70 V. Humblot, M. O. Lorenzo, C. J. Baddeley, S. Haq and R. Raval, *J. Am. Chem. Soc.*, 2004, **126**, 6460–6469.
71 T. J. Lawton, V. Pushkarev, D. Wei, F. R. Lucci, D. S. Sholl, A. J. Gellman and E. C. H. Sykes, *J. Phys. Chem. C*, 2013, **117**, 22290–22297.
72 W. Y. Cheong and A. J. Gellman, *J. Phys. Chem. C*, 2011, **115**, 1031–1035.
73 X. Zhao, R. Zhao and W. Yang, *Langmuir*, 2000, **16**, 9812–9818.
74 R. Sancho and C. Minguillon, *Chem. Soc. Rev.*, 2009, **38**, 797–805.
75 Y. Zhang, D.-R. Wu, D. B. Wang-Iverson and A. A. Tymiak, *Drug Discovery Today*, 2005, **10**, 571–577.
76 A. R. Ribeiro, A. S. Maia, Q. B. Cass and M. E. Tiritan, *J. Chromatogr. B: Anal. Technol. Biomed. Life Sci.*, 2014, **968**, 8–21.
77 Z. A. Al-Othman, A. Al-Warthan, S. D. Alam and I. Ali, *Biomed. Chromatogr.*, 2014, **28**, 1514–1524.
78 J. Martens and R. Bhushan, *Isr. J. Chem.*, 2016, **56**, 990–1009.
79 V. A. Soloshonok, C. Roussel, O. Kitagawa and A. E. Sorochinsky, *Chem. Soc. Rev.*, 2012, **41**, 4180–4188.
80 V. A. Soloshonok, *Angew. Chem., Int. Ed.*, 2006, **45**, 766–769.
81 O. Trapp and V. Schurig, *Tetrahedron: Asymmetry*, 2010, **21**, 1334–1340.
82 M. Heitbaum, F. Glorius and I. Escher, *Angew. Chem., Int. Ed.*, 2006, **45**, 4732–4762.
83 D. Y. Murzin, P. Mäki-Arvela, E. Toukoniitty and T. Salmi, *Catal. Rev.*, 2005, **47**, 175–256.
84 T. Mallat, E. Orglmeister and A. Baiker, *Chem. Rev.*, 2007, **107**, 4863–4890.
85 I. Ojima, *Catalytic asymmetric synthesis*, John Wiley & Sons, Inc., New York, 2004.
86 R. Schmid, *CHIMIA Int. J. Chem.*, 1996, **50**, 110–113.
87 N. Künzle, R. Hess, T. Mallat and A. Baiker, *J. Catal.*, 1999, **186**, 239–241.
88 T. Bürgi and A. Baiker, *Acc. Chem. Res.*, 2004, **37**, 909–917.
89 W. Reschetilowski, U. Böhmer and J. Wiehl, in *Chiral Reactions in Heterogeneous Catalysis*, ed. G. Jannes and V. Dubois, Springer, Berlin, Germany, 1995, pp. 111–118.
90 M. Studer, H. U. Blaser and C. Exner, *Adv. Synth. Catal.*, 2003, **345**, 45–65.
91 J. M. Bonello, F. J. Williams and R. M. Lambert, *J. Am. Chem. Soc.*, 2003, **125**, 2723–2729.
92 C. Baddeley, *Top. Catal.*, 2003, **25**, 17–28.
93 T. Verbiest, S. Van Elshocht, M. Kauranen, L. Hellemans, J. Snauwaert, C. Nuckolls, T. J. Katz and A. Persoons, *Science*, 1998, **282**, 913–915.
94 Y. Yang, R. C. da Costa, M. J. Fuchter and A. J. Campbell, *Nat. Photonics*, 2013, **7**, 634–638.

95 S. Pieraccini, S. Masiero, A. Ferrarini and G. P. Spada, *Chem. Soc. Rev.*, 2011, **40**, 258–271.
96 D. Fichou, *J. Mater. Chem.*, 2000, **10**, 571–588.
97 B. L. Feringa and W. R. Browne, in *Molecular switches*, ed. B. L. Feringa and W. R. Browne, Wiley-VCH Verlag GmbH & Co. KGaA, Weinheim, Germany, 2001, vol. 42.
98 M. Eremtchenko, J. Schaefer and F. Tautz, *Nature*, 2003, **425**, 602–605.
99 F. I. Bohrer, C. N. Colesniuc, J. Park, M. E. Ruidiaz, I. K. Schuller, A. C. Kummel and W. C. Trogler, *J. Am. Chem. Soc.*, 2008, **131**, 478–485.
100 T. Nakanishi, N. Yamakawa, T. Asahi, T. Osaka, B. Ohtani and K. Uosaki, *J. Am. Chem. Soc.*, 2002, **124**, 740–741.
101 L. Addadi and S. Weiner, *Nature*, 2001, **411**, 753–755.
102 M. Zhang, G. Qing and T. Sun, *Chem. Soc. Rev.*, 2012, **41**, 1972–1984.
103 A. Baiker, *Catal. Today*, 2005, **100**, 159–170.
104 D. S. Sholl, A. Asthagiri and T. D. Power, *J. Phys. Chem. B*, 2001, **105**, 4771–4782.
105 A. Baiker, *J. Mol. Catal. A: Chem.*, 2000, **163**, 205–220.
106 S. Iwama, M. Horiguchi, H. Sato, Y. Uchida, H. Takahashi, H. Tsue and R. Tamura, *Cryst. Growth Des.*, 2010, **10**, 2668–2675.
107 R. Bishop, in *Chirality in Supramolecular Assemblies*, ed. R. Keene, John Wiley & Sons, Inc., New York, 2016, pp. 65–93.
108 B. Chion, J. Lajzerowicz, D. Bordeaux, A. Collet and J. Jacques, *J. Phys. Chem.*, 1978, **82**, 2682–2688.
109 J. Huang, S. Chen, I. A. Guzei and L. Yu, *J. Am. Chem. Soc.*, 2006, **128**, 11985–11992.
110 O. Wallach, *Liebigs Ann. Chem.*, 1895, **286**, 119–143.
111 A. Kitaigorodskii, *Acta Crystallogr.*, 1965, **18**, 585–590.
112 K. H. Ernst, *Isr. J. Chem.*, 2017, **57**, 24–30.
113 C. P. Brock, W. B. Schweizer and J. D. Dunitz, *J. Am. Chem. Soc.*, 1991, **113**, 9811–9820.
114 J. Dunitz and A. Gavezzotti, *J. Phys. Chem. B*, 2012, **116**, 6740–6750.
115 A. Gavezzotti and G. Filippini, *J. Am. Chem. Soc.*, 1995, **117**, 12299–12305.
116 A. Gavezzotti and S. Rizzato, *J. Org. Chem.*, 2014, **79**, 4809–4816.
117 A. Otero-de-la-Roza, J. E. Hein and E. R. Johnson, *Cryst. Growth Des.*, 2016, **16**, 6055–6059.
118 B. O. Patrick and C. P. Brock, *Acta Crystallogr., Sect. B: Struct. Sci., Cryst. Eng. Mater.*, 2006, **B62**, 488–497.
119 K. S. Jeong, D. E. Kim, E. Lee, Y. H. Jhon, H. Han, J. Kim and N. Jeong, *Tetrahedron: Asymmetry*, 2009, **20**, 1736–1741.
120 G. Coquerel, in *Novel Optical Resolution Technologies*, ed. K. Sakai, N. Hirayama and R. Tamura, Springer, Berlin, Germany, 2007, pp. 1–51.
121 R. G. Kostyanovsky, F. A. Lakhvich, P. M. Philipchenko, D. A. Lenev, V. Y. Torbeev and K. A. Lyssenko, *Mendeleev Commun.*, 2002, **12**, 147–149.
122 E. M. Arnett, J. Chao, B. Kinzig, M. V. Stewart, O. Thompson and R. J. Verbiar, *J. Am. Chem. Soc.*, 1982, **104**, 389–400.
123 M. V. Stewart and E. M. Arnett, *Top. Stereochem.*, 1982, **13**, 195–262.
124 M. Vaida, L. Shimon, Y. Weisinger-Lewin, F. Frolow, M. Lahav, L. Leiserowitz and R. McMullan, *Science*, 1988, 1475–1479.
125 K. E. Plass, A. L. Grzesiak and A. J. Matzger, *Acc. Chem. Res.*, 2007, **40**, 287–293.
126 N. Nandi and D. Vollhardt, *Curr. Opin. Colloid Interface Sci.*, 2008, **13**, 40–46.
127 S. De Feyter, A. Gesquiere, M. M. Abdel-Mottaleb, P. C. M. Grim, F. C. De Schryver, C. Meiners, M. Sieffert, S. Valiyaveettil and K. Mullen, *Acc. Chem. Res.*, 2000, **33**, 520–531.
128 S. De Feyter and F. C. De Schryver, *J. Phys. Chem. B*, 2005, **109**, 4290–4302.
129 K. H. Ernst, in *Supramolecular Chirality*, ed. M. Crego-Calama and D. Reinboudt, Springer-Verlag, Berlin, Berlin, 2006, vol. 265, pp. 209–252.
130 T. Eralp, A. Cornish, A. Shavorskiy and G. Held, *Top. Catal.*, 2011, **54**, 1414–1428.
131 S. M. Barlow, S. Louafi, D. Le Roux, J. Williams, C. Muryn, S. Haq and R. Raval, *Surf. Sci.*, 2005, **590**, 243–263.
132 M. Parschau, S. Romer and K. H. Ernst, *J. Am. Chem. Soc.*, 2004, **126**, 15398–15399.
133 F. Masini, N. Kalashnyk, M. M. Knudsen, J. R. Cramer, E. Laegsgaard, F. Besenbacher, K. V. Gothelf and T. R. Linderoth, *J. Am. Chem. Soc.*, 2011, **133**, 13910–13913.
134 I. De Cat, Z. Guo, S. J. George, E. W. Meijer, A. P. H. J. Schenning and S. De Feyter, *J. Am. Chem. Soc.*, 2012, **134**, 3171–3177.
135 M. Parschau, D. Passerone, K. H. Rieder, H. J. Hug and K. H. Ernst, *Angew. Chem., Int. Ed.*, 2009, **48**, 4065–4068.
136 I. Lee and F. Zaera, *J. Am. Chem. Soc.*, 2006, **128**, 8890–8898.
137 R. A. Reddy and C. Tschierske, *J. Mater. Chem.*, 2006, **16**, 907–961.
138 J. Weckesser, A. De Vita, J. V. Barth, C. Cai and K. Kern, *Phys. Rev. Lett.*, 2001, **87**, 096101.
139 R. H. Janke, G. Haufe, E.-U. Würthwein and J. H. Borkent, *J. Am. Chem. Soc.*, 1996, **118**, 6031–6035.
140 G. Smith, K. Williams and D. Wonnacott, *J. Org. Chem.*, 1978, **43**, 1–5.
141 K. Mislow, *Top. Stereochem.*, 1999, **22**, 1–82.
142 S. Duhm, Q. Xin, S. Hosoumi, H. Fukagawa, K. Sato, N. Ueno and S. Kera, *Adv. Mater.*, 2012, **24**, 901–905.
143 C. Udhardt, R. Forker, M. Gruenewald, Y. Watanabe, T. Yamada, T. Ueba, T. Munakata and T. Fritz, *Thin Solid Films*, 2016, **598**, 271–275.
144 C. W. Thomas and Y. Tor, *Chirality*, 1998, **10**, 53–59.
145 W. D. Xiao, Y. H. Jiang, K. Ait-Mansour, P. Ruffieux, H. J. Gao and R. Fasel, *J. Phys. Chem. C*, 2010, **114**, 6646–6649.
146 K. Wilson, A. Trant and C. Baddeley, *J. Phys. Chem. C*, 2011, **116**, 1092–1098.
147 K. E. Wilson and C. J. Baddeley, *J. Catal.*, 2011, **278**, 41–49.
148 K. E. Wilson and C. J. Baddeley, *J. Phys. Chem. C*, 2009, **113**, 10706–10711.
149 B. S. Mhatre, S. Dutta, A. Reinicker, B. Karagoz and A. J. Gellman, *Chem. Commun.*, 2016, **52**, 14125–14128.

150 D. Rampulla, A. Francis, K. Knight and A. Gellman, *J. Phys. Chem. B*, 2006, **110**, 10411–10420.
151 D. Rampulla and A. Gellman, *Surf. Sci.*, 2006, **600**, 2823–2829.
152 E. A. Wood, *J. Appl. Phys.*, 1964, **35**, 1306–1312.
153 J. Seibel, M. Parschau and K.-H. Ernst, *J. Am. Chem. Soc.*, 2015, **137**, 7970–7973.
154 I. Destoop, H. Xu, C. Oliveras-Gonzalez, E. Ghijsens, D. B. Amabilino and S. De Feyter, *Chem. Commun.*, 2013, **49**, 7477–7479.
155 I. Destoop, E. Ghijsens, K. Katayama, K. Tahara, K. S. Mali, Y. Tobe and S. De Feyter, *J. Am. Chem. Soc.*, 2012, **134**, 19568–19571.
156 N. Katsonis, H. Xu, R. M. Haak, T. Kudernac, Z. Tomovic, S. George, M. Van der Auweraer, A. P. H. J. Schenning, E. W. Meijer, B. L. Feringa and S. De Feyter, *Angew. Chem., Int. Ed.*, 2008, **47**, 4997–5001.
157 N. Katsonis, E. Lacaze and B. L. Feringa, *J. Mater. Chem.*, 2008, **18**, 2065–2073.
158 T. Chen, S.-Y. Li, D. Wang, M. Yao and L.-J. Wan, *Angew. Chem., Int. Ed.*, 2015, **54**, 4309–4314.
159 L. Xu, X. Miao, L. Cui, P. Liu, X. Chen and W. Deng, *Nanoscale*, 2015, **7**, 11734–11745.
160 T. Chen, D. Wang, X. Zhang, Q.-L. Zhou, R.-B. Zhang and L.-J. Wan, *J. Phys. Chem. C*, 2009, **114**, 533–538.
161 Y. Yang and C. Wang, *Curr. Opin. Colloid Interface Sci.*, 2009, **14**, 135–147.
162 L. Xu, X. Miao, B. Zha and W. Deng, *J. Phys. Chem. C*, 2012, **116**, 16014–16022.
163 R. H. Perry, C. P. Wu, M. Nefliu and R. G. Cooks, *Chem. Commun.*, 2007, 1071–1073.
164 S. P. Fletcher, R. B. Jagt and B. L. Feringa, *Chem. Commun.*, 2007, 2578–2580.
165 C. Viedma, W. L. Noorduin, J. E. Ortiz, T. de Torres and P. Cintas, *Chem. Commun.*, 2011, **47**, 671–673.
166 A. Bellec and J.-C. Guillemin, *Chem. Commun.*, 2010, **46**, 1482–1484.
167 A. Bellec and J.-C. Guillemin, *J. Fluorine Chem.*, 2010, **131**, 545–548.
168 Y. Yun and A. J. Gellman, *Langmuir*, 2015, **31**, 6055–6063.
169 Y. Yun, D. Wei, D. S. Sholl and A. J. Gellman, *J. Phys. Chem. C*, 2014, **118**, 14957–14966.
170 A. J. Gellman and Y. Yun, *Nat. chem.*, 2015, **7**, 520–525.
171 Y. Yun and A. J. Gellman, *Angew. Chem., Int. Ed.*, 2013, **52**, 3394–3397.
172 S. Karakalos, J. Hong and F. Zaera, *Angew. Chem., Int. Ed.*, 2016, **55**, 6225–6228.
173 S. Karakalos and F. Zaera, *J. Phys. Chem. C*, 2015, **119**, 13785–13790.
174 S. J. Sowerby, W. M. Heckl and G. B. Petersen, *J. Mol. Evol.*, 1996, **43**, 419–424.
175 F. Stevens, D. J. Dyer and D. M. Walba, *Angew. Chem., Int. Ed.*, 1996, **35**, 900–901.
176 S. De Feyter, P. C. M. Grim, M. Rucker, P. Vanoppen, C. Meiners, M. Sieffert, S. Valiyaveettil, K. Mullen and F. C. De Schryver, *Angew. Chem., Int. Ed.*, 1998, **37**, 1223–1226.
177 G. Ertl and J. Küppers, *Low energy electrons and surface chemistry*, VCH Verlagsgellschaft Weinheim, Germany, 1985.
178 C. Bai, *Scanning tunneling microscopy and its application*, Springer, New York, 2000.
179 E. Meyer, H. J. Hug and R. Bennewitz, *Scanning probe microscopy: the lab on a tip*, Springer, New York, 2013.
180 H. L. Tierney, C. J. Murphy and E. C. H. Sykes, *Phys. Rev. Lett.*, 2011, **106**, 010801.
181 K. H. Ernst, Y. Kuster, R. Fasel, M. Muller and U. Ellerbeck, *Chirality*, 2001, **13**, 675–678.
182 R. Fasel, A. Cossy, K. H. Ernst, F. Baumberger, T. Greber and J. Osterwalder, *J. Chem. Phys.*, 2001, **115**, 1020–1027.
183 T. Eralp, A. Shavorskiy, Z. V. Zheleva, G. Held, N. Kalashnyk, Y. Ning and T. R. Linderoth, *Langmuir*, 2010, **26**, 18841–18851.
184 M. Parschau, T. Kampen and K. H. Ernst, *Chem. Phys. Lett.*, 2005, **407**, 433–437.
185 M. Parschau, B. Behzadi, S. Romer and K. H. Ernst, *Surf. Interface Anal.*, 2006, **38**, 1607–1610.
186 S. Romer, B. Behzadi, R. Fasel and K. H. Ernst, *Chem. – Eur. J.*, 2005, **11**, 4149–4154.
187 Q. Chen, C. W. Lee, D. Frankel and N. Richardson, *PhysChemComm*, 1999, **2**, 41–44.
188 R. Fasel, M. Parschau and K. H. Ernst, *Nature*, 2006, **439**, 449–452.
189 M. Linares, A. Minoia, P. Brocorens, D. Beljonne and R. Lazzaroni, *Chem. Soc. Rev.*, 2009, **38**, 806–816.
190 C.-A. Palma, P. Samori and M. Cecchini, *J. Am. Chem. Soc.*, 2010, **132**, 17880–17885.
191 P. Szabelski and S. De Feyter, *CrystEngComm*, 2011, **13**, 5542–5550.
192 N. Martsinovich and A. Troisi, *J. Phys. Chem. C*, 2010, **114**, 4376–4388.
193 R. B. Rankin and D. S. Sholl, *Surf. Sci.*, 2004, **548**, 301–308.
194 R. B. Rankin and D. S. Sholl, *Surf. Sci.*, 2005, **574**, L1–L8.
195 L. Mao, H. H. Harris and K. J. Stine, *J. Chem. Inf. Comp. Sci.*, 2002, **42**, 1179–1184.
196 I. Paci, *J. Phys. Chem. C*, 2010, **114**, 19425–19432.
197 I. Paci, I. Szleifer and M. A. Ratner, *J. Am. Chem. Soc.*, 2007, **129**, 3545–3555.
198 I. Medved, A. Trník and D. Huckaby, *J. Stat. Mech.: Theory Exp.*, 2010, P12027.
199 H. Xu, W. J. Saletra, P. Iavicoli, B. Van Averbeke, E. Ghijsens, K. S. Mali, A. P. H. J. Schenning, D. Beljonne, R. Lazzaroni, D. B. Amabilino and S. De Feyter, *Angew. Chem., Int. Ed.*, 2012, **51**, 11981–11985.
200 M. Yu, J. Wang, M. Mura, Q.-Q. Meng, W. Xu, H. Gersen, E. Laegsgaard, I. Stensgaard, R. E. A. Kelly, J. Kjems, T. R. Linderoth, L. N. Kantorovich and F. Besenbacher, *ACS Nano*, 2011, **5**, 6651–6660.
201 N. M. Santagata, A. M. Lakhani, B. F. Davis, P. Luo, M. B. Nardelli and T. P. Pearl, *J. Phys. Chem. C*, 2010, **114**, 8917–8925.
202 J. S. Prauzner-Bechcicki, S. Godlewski, J. Budzioch, G. Goryl, L. Walczak, P. Sehnal, I. G. Stara, I. Stary, F. Ample,

C. Joachim and M. Szymonski, *PhysChemComm*, 2010, **11**, 3522–3528.
203 J. D. Horvath and A. J. Gellman, *J. Am. Chem. Soc.*, 2002, **124**, 2384–2392.
204 J. D. Horvath, L. Baker and A. J. Gellman, *J. Phys. Chem. C*, 2008, **112**, 7637–7643.
205 C. Fleming, M. King and M. Kadodwala, *J. Phys. Chem. C*, 2008, **112**, 18299–18302.
206 Ž. Šljivančanin, K. V. Gothelf and B. Hammer, *J. Am. Chem. Soc.*, 2002, **124**, 14789–14794.
207 T. Greber, Z. Sljivancanin, R. Schillinger, J. Wider and B. Hammer, *Phys. Rev. Lett.*, 2006, **96**, 056103.
208 J. Wellendorff, T. L. Silbaugh, D. Garcia-Pintos, J. K. Nørskov, T. Bligaard, F. Studt and C. T. Campbell, *Surf. Sci.*, 2015, **640**, 36–44.
209 J. Barth, H. Brune, G. Ertl and R. Behm, *Phys. Rev. B: Condens. Matter Mater. Phys.*, 1990, **42**, 9307.
210 A. D. Gordon, S. Karakalos and F. Zaera, *Surf. Sci.*, 2014, **629**, 3–10.
211 D. Costa, C.-M. Pradier, F. Tielens and L. Savio, *Surf. Sci. Rep.*, 2015, **70**, 449–553.
212 A. J. Gellman and Y. Yun, *Angew. Chem., Int. Ed.*, 2013, **52**, 3394–3397.
213 Y. Yun and A. J. Gellman, *J. Phys. Chem. C*, 2016, **120**, 27285–27295.
214 H. Iwai and C. Egawa, *Langmuir*, 2010, **26**, 2294–2300.
215 T. Huang, Z. P. Hu, B. Wang, L. Chen, A. D. Zhao, H. Q. Wang and J. G. Hou, *J. Phys. Chem. B*, 2007, **111**, 6973–6977.
216 L. Atanasoska, J. Buchholz and G. Somorjai, *Surf. Sci.*, 1978, **72**, 189–207.
217 S. Haq, A. Massey, N. Moslemzadeh, A. Robin, S. M. Barlow and R. Raval, *Langmuir*, 2007, **23**, 10694–10700.
218 S. N. Patole, C. J. Baddeley, A. Schuler, D. O'Hagan and N. V. Richardson, *Langmuir*, 2009, **25**, 1412–1416.
219 P. Iavicoli, H. Xu, T. Keszthelyi, J. Telegdi, K. Wurst, B. Van Averbeke, W. J. Saletra, A. Minoia, D. Beljonne and R. Lazzaroni, *Chirality*, 2012, **24**, 155.
220 S.-Y. Li, T. Chen, L. Wang, B. Sun, D. Wang and L.-J. Wan, *Langmuir*, 2016, **32**, 6830–6835.
221 Y. U. Cai and S. L. Bernasek, *J. Am. Chem. Soc.*, 2003, **125**, 1655–1659.
222 Q. H. Yuan, C. J. Yan, H. J. Yan, L. J. Wan, B. H. Northrop, H. Jude and P. J. Stang, *J. Am. Chem. Soc.*, 2008, **130**, 8878–8879.
223 T. Balandina, M. W. van der Meijden, O. Ivasenko, D. Cornil, J. Cornil, R. Lazzaroni, R. M. Kellogg and S. De Feyter, *Chem. Commun.*, 2013, **49**, 2207–2209.
224 M. Kunitake, T. Hattori, S. Miyano and K. Itaya, *Langmuir*, 2005, **21**, 9206–9210.
225 R. Raval, *J. Phys.: Condens. Matter*, 2002, **14**, 4119–4132.
226 Y. Izumi, *Adv. Catal.*, 1983, **32**, 215–271.
227 M. A. Keane and G. Webb, *J. Catal.*, 1992, **136**, 1–15.
228 K. H. Ernst, M. Bohringer, C. F. McFadden, P. Hug, U. Muller and U. Ellerbeck, *Nanotechnology*, 1999, **10**, 355–361.
229 M. Gingras, *Chem. Soc. Rev.*, 2013, **42**, 1051–1095.
230 A. Kuhnle, T. R. Linderoth, B. Hammer and F. Besenbacher, *Nature*, 2002, **415**, 891–893.
231 A. G. Mark, M. Forster and R. Raval, *ChemPhysChem*, 2011, **12**, 1474–1480.
232 N. Katsonis, A. Minoia, T. Kudernac, T. Mutai, H. Xu, H. Uji-i, R. Lazzaroni, S. De Feyter and B. L. Feringa, *J. Am. Chem. Soc.*, 2008, **130**, 386–387.
233 R. Ouyang, J. Yan, P. S. Jensen, E. Ascic, S. Gan, D. Tanner, B. Mao, L. Niu, J. Zhang and C. Tang, *ChemPhysChem*, 2015, **16**, 928–932.
234 K. H. Ernst, *Acc. Chem. Res.*, 2016, **49**, 1182–1190.
235 Y. Shen and C.-F. Chen, *Chem. Rev.*, 2011, **112**, 1463–1535.
236 J. Seibel, M. Parschau and K. H. Ernst, *J. Phys. Chem. C*, 2014, **118**, 29135–29141.
237 M. Parschau, R. Fasel and K. H. Ernst, *Cryst. Growth Des.*, 2008, **8**, 1890–1896.
238 J. Seibel, L. Zoppi and K. H. Ernst, *Chem. Commun.*, 2014, **50**, 8751–8753.
239 J. Seibel, O. Allemann, J. S. Siegel and K. H. Ernst, *J. Am. Chem. Soc.*, 2013, **135**, 7434–7437.
240 M. Stohr, S. Boz, M. Schaer, N. Manh-Thuong, C. A. Pignedoli, D. Passerone, W. B. Schweizer, C. Thilgen, T. A. Jung and F. Diederich, *Angew. Chem., Int. Ed.*, 2011, **50**, 9982–9986.
241 C. Le Poulennec, J. Cousty, Z. Xie and C. Mioskowski, *Surf. Sci.*, 2000, **448**, 93–100.
242 K. H. Ernst, Y. Kuster, R. Fasel, C. F. McFadden and U. Ellerbeck, *Surf. Sci.*, 2003, **530**, 195–202.
243 A. Robin, P. Iavicoli, K. Wurst, M. S. Dyer, S. Haq, D. B. Amabilino and R. Raval, *Cryst. Growth Des.*, 2010, **10**, 4516–4525.
244 S. Godlewski, J. S. Prauzner-Bechcicki, J. Budzioch, L. Walczak, I. G. Stara, I. Stary, P. Sehnal and M. Szymonski, *Surf. Sci.*, 2012, **606**, 1600–1607.
245 J. D. Fuhr, M. W. van der Meijden, L. J. Cristina, L. M. Rodríguez, R. M. Kellogg, J. E. Gayone, H. Ascolani and M. Lingenfelder, *Chem. Commun.*, 2017, **53**, 130–133.
246 M. Forster, M. S. Dyer, M. Persson and R. Raval, *Top. Catal.*, 2011, **54**, 13–19.
247 M. Forster, M. S. Dyer, S. D. Barrett, M. Persson and R. Raval, *J. Phys. Chem. C*, 2011, **115**, 1180–1185.
248 B. Ohtani, A. Shintani and K. Uosaki, *J. Am. Chem. Soc.*, 1999, **121**, 6515–6516.
249 M. Han, D. Wang, J. Hao, L. Wan, Q. Zeng, Q. Fan and C. Bai, *Anal. Chem.*, 2004, **76**, 627–631.
250 D. Wang, Q. M. Xu, L. J. Wan, C. L. Bai and G. Jin, *Langmuir*, 2003, **19**, 1958–1962.
251 P. Qian, H. Nanjo, T. Yokoyama and T. M. Suzuki, *Chem. Lett.*, 1998, 1133–1134.
252 W. Mamdouh, H. Uji-i, A. Gesquiere, S. De Feyter, D. B. Amabilino, M. M. S. Abdel-Mottaleb, J. Veciana and F. C. De Schryver, *Langmuir*, 2004, **20**, 9628–9635.
253 Y. G. Cai and S. L. Bernasek, *J. Phys. Chem. B*, 2005, **109**, 4514–4519.
254 J. B. Lin, Z. X. Guo, J. Plas, D. B. Amabilino, S. De Feyter and A. Schenning, *Chem. Commun.*, 2013, **49**, 9320–9322.

255 A. M. Lakhani, D. J. DeWitt, N. M. Sant'Agata and T. P. Pearl, *J. Phys. Chem. C*, 2007, **111**, 5750–5755.
256 A. Kuhnle, T. R. Linderoth and F. Besenbacher, *Top. Catal.*, 2011, **54**, 1384–1391.
257 M. Taniguchi, H. Nakagawa, A. Yamagishi and K. Yamada, *Surf. Sci.*, 2002, **507**, 458–462.
258 M. Taniguchi, H. Nakagawa, A. Yamagishi and K. Yamada, *Surf. Sci.*, 2000, **454**, 1005–1009.
259 P. Rahe, M. Nimmrich, A. Greuling, J. Schutte, I. G. Stara, J. Rybacek, G. Huerta-Angeles, I. Stary, M. Rohlfing and A. Kuhnle, *J. Phys. Chem. C*, 2010, **114**, 1547–1552.
260 X. Y. Zhao, R. G. Zhao and W. S. Yang, *Surf. Sci.*, 1999, **442**, L995–L1000.
261 C. Egawa, H. Iwai, M. Kabutoya and S. Oki, *Surf. Sci.*, 2003, **532**, 233–236.
262 M. Lingenfelder, G. Tomba, G. Costantini, L. C. Ciacchi, A. De Vita and K. Kern, *Angew. Chem., Int. Ed.*, 2007, **46**, 4492–4495.
263 C. Roth, M. Parschau and K. H. Ernst, *ChemPhysChem*, 2011, **12**, 1572–1577.
264 M. Forster, M. S. Dyer, M. Persson and R. Raval, *Angew. Chem., Int. Ed.*, 2010, **49**, 2344–2348.
265 C. Roth, D. Passerone and K.-H. Ernst, *Chem. Commun.*, 2010, **46**, 8645–8647.
266 S. Haq, N. Liu, V. Humblot, A. P. J. Jansen and R. Raval, *Nat. Chem.*, 2009, **1**, 409–414.
267 B. Behzadi, S. Romer, R. Fasel and K. H. Ernst, *J. Am. Chem. Soc.*, 2004, **126**, 9176–9177.
268 M. Parschau and K. H. Ernst, *Angew. Chem., Int. Ed.*, 2015, **54**, 14422–14426.
269 M. Nakamura, H. Huang, K. Kanazawa, A. Taninaka, S. Yoshida, O. Takeuchi and H. Shigekawa, *Jpn. J. Appl. Phys.*, 2015, **54**, 08LB05.
270 D. C. Madden, M. L. Bentley, S. J. Jenkins and S. M. Driver, *Surf. Sci.*, 2014, **629**, 81–87.
271 S. Karakalos, T. J. Lawton, F. R. Lucci, E. C. H. Sykes and F. Zaera, *J. Phys. Chem. C*, 2013, **117**, 18588–18594.
272 X. Y. Zhao, H. Wang, R. G. Zhao and W. S. Yang, *Mater. Sci. Eng., C*, 2001, **16**, 41–50.
273 G. A. Somorjai and Y. Li, *Introduction to surface chemistry and catalysis*, John Wiley & Sons, New York, 2010.
274 Y. H. Wei, K. Kannappan, G. W. Flynn and M. B. Zimmt, *J. Am. Chem. Soc.*, 2004, **126**, 5318–5322.
275 M. Hibino, A. Sumi, H. Tsuchiya and I. Hatta, *J. Phys. Chem. B*, 1998, **102**, 4544–4547.
276 D. G. Yablon, L. C. Giancarlo and G. W. Flynn, *J. Phys. Chem. B*, 2000, **104**, 7627–7635.
277 A. Miura, P. Jonkheijm, S. De Feyter, A. Schenning, E. W. Meijer and F. C. De Schryver, *Small*, 2005, **1**, 131–137.
278 F. Tao and S. L. Bernasek, *Chem. Rev.*, 2007, **107**, 1408–1453.
279 X. Shao, X. Luo, X. Hu and K. Wu, *J. Phys. Chem. B*, 2006, **110**, 15393–15402.
280 J. P. Rabe and S. Buchholz, *Science*, 1991, **253**, 424–427.
281 B. Venkataraman, J. J. Breen and G. W. Flynn, *J. Phys. Chem.*, 1995, **99**, 6608–6619.
282 C. Cai, B. Müller, J. Weckesser, J. V. Barth, Y. Tao, M. M. Bösch, A. Kündig, C. Bosshard, I. Biaggio and P. Günter, *Adv. Mater.*, 1999, **11**, 750–754.
283 J. V. Barth, J. Weckesser, G. Trimarchi, M. Vladimirova, A. De Vita, C. Z. Cai, H. Brune, P. Gunter and K. Kern, *J. Am. Chem. Soc.*, 2002, **124**, 7991–8000.
284 F. Vidal, E. Delvigne, S. Stepanow, N. Lin, J. V. Barth and K. Kern, *J. Am. Chem. Soc.*, 2005, **127**, 10101–10106.
285 B. I. Kim, C. Z. Cai, X. B. Deng and S. S. Perry, *Surf. Sci.*, 2003, **538**, 45–52.
286 J. V. Barth, J. Weckesser, C. Z. Cai, P. Gunter, L. Burgi, O. Jeandupeux and K. Kern, *Angew. Chem., Int. Ed.*, 2000, **39**, 1230–1234.
287 N. Lin, S. Stepanow, F. Vidal, J. V. Barth and K. Kern, *Chem. Commun.*, 2005, 1681–1683.
288 J. H. Kang, R. L. Toomes, M. Polcik, M. Kittel, J. T. Hoeft, V. Efstathiou, D. P. Woodruff and A. M. Bradshaw, *J. Chem. Phys.*, 2003, **118**, 6059–6071.
289 V. Efstathiou and D. P. Woodruff, *Surf. Sci.*, 2003, **531**, 304–318.
290 Q. Chen, D. J. Frankel and N. V. Richardson, *Surf. Sci.*, 2002, **497**, 37–46.
291 Z. V. Zheleva, T. Eralp and G. Held, *J. Phys. Chem. C*, 2012, **116**, 618–625.
292 X. Y. Zhao, H. Yan, R. G. Zhao and W. S. Yang, *Langmuir*, 2003, **19**, 809–813.
293 K. Mae and Y. Morikawa, *Surf. Sci.*, 2004, **553**, L63–L67.
294 R. L. Toomes, J.-H. Kang, D. P. Woodruff, M. Polcik, M. Kittel and J.-T. Hoeft, *Surf. Sci.*, 2003, **522**, L9–L14.
295 M. Bohringer, W. D. Schneider and R. Berndt, *Angew. Chem., Int. Ed.*, 2000, **39**, 792–795.
296 M. Bohringer, K. Morgenstern, W. D. Schneider and R. Berndt, *Angew. Chem., Int. Ed.*, 1999, **38**, 821–823.
297 J. Prinz, O. Groening, H. Brune and R. Widmer, *Angew. Chem., Int. Ed.*, 2015, **54**, 3902–3906.
298 B. Yang, Y. L. Wang, H. Y. Cun, S. X. Du, M. C. Xu, Y. Wang, K. H. Ernst and H. J. Gao, *J. Am. Chem. Soc.*, 2010, **132**, 10440–10444.
299 J. Yoon, W. Son, H. Kim, K. Chung, S. Han and S. Kahng, *Nanotechnology*, 2011, **22**, 275705.
300 W. Xu, R. E. A. Kelly, H. Gersen, E. Laegsgaard, I. Stensgaard, L. N. Kantorovich and F. Besenbacher, *Small*, 2009, **5**, 1952–1956.
301 D. Rohde, C. J. Yan, H. J. Yan and L. J. Wan, *Angew. Chem., Int. Ed.*, 2006, **45**, 3996–4000.
302 W. Mamdouh, M. Dong, R. E. A. Kelly, L. N. Kantorovich and F. Besenbacher, *J. Phys. Chem. B*, 2007, **111**, 12048–12052.
303 M. E. Stawasz and B. A. Parkinson, *Langmuir*, 2003, **19**, 10139–10151.
304 S. De Feyter, A. Gesquiere, K. Wurst, D. B. Amabilino, J. Veciana and F. C. De Schryver, *Angew. Chem., Int. Ed.*, 2001, **40**, 3217–3220.
305 S. Ahn, J. T. Henssler and A. J. Matzger, *Chem. Commun.*, 2011, **47**, 11432–11434.
306 D. G. Yablon, D. Wintgens and G. W. Flynn, *J. Phys. Chem. B*, 2002, **106**, 5470–5475.

307 R. Lim, J. Li, S. F. Y. Li, Z. Feng and S. Valiyaveettil, *Langmuir*, 2000, **16**, 7023–7030.
308 Q. Chen, T. Chen, D. Wang, H. B. Liu, Y. L. Li and L. J. Wan, *Proc. Natl. Acad. Sci. U. S. A.*, 2010, **107**, 2769–2774.
309 Q. Chen, T. Chen, X. Zhang, L.-J. Wan, H.-B. Liu, Y.-L. Li and P. Stang, *Chem. Commun.*, 2009, 3765–3767.
310 A. Gesquiere, P. Jonkheijm, A. Schenning, E. Mena-Osteritz, P. Bauerle, S. De Feyter, F. C. De Schryver and E. W. Meijer, *J. Mater. Chem.*, 2003, **13**, 2164–2167.
311 H. Zhou and J. D. Wuest, *Langmuir*, 2013, **29**, 7229–7238.
312 J. Zhang, B. Li, X. F. Cui, B. Wang, J. L. Yang and J. G. Hou, *J. Am. Chem. Soc.*, 2009, **131**, 5885–5890.
313 M. Lukas, R. E. A. Kelly, L. N. Kantorovich, R. Otero, W. Xu, E. Laegsgaard, I. Stensgaard and F. Besenbacher, *J. Chem. Phys.*, 2009, **130**, 024705.
314 R. Otero, M. Schock, L. M. Molina, E. Laegsgaard, I. Stensgaard, B. Hammer and F. Besenbacher, *Angew. Chem., Int. Ed.*, 2005, **44**, 2270–2275.
315 C. B. France and B. A. Parkinson, *J. Am. Chem. Soc.*, 2003, **125**, 12712–12713.
316 M. Kiel, K. Duncker, C. Hagendorf and W. Widdra, *Phys. Rev. B: Condens. Matter Mater. Phys.*, 2007, **75**, 195439.
317 A. Dmitriev, H. Spillmann, S. Stepanow, T. Strunskus, C. Woll, A. P. Seitsonen, M. Lingenfelder, N. Lin, J. V. Barth and K. Kern, *ChemPhysChem*, 2006, **7**, 2197–2204.
318 S. Stepanow, N. Lin, F. Vidal, A. Landa, M. Ruben, J. V. Barth and K. Kern, *Nano Lett.*, 2005, **5**, 901–904.
319 R. Cortes, A. Mascaraque, P. Schmidt-Weber, H. Dil, T. U. Kampen and K. Horn, *Nano Lett.*, 2008, **8**, 4162–4167.
320 Q. Chen, D. J. Frankel and N. V. Richardson, *Langmuir*, 2002, **18**, 3219–3225.
321 F. Song, W. D. Dou, H. Huang, H. Y. Li, P. M. He, S. N. Bao, Q. Chen and W. Z. Zhou, *Chem. Phys. Lett.*, 2008, **452**, 275–280.
322 H. Cun, Y. Wang, B. Yang, L. Zhang, S. Du, Y. Wang, K.-H. Ernst and H.-J. Gao, *Langmuir*, 2010, **26**, 3402–3406.
323 B. V. Rao, K. Y. Kwon, J. Zhang, A. W. Liu and L. Bartels, *Langmuir*, 2004, **20**, 4406–4412.
324 K. Kanazawa, A. Taninaka, H. Huang, M. Nishimura, S. Yoshida, O. Takeuchi and H. Shigekawa, *Chem. Commun.*, 2011, **47**, 11312–11314.
325 C. Villagomez, O. Guillermet, S. Goudeau, F. Ample, H. Xu, C. Coudret, X. Bouju, T. Zambelli and S. Gauthier, *J. Chem. Phys.*, 2010, **132**, 074705.
326 E. V. Iski, H. L. Tierney, A. D. Jewell and E. C. H. Sykes, *Chem. – Eur. J.*, 2011, **17**, 7205–7212.
327 Y. J. Hwang, A. Kim, E. Y. Hwang and S. Kim, *J. Am. Chem. Soc.*, 2005, **127**, 5016–5017.
328 L. Merz, H. Guntherodt, L. J. Scherer, E. C. Constable, C. E. Housecroft, M. Neuburger and B. A. Hermann, *Chem. – Eur. J.*, 2005, **11**, 2307–2318.
329 A. Ulman, *Chem. Rev.*, 1996, **96**, 1533–1554.
330 O. Ikkala and G. ten Brinke, *Science*, 2002, **295**, 2407–2409.
331 A. Fisher and P. Blöchl, *Phys. Rev. Lett.*, 1993, **70**, 3263.
332 K. Sun, M. Lan and J.-Z. Wang, *Phys. Chem. Chem. Phys.*, 2015, **17**, 26220–26224.
333 L. Wang, S. Chen, L. Liu, D. C. Qi, X. Y. Gao, J. Subbiah, S. Swaminathan and A. T. S. Wee, *J. Appl. Phys.*, 2007, **102**, 063504.
334 L. Wang, H. H. Kong, X. Chen, X. L. Du, F. Chen, X. Q. Liu and H. M. Wang, *Appl. Phys. Lett.*, 2009, **95**, 093102.
335 M. Pivetta, M. C. Blüm, F. Patthey and W.-D. Schneider, *ChemPhysChem*, 2010, **11**, 1558–1569.
336 J. A. Miwa, F. Cicoira, S. Bedwani, J. Lipton-Duffin, D. F. Perepichka, A. Rochefort and F. Rosei, *J. Phys. Chem. C*, 2008, **112**, 10214–10221.
337 J. A. Miwa, F. Cicoira, J. Lipton-Duffin, D. F. Perepichka, C. Santato and F. Rosei, *Nanotechnology*, 2008, **19**, 424021.
338 M. Pivetta, M. C. Blüm, F. Patthey and W. D. Schneider, *J. Phys. Chem. B*, 2009, **113**, 4578–4581.
339 M. C. Blüm, E. Cavar, M. Pivetta, F. Patthey and W. D. Schneider, *Angew. Chem., Int. Ed.*, 2005, **44**, 5334–5337.
340 J. Sadowski, T. Nagao, S. Yaginuma, Y. Fujikawa, A. Al-Mahboob, K. Nakajima, T. Sakurai, G. Thayer and R. Tromp, *Appl. Phys. Lett.*, 2005, **86**, 073109.
341 K. Tahara, S. Okuhata, J. Adisoejoso, S. B. Lei, T. Fujita, S. De Feyter and Y. Tobe, *J. Am. Chem. Soc.*, 2009, **131**, 17583–17590.
342 N. Jiang, Y. L. Wang, Q. Liu, Y. Y. Zhang, Z. T. Deng, K. H. Ernst and H. J. Gao, *Phys. Chem. Chem. Phys.*, 2010, **12**, 1318–1322.
343 L. Cheng, Y. Li, C. Zhang, Z.-L. Gong, Q. Fang, Y.-W. Zhong, B. Tu, Q. Zeng and C. Wang, *ACS Appl. Mater. Interfaces*, 2016, 32004–32010.
344 C. Busse, S. Weigelt, L. Petersen, E. Laegsgaard, F. Besenbacher, T. R. Linderoth, A. H. Thomsen, M. Nielsen and K. V. Gothelf, *J. Phys. Chem. B*, 2007, **111**, 5850–5860.
345 T. Huang, Z. P. Hu, A. D. Zhao, H. Q. Wang, B. Wang, J. L. Yang and J. G. Hou, *J. Am. Chem. Soc.*, 2007, **129**, 3857–3862.
346 F. Tao and S. L. Bernasek, *J. Phys. Chem. B*, 2005, **109**, 6233–6238.
347 T. Chen, W.-H. Yang, D. Wang and L.-J. Wan, *Nat. Commun.*, 2013, **4**, 1389.
348 S. Berner, M. de Wild, L. Ramoino, S. Ivan, A. Baratoff, H. J. Guntherodt, H. Suzuki, D. Schlettwein and T. A. Jung, *Phys. Rev. B: Condens. Matter Mater. Phys.*, 2003, **68**, 115410.
349 W. Auwärter, A. Weber-Bargioni, A. Riemann, A. Schiffrin, O. Gröning, R. Fasel and J. Barth, *J. Chem. Phys.*, 2006, **124**, 194708.
350 A. Nuermaimaiti, V. S-Falk, J. L. Cramer, K. L. Svane, B. Hammer, K. V. Gothelf and T. R. Linderoth, *Chem. Commun.*, 2016, **52**, 14023–14026.
351 J. Kuntze, X. Ge and R. Berndt, *Nanotechnology*, 2004, **15**, S337–S340.
352 T. G. Gopakumar, F. Matino, B. Schwager, A. Bannwarth, F. Tuczek, J. Kroger and R. Berndt, *J. Phys. Chem. C*, 2010, **114**, 18247–18251.
353 G. Schull, N. Néel, M. Becker, J. Kröger and R. Berndt, *New J. Phys.*, 2008, **10**, 065012.

354 N. Liu, S. Haq, G. R. Darling and R. Raval, *Angew. Chem., Int. Ed.*, 2007, **46**, 7613–7616.
355 M. Schock, R. Otero, S. Stojkovic, F. Hummelink, A. Gourdon, E. Laegsgaard, I. Stensgaard, C. Joachim and F. Besenbacher, *J. Phys. Chem. B*, 2006, **110**, 12835–12838.
356 A. Mugarza, N. Lorente, P. Ordejon, C. Krull, S. Stepanow, M. L. Bocquet, J. Fraxedas, G. Ceballos and P. Gambardella, *Phys. Rev. Lett.*, 2010, **105**, 115702.
357 U. Schlickum, R. Decker, F. Klappenberger, G. Zoppellaro, S. Klyatskaya, W. Auwarter, S. Neppl, K. Kern, H. Brune, M. Ruben and J. V. Barth, *J. Am. Chem. Soc.*, 2008, **130**, 11778–11782.
358 W. D. Xiao, X. L. Feng, P. Ruffieux, O. Groning, K. Mullen and R. Fasel, *J. Am. Chem. Soc.*, 2008, **130**, 8910–8912.
359 M. E. Canas-Ventura, K. Ait-Mansour, P. Ruffieux, R. Rieger, K. Mullen, H. Brune and R. Fasel, *ACS Nano*, 2011, **5**, 457–469.
360 K. Sun, T. N. Shao, J. L. Xie, M. Lan, H. K. Yuan, Z. H. Xiong, J. Z. Wang, Y. Liu and Q. K. Xue, *Small*, 2012, **8**, 2078–2082.
361 P. Donovan, A. Robin, M. S. Dyer, M. Persson and R. Raval, *Chem. – Eur. J.*, 2010, **16**, 11641–11652.
362 M. Parschau, R. Fasel, K. H. Ernst, O. Groning, L. Brandenberger, R. Schillinger, T. Greber, A. R. Seitsonen, Y. T. Wu and J. S. Siegel, *Angew. Chem., Int. Ed.*, 2007, **46**, 8258–8261.
363 D. Jiang, Y. Lu, J. Ling, X. Leng, X. Liu and L. Wang, *Surf. Rev. Lett.*, 2016, **23**, 1650061.
364 M. Treier, P. Ruffieux, P. Groning, S. X. Xiao, C. Nuckolls and R. Fasel, *Chem. Commun.*, 2008, 4555–4557.
365 F. Chen, X. Chen, L. Liu, X. Song, S. Liu, J. Liu, H. Ouyang, Y. Cai, X. Liu and H. Pan, *Appl. Phys. Lett.*, 2012, **100**, 081602.
366 C. Vericat, M. Vela, G. Benitez, P. Carro and R. Salvarezza, *Chem. Soc. Rev.*, 2010, **39**, 1805–1834.
367 L. Srisombat, A. C. Jamison and T. R. Lee, *ACS Appl. Mater. Interfaces*, 2011, **390**, 1–19.
368 N. S. Bhairamadgi, S. P. Pujari, F. G. Trovela, A. Debrassi, A. A. Khamis, J. M. Alonso, A. A. Al Zahrani, T. Wennekes, H. A. Al-Turaif and C. van Rijn, *Langmuir*, 2014, **30**, 5829–5839.
369 K. Fukuda, T. Yokota, K. Kuribara, T. Sekitani, U. Zschieschang, H. Klauk and T. Someya, *Appl. Phys. Lett.*, 2010, **96**, 17.
370 O. Seitz, P. G. Fernandes, R. Tian, N. Karnik, H.-C. Wen, H. Stiegler, R. A. Chapman, E. M. Vogel and Y. J. Chabal, *J. Mater. Chem.*, 2011, **21**, 4384–4392.